Essential Host Factors for Human Parvovirus B19 Replication

By

Safder Saieed Ganaie

Submitted to the graduate degree program in Microbiology, Molecular Genetics & Immunology and the Graduate Faculty of the University of Kansas in partial fulfillment of the requirements for the degree of Doctor of Philosophy.

Dissertation Committee:

_____

Jianming Qiu, PhD, Chair

_____

Joe Lutkenhaus, PhD

_____

Edward B. Stephens, PhD

_____

Wolfram R. Zuckert, PhD

_____

Vargheese Chennathukuzhi, PhD

_____

Severin O. Gudima, PhD

Date defended: April 20, 2018

The dissertation committee for Safder Saieed Ganaie certifies that this is the approved version of the following dissertation:

Essential Host Factors for Human Parvovirus B19 Replication

_____

Jianming Qiu, PhD, Chair

Date Approved: May 4, 2018

Abstract

Parvovirus B19 (B19V) is a small, non-enveloped virus that contains a single-stranded DNA (ssDNA) genome of 5.6 kb in size. B19V is pathogenic to humans and causes bone marrow failure diseases and various other inflammatory disorders. B19V infection exhibits high tropism for human erythroid progenitor cells (EPCs) in the bone marrow and fetal liver. The exclusive restriction of B19V replication to erythroid lineage cells is partly due to the expression of receptor and co-receptor(s) on the cell surface of human EPCs and partly depends on the intracellular factors essential for virus replication. On this rationale, we tried to investigate the essential host factors for efficient virus replication. Our results demonstrated that signal transducer and activator of transcription 5 (STAT5) and RNA-binding motif protein-38 (RBM38) are two of these important host factors that ensure virus DNA replication and pre-mRNA processing, respectively, during B19V infection. The stages of erythropoiesis during which STAT5 is activated and RBM38 is expressed, are highly susceptible to B19V infection, thus suggesting that these two factors are among the key determinants of the B19V restriction to human EPCs.

B19V requires erythropoietin (EPO) signaling and hypoxia for its efficient replication. EPO to EPO receptor signaling activates JAK2-STAT5 pathway that phosphorylates STAT5. In our first study, we show that phosphorylated STAT5 is critical for B19V replication. Upon *in-silico* analysis, we identified a consensus STAT5 binding element adjacent to the NS1-binding elements within the minimal origin of viral DNA replication (Ori) in the B19V genome. The phosphorylated STAT5 specifically interacts with viral Ori both *in vivo* and *in vitro,* and is actively recruited within the viral DNA replication centers. Furthermore, our study shows a novel interaction between STAT5 and the minichromosome maintenance (MCM) complex. Our

proposed model suggests that STAT5 directly facilitates viral DNA replication by recruiting MCM complex into viral DNA replication centers. Interestingly, we found that pimozide, a STAT5 phosphorylation inhibitor and an FDA-approved drug, inhibits B19V replication in *ex vivo* expanded EPCs, suggesting that pimozide could be a promising antiviral drug for the treatment of B19V-related pathologies.

B19V expresses a single precursor mRNA (pre-mRNA), which undergoes alternative splicing and alternate polyadenylation to generate 12 viral mRNA transcripts. Splicing at the second 5' donor site (D2) of the B19V pre-mRNA is essential for the expression of VP1, VP2 and 11-kDa. We have previously identified that a *cis*-acting intronic splicing enhancer 2 (ISE2) that lies immediately after the D2 site facilitates recognition of the D2 donor for its efficient splicing. In our second study, we described that ISE2 harbors a consensus RBM38 binding sequence–5'-UGUGUG-3'. RBM38 is expressed during the middle stage of erythropoiesis. We first confirmed that the RBM38 binds specifically with the ISE2 element *in vitro*. Knockdown of RBM38 significantly decreases the level of the spliced mRNA at D2 that encodes 11-kDa protein and, thereafter, the expression of the 11-kDa protein. Importantly, we found that the 11-kDa protein enhances viral DNA replication and virion release. Accordingly, knockdown of RBM38 decreases virus replication *via* downregulating 11-kDa expression. Taken together, these results suggest that the 11-kDa protein facilitates B19V DNA replication, and that RBM38 is an essential host factor for the splicing of B19V pre-mRNA from D2 to A2-2 sites and for the expression of the 11-kDa protein. In conclusion, we identified two host factors, STAT5 and RBM38, which play important roles in B19V replication. We provide a mechanistic overview of how STAT5 facilitates virus DNA replication and RBM38 promotes the splicing of B19V pre-mRNA that ensures the expression of 11-kDa protein.

Acknowledgments

I would like to thank my mentor Dr. Jianming Qiu, whose encouragement and unreserved support all these years has enabled me to grow as a student and a scientist-to-be. The projects would not have been fruitful without his encouragement and help. I truly enjoyed working with him all these years. Dr. Qiu's skillful guidance, innovative ideas and stoic patience are greatly appreciated.

Dr. Mohammad Mir, my inspiring first mentor, gave me an opportunity to prove myself and guided me through my initial PhD study and for that I will always be grateful and indebted to him.

I wish to express my profound gratitude and sincere thanks to all the members of my comprehensive exam and thesis committee for stimulating discussions and valuable advice – Dr. Joe Lutkenhaus, Dr. Edward Stephens, Dr. Wolfram Zuckert, Dr. Thomas Yankee, Dr. Severin Gudima and Dr. Vargheese Chennathukuzhi.

My sincere thanks to Dr. Michael Parmely for his help and Microbiology Department staff; Kathy Mackay, Elizabeth Jenkins, Bob Gum and Jeff Fischer for their support all these years. I also thank Richard Hastings for his help with Flow cytometry.

For their friendship and support, I also thank my present and past colleagues, Zekun Wang, Peng Xu, Wei Zou, Xuefeng Deng, Weiran Shen, Fang Cheng, Sheema Mir and Nilshad Salim.

Lastly, I express my love and respect to my family and friends for their understanding and for always being there for me.

Table of Contents

List of Figures

Chapter 1:

Overview of Parvovirus B19 Replication and Infection[1]

[1] A version of this chapter has been accepted for publication in Frontiers in Cellular and Infection Microbiology: Ganaie SS and Qiu J; Front. Cell. Infect. Microbiol. | doi: 10.3389/fcimb.2018.00166. https://www.frontiersin.org/articles/10.3389/fcimb.2018.00166/abstract

Abstract

Human parvovirus B19 (B19V) infects erythroid progenitor cells in the bone marrow and fetal liver. The specific tropism of B19V for erythroid precursor cells partially relies on the intracellular factors in erythroid-lineage cells. In human $CD36^{+}$ erythroid progenitor cells (EPCs), erythropoietin signaling is not only required for the cell differentiation and development, but is also indispensable for B19V replication. Specifically, **S**ignal **T**ransducer and **A**ctivator of **T**ranscription- **5 (**STAT5) activation is critical for viral DNA replication. B19V replication-induced DNA damage response (DDR) also plays an important role in the virus replication. B19V multiplies efficiently under hypoxic conditions. B19V induces cell cycle arrest, initially at late S-phase, during which B19V fully exploits S-phase factors to replicate the viral genomes. Later B19V causes G2 arrest that leads to cell death of EPCs. B19V encodes a single precursor mRNA, which harbors two splice donor sites and four acceptor sites. The use of extensive alternate splicing and alternative polyadenylation generates at least 12 different species of mRNA transcripts. Both the processes of alternate splicing and alternative polyadenylation are tightly regulated through *cis-acting* elements and *trans-acting* factors flanking the splice donor or acceptor sites. In this introductory chapter, we focus on recent advances in the molecular virology and pathogenesis of B19V infection.

Introduction

Parvovirus B19 (B19V) is a small, non-enveloped virus that has a diameter of approximately 23-26 nm and contains a linear single-stranded DNA genome of 5.6 kb, flanked by two identical terminal hairpin structures (**Fig. 1-1A**) (1). B19V belongs to *Erythroparvovirus* of the *Parvoviridae* family. The name B19 was coined after the sample number containing the virus; panel B and no.19, during the screening of hepatitis B virus (2). B19V infection causes several diseases in humans, including like fifth disease in children, transient aplastic crisis, non-immune hydrops fetalis in pregnant women, persistent anemia in immunocompromised patients, arthropathy, cardiomyopathy and inflammation of various other tissues (1).

In this chapter, we focus on recent advances in B19V tropism, viral DNA replication and viral transcription. Importantly, we will focus on four key factors involved in B19V replication that are: a) erythropoietin (EPO) signaling; b) hypoxia; c) DNA damage response (DDR); and d) late S-phase arrest. We also summarize the new advancements in B19V pre-mRNA processing and its regulation. We also discuss host factors STAT5 and RBM38 (**R**NA-**B**inding **M**otif protein- **38**), which regulate virus replication and mRNA processing, respectively. Lastly, we discuss the underlying mechanism of NS1 induced cell cycle arrest, B19V pathogenesis, and the future directions in the development of therapeutics for B19V infection.

Viral entry and determinants of viral tropism

Productive infection of B19V is restricted to human erythroid progenitor cells, particularly, during the stages of burst forming unit-erythroid (BFU- E) to colony forming unit-erythroid (CFU-E) (3,4). B19V infects *ex vivo* expanded EPCs from human bone marrow (3-5), peripheral and umbilical blood (6-9) and the fetal liver (10,11). In addition to expanded primary EPCs, various other cell lines have been used for B19V infection, including MB-02, UT7/Epo and UT7/Epo-S1 (megakaryoblastoid cell lines) (12-14) and JK-1, KU812-Ep6 (erythroid leukemia cell lines) (15,16). For efficient B19V replication, erythropoietin and hypoxia play a critical role under *in vitro* conditions (17,18). B19V also infects endothelial cells of various tissues, but the infection is largely non-productive (19). In addition, U937 cells, circulating angiogenic cells (CACs) and $CD34^{+}$ endothelial progenitor cells from bone marrow have also been reported to be susceptible to B19V infection (20-22). All these cells either express viral receptor/co-receptors or use an antibody dependent route via c1q receptor for viral entry (23).

The primary receptor for B19V is globoside or P antigen (**Fig. 1-2**) (24). However, all P antigen expressing cells are not permissive to B19V (25). Various other co-receptors like Ku80 (26), integrin α5β1 (27) and antibody-mediated B19V entry routes (23) are presumed to be involved in B19V entry. Importantly, the B19V capsid binds its primary receptor, P antigen and undergoes a conformational change, exposing VP1u, a unique (273 aa) N-terminus of the VP1 capsid protein (**Fig. 1-2**) (28-30). Since Ku80 and α5β1 integrin haven't been shown to interact with VP1u, it has been hypothesized that VP1u interacts with some unknown co-receptor for subsequent internalization. Further, the N-terminal 100 amino acids of VP1u are required for internalization, which implies that the PLA2 (phospholipase A2) activity of VP1u is not essential for viral entry (31). Interestingly, the VP1u region (without capsid) is efficiently internalized by

B19V-permissive cells (32,33), which suggests that primary interaction of B19V with P antigen is required only for externalization of VP1u. Mature RBCs also express P antigen and hence show primary attachment to B19V, as the virus is not internalized (29). It is presumed that this primary interaction may be responsible for systemic dissemination of the virus. Similar to other parvoviruses, B19V uses the endocytic pathway but escapes lysosomal degradation to enter the nucleus for subsequent replication, transcription and packaging (**Fig. 1**-**2**) (34,35).

Gene expression, splicing, and its regulation

Upon entry of the virus into the nucleus, the B19V ssDNA genome is converted to double-stranded replicative form (dsRF), which acts a template for both DNA replication and transcription (**Fig. 1-2**) (36). The dsRF viral DNA has a unique but single promoter at map unit 6 (P6) that expresses a single precursor mRNA (pre-mRNA) (**Fig. 1-1B**) (37,38). The P6 promoter has an upstream enhancer region and NS1 elements that bind transcription factors (e.g. CREBP, GATA, Oct1 etc.) and NS1 protein, respectively, for promoter transactivation (39-42). B19V pre-mRNA undergoes alternative splicing and polyadenylation to express at least 12 mature mRNA transcripts that encode two structural (VP1 & VP2) and three non-structural (NS1, 7.5-kDa & 11-kDa) proteins (43-45). The pre-mRNA contains two splice donor sites (D1 & D2) and four acceptor sites (A1-1, A1-2, A2-1 & A2-2) (**Fig. 1-1B**) (1). In addition, it harbors two proximal [(pA)p]1/2 and a distal [p(pA)d] polyadenylation sites (**Fig. 1-1B**) (1). Unspliced mRNA transcripts (R1&R1') that polyadenylate at (pA)p encode the NS1 protein while those spliced at A1-1 (R2 & R2') and use (pA)p sites encode the 7.5-kDa protein (**Fig. 1-1B**). The mRNA transcripts polyadenylated at (pA)d and where 1^{st} intron (R4 & R5), 1^{st} and 2^{nd} (R6 & R7), or 1^{st} , 2^{nd} and 3^{rd} introns (R8 & R9) are spliced out encode the VP1, VP2 and 11-kDa proteins, respectively (**Fig. 1-1B**) (44,46,47). Whether other mRNAs (R3 & R3') encode a protein or play any role during virus infection is unknown.

While the B19V mRNAs are splice products from a single pre-mRNA, the expression levels of the different encoded proteins vary considerably. Therefore, the virus must employ different strategies to regulate the level of gene expression. In absence of viral DNA replication, most mRNA transcripts polyadenylate at (pA)p leading to the expression of NS1 and 7.5-kDa proteins in both B19V-permisssive or non-permissive cells (**Fig. 1B**) (48). Viral DNA

replication facilitates the read through of (pA)p and overcomes the blockade to express mRNAs that polyadenylate at (pA)d encoding for the VP1, VP2 and 11-kDa proteins (49). Thus, the early and late phases of virus infection are dominated by NS1-encoding and VP/11-kDa-encoding mRNAs, respectively (50). An alternative model for virus infection was also proposed suggesting that B19V genome be considered as single, two state replicative and transcription unit, where the increase in viral RNA correlates with viral DNA levels (51). Next, the central exon or exon 2 (spanning A1-1/2 to D2) harbors serine arginine (SR) protein binding GAA motifs, and the GAA motif between A1-1 and A1-2, constitutes exon splicing enhancer 1 (ESE1), which defines exon-2 and facilitates splicing at A1-1. The 5' end of exon 2 promotes splicing at A1-2 and serves as exon splicing enhancer 2 (ESE2) (52). Splicing at second donor site (D2) is critical for the expression of capsid and 11-kDa encoding mRNAs, and also competes with polyadenylation at (pA)p (53). Binding of U1 snRNA to D2 splice donor site inhibits polyadenylation at (pA)p (52). D2 is a weak splice donor site and requires two *cis-acting* elements: exon splicing enhancer 3 (ESE3) and intron splicing enhancer 2 (ISE2) for its efficient splicing (52). Hence, the interplay of *cis-acting* elements and *trans-acting* factors determine the splicing efficiency of different splice sites to regulate the expression of different mRNA species. While looking for the *trans-acting* factors that bind ISE2, our results in chapter 3 demonstrate that RNA binding protein-RBM38, expressed in the middle stages of erythropoiesis, promotes the expression of 11-kDa protein. Specifically, RBM38 binds ISE2 and promotes splicing of the third intron (D2 to A2-2), that results in the production of 11-kDa encoding mRNAs. Therefore, RBM38 is one of the essential *trans-acting* factors that regulates the expression of 11-kDa protein (54)**.**

Viral Proteins and their functions

B19V expresses two structural proteins (VP1 & VP2) and three non-structural proteins (NS1, 11-kDa & 7.5-kDa).

Non-structural proteins.

Non-structural protein 1 (NS1). NS1 is 671 amino acid long protein that has a MW of ~ 78 kDa by SDS-PAGE. NS1 contains two nuclear localization signals; KKPR (177-179) and KKCGKK (316-321) (**Fig. 1-3**) and is found predominantly in the nucleus of infected cells (43,55-57). NS1 contains a DNA binding and endonuclease domain at N-terminus (58), ATPase and NTP-binding domains in the central region (59) and a transactivation domain at its C-terminus (60) **(Fig. 1-3).** NS1 is critical for virus DNA replication (61), and binds NSBEs (NS1 binding elements) of the minimum origin of replication of B19V dsRF DNA (**Fig. 1-4**) (58). Upon NS1 binding to NSBEs, it presumably opens up the dsRF DNA and nicks the ssDNA substrate at trs (terminal resolution site) (**Fig. 1-2**) (62). With the assistance of Sp1/Sp3, NS1 binds P6 promoter for its transactivation (63,64). NS1 induces apoptosis via NTP-binding motif (328-335 amino acid) (59,65,66), a DNA damage response (60,67) and cell cycle arrest (57,68-70). The putative transactivation domain TAD2 of NS1 is critical for cell cycle arrest and the transactivation of host genes. NS1 is thought to be a global transactivator as the expression of NS1 protein in UT7/Epo-S1 affected around 1,770 genes, by upregulating 1,064 genes and downregulating 706 genes (70). In short, NS1 is a multifunctional protein and plays various roles during B19V infection (**Fig. 1-5**).

11-kDa protein. The 11-kDa protein is expressed at high levels during B19V infection and localizes more in cytoplasm than nucleus of infected cells. The abundance of the 11-kDa protein in cytoplasm of infected cells is at least 100 times greater than NS1 protein (47,71). The

11-kDa protein is potent inducer of apoptosis during B19V infection and involves caspase-10 (**Fig. 1-2**) (71). In chapter 3, our results demonstrate that the 11-kDa protein enhances viral DNA replication (~10 fold), and thus determines virion production (54). Finally, the 11-kDa protein has also been implicated in VP2 production and its distribution (61).

7.5-kDa protein. The function(s) of 7.5-kDa are still unknown.

Structural proteins.

Capsid proteins (VP1 & VP2). VP1 is a minor capsid protein, 781 amino acids long (~ 84 kDa) (56). VP1 shares the same C-terminus with VP2, with extra 273 amino acids, called as VP1-unique (VP1u) (43,56). VP2 is a major capsid protein, 554 amino acid long (~ 58 kDa) (56). VP1 expression is low (72) and with VP2 assemble into viral capsid (VP1:VP2= 1:20) (**Fig. 1-2**) (56). VP2 has nuclear localization signal at C-terminus, therefore both proteins are found in the nucleus of infected cells(73). The capsid first interacts with P antigen (**Fig. 1-2**) (24) and thereafter first 100 amino acids of VP1u help in internalization of the virus particles (31). VP1u region from 128 to 160 amino acids exhibits phospholipase A2 activity (74-76), which is possibly used to evade lysosomal fusion and ensure nuclear entry of the virions.

B19 replication and its regulation

B19V replication takes place in the nucleus of the infected cells. The single-stranded genome of the virus is first converted to dsRF DNA. B19V genome (RF) contains two 67-bp (nt 5214 - 5280) long minimum origin of replication (Ori) at both ends (77). Although the origins function independently, but both origins are required for the efficient DNA replication of the virus (78). B19V genome can replicate without inverted terminal repeats (ITR), however, ITRs significantly enhance viral DNA replication (78). Ori contains NS1 binding elements (NSBEs) (58), terminal resolution site (trs) (62), STAT5 binding site, and potential host factor binding sites (**Fig. 1-4**) (78). NS1 binds NSBEs and nicks DNA at trs (62), whereas STAT5 binds Ori and recruits MCM (**M**ini**c**hromosome **M**aintenance) complex (78). After NS1 nicking, DNA replication continues, and presumably follows rolling hairpin model of replication (**Fig. 1-2**), as suggested for other parvoviruses (79). Upon microarray analysis of dynamic transcriptome of B19V infected EPCs, we recently found that DNA metabolism, DNA replication, DNA repair, DNA damage response, cell cycle and cell cycle arrest pathways are significantly altered upon virus infection (80). Broadly, B19V replication is regulated by the following factors:

I. EPO-signaling.

In response to low oxygen tension, human kidney interstitial fibroblasts secrete EPO, a glycoprotein cytokine that promotes the differentiation and development of erythroid progenitors that results in the production of mature RBCs (81). During erythropoiesis, pluripotent hematopoietic stem cells (HSCs, $CD34^{+}$) are differentiated into enucleated erythrocytes, encompassing the following stages – BFU-Es, CFU-Es, normoblasts, erythroblasts, reticulocytes and finally the mature erythrocytes (81,82). The earlier stages of differentiation are EPO-independent (82**),** and rely on factors like, stem cell factor (SCF) (83,84), IL-6 (85) and IL-3

(83). However, the late stage differentiation process requires EPO (82,86). The exclusive tropism of B19V for erythroid progenitor cells partly depends on the expression of receptor and co-receptors on the cell surface and partly on the essential host cellular factors for efficient virus replication. Erythroid lineage cells depend on EPO for survival (87), but B19V also needs EPO for its replication (17). BFU-Es and CFU-Es, the late stage erythroids, are highly susceptible to B19V infection (88). B19V-semi permissive cell lines (e.g. UT7/Epo-S1) depend on EPO for cell proliferation and survival. Interestingly, B19V-permissivity of these cell lines strictly depends on EPO (**Fig. 1-2**) (88). $CD36^+$ EPCs differentiated from $CD34^+$ in absence of EPO are not permissive to B19V infection and B19V genome replicates only in the presence of EPO and requires phosphorylated Janus kinase 2 (JAK2) (17). EPO binds EPO-receptor and activates ERK, Phosphoinositide 3-kinase (PI3K) and JAK2-STAT5 pathways (**Fig. 1-2**) (89). JAK2-STAT5 pathway is essential for B19V replication while the ERK pathway negatively regulates B19V replication and PI3K is dispensable for virus replication (18). Although EPO signaling activates ERK pathway, B19V inhibits the ERK pathway presumably through its 11-kDa protein (18,90). Therefore, B19V fine tunes the EPO-signaling that favors efficient virus replication. In order to understand the underlying mechanism of STAT5 dependent B19V replication, we demonstrate in chapter 2 that STAT5 phosphorylation is critical for B19V DNA replication (78). The viral Ori harbors a STAT5 binding site (**Fig. 1-4**) and phosphorylated STAT5 binds viral origins both *in-vivo* as well as *in-vitro* (78). The mutation of STAT5 binding site within viral origins completely abolishes viral DNA replication (78). Importantly, STAT5 interacts with MCM complex. The disruption of STAT5-Ori complex leads to decrease in virus DNA replication and the abundance of MCM complex decreased significantly at the viral Ori (78).

Therefore, our proposed model shows that B19V utilizes STAT5 interaction with viral Ori to recruit MCM complex for the initiation of viral DNA replication (78).

II. Hypoxia.

During the propagation of B19V in *ex-vivo* expanded $CD36^{+}$ EPCs, progeny virion production is not as efficient as under natural conditions in human bone marrow on B19V infection of EPCs. The viremia in B19V infected patients goes up to 10^{13} genomic copies per ml of plasma (91,92), which indicates the requirement of other factors in determining the production of virions. Oxygen tension is low in bone marrow (93) and lower oxygen pressure favors erythroid cell development in culture (94)**.** Interestingly, B19V infected human EPCs at hypoxia (1% O_2) enhances viral gene expression, viral replication, and virus production. Hypoxia augmentation of B19V replication is independent of PHD/HIFα pathway. Hypoxia also enabled the B19V-infected pluripotent erythroid cells (KU812F) to yield high progeny virions (95). Increase in the productive B19V infection under hypoxic conditions wasn't due to increase in the B19V entry or intracellular trafficking of the virus and HIF-1 was shown not to play any role in hypoxia-induced enhancement in B19V infectivity (18)**.** However, hypoxia regulates EPO/EPO-receptor signaling pathway by upregulating STAT5 and downregulating MEK activation, thereby enhancing B19V DNA replication in both B19V-infected EPCs and M20 (infectious clone)-transfected UT7/Epo-S1cells (18)**.** We strongly believe that upregulation of STAT5 and downregulation of MEK/ERK signaling during hypoxia promote virus replication. The B19V infectious clone grows rapidly (~80 times) in UT7/Epo-S1 cells under hypoxia (18). The culture of EPCs or UT7/Epo-S1 cells under hypoxia for B19V propagation is currently the best culture system in use. The efficient replication of M20 infectious clone and the subsequent production of infectious virions holds promise to study B19V replication and the underlying mechanism(s) of

replication. Also, mutagenesis of B19V molecular clone M20 could help to understand the role of individual viral proteins and the specific protein domains in virus replication.

III. Late S phase cell cycle.

B19V DNA replication is dependent on host cellular DNA replication, since the virus doesn't encode a viral DNA polymerase (96). B19V induces cell cycle arrest in both virus-infected $CD36^{+}$ EPCs and UT7/Epo-S1 or M20 transfected UT7/Epo-S1 cells at G2/M (14,68). Virus infected UT7/Epo-S1-arrested cells display 4N DNA content and (5'-bromo-2-deoxy-uridine) BrdU-pulse labeling for *de novo* DNA synthesis along with DAPI staining indicates that the cells are precisely in late-S phase (68). Upon B19V infection of UT7/Epo-S1, cyclin A, cyclin B1 and phosphorylated cell division cycle 2 (CDC2) were shown to accumulate and CDC2-cyclinB1 complex displayed enhanced kinase activity (14)**.** The sequestration of cyclin B1 to the cytoplasm in B19V-infected cells indicates that B19V somehow prevents its import to nucleus, thus results into cell cycle arrest at G2 phase (14)**.** NS1 alone has been shown to induce a true G2/M cell cycle arrest, doesn't show BrdU incorporation but displays 4N DNA content (68), and de-regulation of E2F family transcription factors have been implicated for such arrest (57).

While B19V induces DDR that promotes virus replication, virus-induced DDR is not involved in cell cycle arrest at G2/M (60)**.** Like other autonomous parvoviruses, B19V infection also induces arrest at S phase (67,68)**.** Therefore, B19V induced late S phase arrest is possibly an outcome of replication-induced S phase arrest and NS1-induced G2/M arrest. Various S phase replication factors like polymerase delta (pol δ), proliferating cell nuclear antigen (PCNA), replication factor C-subunit 1 (RFC-1), the MCM complex except the DNA repair DNA polymerases are actively recruited to viral replication centers with pol δ and pol α essential for viral DNA replication (68,80). It is likely that like other parvoviruses (97-99), B19V exploits the

cell cycle arrest at late S phase and uses S phase factors for viral DNA replication. In addition, replication protein A-32 (RPA32) also colocalizes with viral replicating machinery. Although phosphorylated RPA32 forms also show colocalization, phosphorylation itself seems dispensable for virus replication (80), supporting the observation that B19V uses S phase for genome amplification.

IV. DNA damage response (DDR).

DNA damage response (DDR) is a cellular defense mechanism to preserve genomic stability and integrity in response to double strand breaks (DSBs), single strand DNA breaks, or installed replication (100). There are three major kinases (mediators) responsible for signaling downstream DDR effects, including Ataxia telangiectasia mutated (ATM), Ataxia telangiectasia and Rad3 related (ATR), and DNA dependent protein kinase, catalytic subunit (DNA-PKcs). Apart from recognizing the damaged cellular DNA, DDR is also activated by various DNA viruses either to combat the infection by invoking innate immune response or to facilitate viral DNA replication (96,101). B19V infection induces a DDR by activating all the three PI3K kinases (ATR, ATM and DNA-PKcs) (67). Phosphorylated ATM, ATR, DNA-PKcs and their downstream effectors (CHK1, CHK2 and Ku70/80) localize within the virus replication centers. Activated ATR and DNA-PKcs, but not ATM were found essential for B19V replication (60,67). Further, it was found that mere expression of the viral genes didn't lead to the phosphorylation of RPA32 and γH2AX, a hallmark of DDR (60). Interestingly, NS1 itself phosphorylates ATR to induces cell cycle arrest, however, such activation of ATR doesn't lead to phosphorylation of RPA32 and γH2AX (70). It was found that replicating, infectious clone-M20, but not a replication deficient M20 mutant, led to the induction of DDR (60), which implies that the replication process *per se* is responsible for inducing DDR.

Viral pathogenesis

Infection with B19V is a global concern and has a seroprevalence against the virus that varies from region to region and between the different age groups. The seroprevalence among children below the age of 5 years is 2-20%, between the age group of 5-18 years 15-40% and among adults 40-80%(1,102). The virus infection is contracted via inhalation, blood transfusion and from pregnant woman to fetus (103,104). It is still unknown how the virus penetrates the respiratory and placental barriers to reach the bone marrow and the fetal liver, respectively. The incubation time varies between 4-14 days, accompanied with prodromal symptoms like fever, headache, malaise and myalgia (1,105). After 2-3 weeks, the rash and joint symptoms become visible, which are believed to have an immunopathological origin (106). B19V is an etiological agent of erythema infectiosum, arthopathy, hydrops fetalis, transient aplastic crisis, and of a persistent infection in immunocompromised patients that causes pure red cell aplasia (PRCA) (1,107). Erythema infectiosum or "slapped cheek" is also called Fifth disease in children. Following the virus infection, the rashes appear first on the cheeks of the infected children as facial erythema, almost 18 days after infection, which then extend to trunk and proximal extremities as erythematous maculopapular eruptions (1,107,108). In adults, B19V causes arthralgia and arthritis, resembling rheumatoid arthritis and joint symptoms that can last for months post- infection (107,109). The parvovirus infection in pregnant women causes non-immune hydrops fealis due to severe anemia in fetuses, which leads to miscarriage and intrauterine fetal death (1,110). Transient aplastic crisis was the first disease linked to B19V and is a direct outcome of virus mediated cytotoxicity of erythroid progenitor cells(107). The B19V infection in children also leads to thrombocytopenia and immune mediated neutropenia

(107,111). In addition, the virus infection is also associated with myocarditis, encephalitis, hepatitis, glomerulonephritis and nephrotic syndrome. (1,107).

Productive infection of B19V induces cell cycle arrest and erythroid cell death.

B19V infection induces cell cycle arrest at G2 phase (14). Upon further analyses of the cell cycle during the virus infection, it was found that the arrest at G2 phase has 4N DNA content but also incorporates BrdU, a thymidine analog, suggesting that the infected cells are in late S phase (68). During early infection, the cells are precisely at late S phase, however, at the late phase of infection most infected cells are found in G2 phase (68). Interestingly, the expression of NS1 induces a true G2 arrest where cells don't incorporate BrdU but only exhibit 4N DNA content (68). There are many players responsible for inducing cell cycle arrest during B19V infection. During the B19V induced cell cycle arrest of UT7/Epo-S1 cells, it was observed that nuclear import of CDC2/cyclin B1 is prevented (14). NS1 itself causes a true G2 arrest by importing the repressive E2F transcription factors (E2F4/E2F5) (57). A putative NS1 transactivation domain-2 (TAD2) was found responsible for NS1-induced G2 arrest (60). Recently, the underlying mechanism of NS1 induced cell cycle arrest was explored in much detail (70). NS1-TAD2 domain transactivates several host genes that lead to the activation of ATR. Activated ATR phosphorylates cell division cycle 25C (CDC25C) at serine-216 through the activation of CHK1 (70). Phosphorylated CDC25C at S216 reduces its phosphatase activity and renders it complexed with 14-3-3 protein in the cytoplasm (112). As a result, inactive CDC25C is unable to dephosphorylate cyclin B1/CDK1 (pT14/Y15) complex to activate it. An active cyclin B1/CDK1 complex is essential for G2 to M transition (113)**.** In NS1-expressing UT7/Epo-S1 cells, nuclear entry of cyclin B1/CDK1 complex is not hampered, rather the complex exhibits reduced kinase activity (70). Hence, B19V NS1 induces G2 arrest by activating

the ATR-CDC25C-CDK1 pathway (70). NS1 activation of ATR doesn't lead to the activation of γH2AX and RPA32, a hallmark of DDR (60,70). Moreover, DNA replication induced DDR and thereafter, activation of ATR leads to the arrest of cells at late S phase (68). It appears that NS1 or DNA replication mediated activation of ATR transduce signaling through different downstream pathways and results in cells arrested at different phases of cell cycle. The last factor implicated in B19V infection induced cell cycle arrest is the viral genome itself. A nucleotide sequence 5'-GTTTTG T-3' from the viral promoter region arrests BFU-E progenitor cells at S and G2/M phase. This promoter sequence is a CpG oligodoxynucleotide-2006 analog that is a ligand of toll-like receptor 9 (TLR9). It appears that viral genomic replication initially stalls infected cells at late S phase and later with the help of NS1 arrests at G2/M, which eventually leads to cell death. B19V infection specifically targets BFU-E and CFU-E progenitors (114), disrupts erythropoiesis and results in the transient aplastic crisis (115). The virus-induced cell death is apoptotic in nature and involves caspase-3/6/8 activation (65,116). B19V NS1 activates the extrinsic apoptotic pathway involving the TNF-α pathway in $CD36^{+}$ EPCs or UT7/Epo cells (116). The B19V encoded 11-kDa protein is also implicated in causing cell death through apoptosis, which involves caspase-10 (71). It was found that 11-kDa is a more potent inducer of apoptosis than NS1 (71).

Non-productive infection of B19V causes inflammatory diseases of various tissues.

Virus infection is seen in non-erythroid cells as well. The virus uses an alternative entry route by complexing with antibody and entering through complement factor C1q and C1q receptor mediated endocytosis (23). There is no clear evidence that B19V replicates or produces virions in any non-erythroid cell lineage, hence the infection is considered largely non-productive.

B19V predominantly infects endothelial cells of various tissues (e.g., aorta, umbilical vein and pulmonary arteria etc.) (23). Other cell lines infected include U937 cells (20), circulatory angiogenic cells (CACs) and $CD34^{+}KDR^{+}$ endothelial progenitor cells (21,22). B19V infection appears to be persistent and viral genes are silenced through methylation of CpG sites on the DNA (117). Even after the infection is resolved, the viral DNA can be found in various tissues like spleen, liver, tonsils, testes and brain (19,118).

Upon infection, the infected tissue evokes host-cellular response against the virus which culminates in a several pathologies. B19V infection has been linked to several inflammatory diseases like cardiomyopathy, rheumatoid arthritis, hepatitis, vasculitis and meningoencephalitis (1,19). B19V infection or the expression of viral proteins can modulate the immune response. NS1 upregulates IFNAR1 and IL-2 (inflammatory response) and downregulates OAS1 and TYK2 (antiviral response) through the activation of STAT3/PIAS3 signaling pathway in human endothelial cells (HMEC-1) (119). The increase in the expression of inflammatory molecules like NF-κB, IL-6 and COX2 correlated with expression of viral capsid proteins in the colon, thyroid and synoviocytes (120-123). Particularly, in synoviocytes, VP1u phospholipase A2 activity is implicated in the production of inflammatory response (121). NS1 induces apoptosis in hepatocytes through the activation of caspse-3 and caspase-9 (66,124). In summary, B19V infection of non-erythroid tissues evokes inflammatory responses that lead to various pathologies. However, with the exception of the placental endothelium (125), no other non-erythroid cell type supports B19V multiplication.

B19V induced immune responses

The virus infection elicits a strong humoral immune response (126). Initially, the IgM antibodies are produced followed by IgG after several days post-infection, which provide few

months to lifelong protection, respectively (106,126,127). The antibody response is directed against VP1 (74), VP2 (128), and the NS1 (129) proteins. However, the neutralizing antibodies produced are against VP1u, the N-terminal (1-80 aa) region of the VP1 protein (130). The $CD8^+$ T cells response has also been observed in B19V infected patients, which sustains for several months even after the clearance of the virus (131). The T cell-mediated response is specifically directed against the VP1 and VP2 proteins, in which the antigen is presented to $CD4^+$ T cell by class II molecules (132). Of note, the T cell response is of Th1 type and involves the release of IFN- γ, IL-2, IL-12, and IL-15 (133,134). B19V-induced innate immune responses are not well established. There are few studies which show that the viral proteins (NS1 & VP2) regulate the expression of defensins, TLR-4/5/7/9 (135) and TLR9 can recognize CpG ODN-2006, the P6 promoter region of the genome (136).

Conclusion and future directions

It has been reported that almost 40-60% of the world's population is infected with parvovirus B19 (137). However, such persistent infection is at sub-immunogenic levels, as viral load is kept under control by our immune system, particularly by neutralizing antibodies against B19V VP1u region. During times when patients are under immune suppression or infected with other pathogens, the viral load increases and causes extensive cell death of erythroid progenitor cells and leads to various inflammatory diseases as described above.

There is no specific treatment for B19V infection, except IVIG treatment or blood transfusion, so there is a need to develop antivirals for B19V infection. The new advancements in the field of B19V viral replication have identified various critical steps during the process of virus replication. One such important step is NS1 binding to the viral origin and subsequent nicking of B19V DNA at trs (58). Recently, *in-vitro* nicking assay for NS1 was developed (62), which could be utilized to screen for inhibitors of NS1 nicking. Furthermore, since the VP1u region is essential for viral entry, peptide analogs of VP1u (1-100) (31) or neutralizing monoclonal antibodies (138) against VP1u can be employed to check B19V entry. In chapter 2, our study demonstrated that STAT5 phosphorylation is essential for B19V DNA replication (78). Pimozide, a STAT5 inhibitor and an FDA-approved drug abolishes virus replication in $CD36^{+}$ EPCs (78). Therefore, pimozide could be a potential drug for B19V infection and can be repurposed for B19 related pathologies and included in prophylactic anti-virals for transplant recipients. However, the development of new antivirals against B19V infection needs an animal model to validate any new treatment. Currently, simian parvovirus (SPV) infection of cynomolgus monkeys (139) can be employed to screen anti-B19 antivirals

Fig. 1-1. Transcription map of Parvovirus B19.

(A) Linear ssDNA genome of B19V. The genome is flanked by two inverted terminal repeats (ITRs), containing unpaired and mismatched bases, shown as bulges and bubbles, respectively. **(B)** Double stranded replicative form of B19V genome. The viral promoter denoted as P6 transcribes a single precursor mRNA (pre-mRNA). Pre-mRNA has two donor sites (D1 & D2) and four acceptor sites (A1-1, A1-2, A2-1, and A2-2). Using alternative splicing and polyadenylation, pre-mRNA is processed into at least 12 different mRNAs (only R1-R9 shown here). Mature mRNAs polyadenylate at (pA)p or (pA)d sites. At least five different proteins are known to be encoded by different species of mRNA transcripts. Different colors indicate the use of different open reading frames for the translation of proteins. Question marks indicate mRNAs encoding unknown proteins.

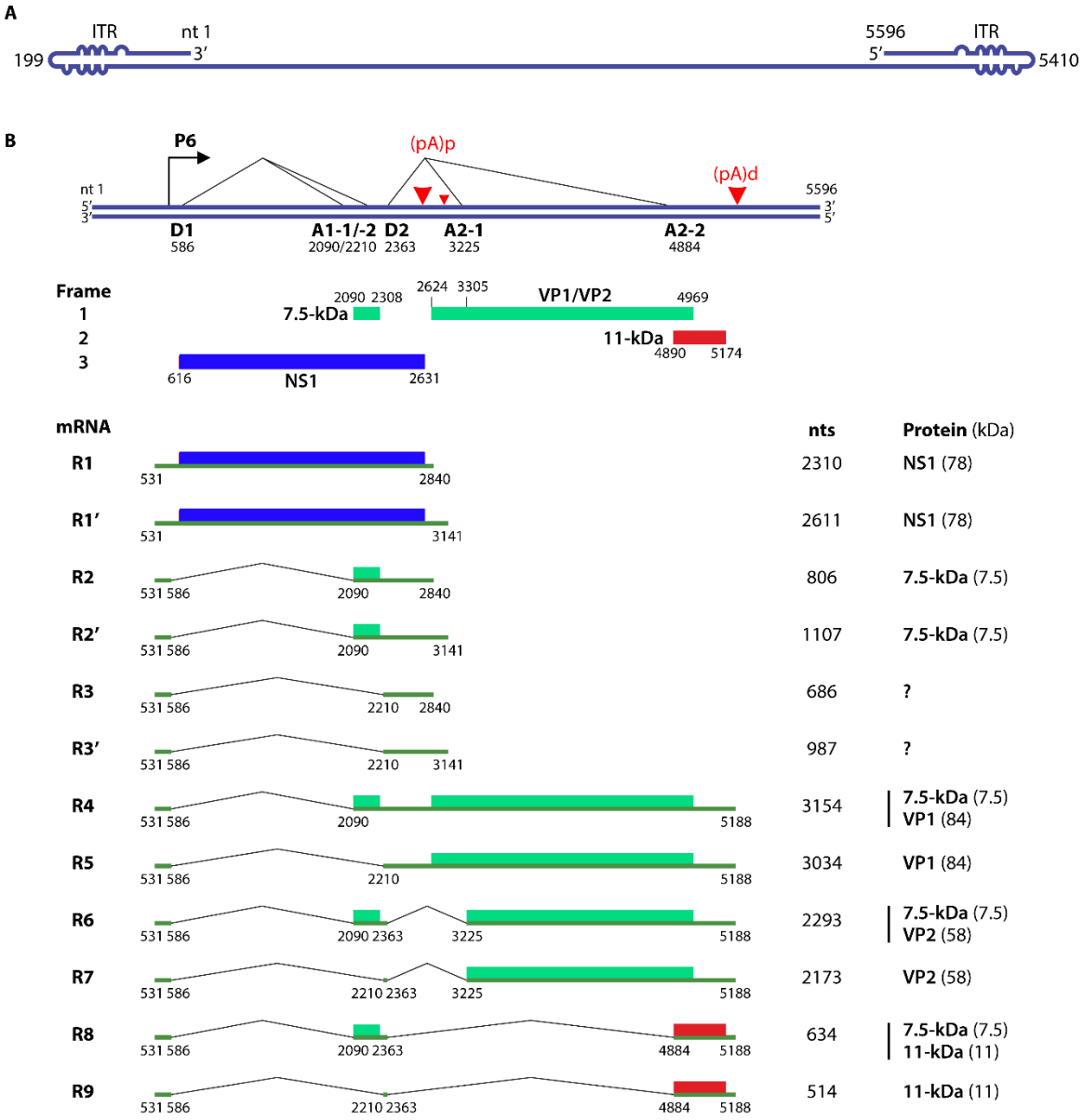
A
ITR
nt 1
199
3′
5596
ITR
5′
5410
B
P6
(pA)p
(pA)d
nt 1
5596
D1
586
A1-1/-2
2090/2210
D2
2363
A2-1
3225
A2-2
4884
Frame
1
2
3
2090 2308
7.5-kDa
2624 3305
VP1/VP2
4969
11-kDa
4890 5174
616
NS1
2631
mRNA
nts
Protein (kDa)
R1
531
2840
2310
NS1 (78)
R1′
531
3141
2611
NS1 (78)
R2
531 586
2090
2840
806
7.5-kDa (7.5)
R2′
531 586
2090
3141
1107
7.5-kDa (7.5)
R3
531 586
2210
2840
686
?
R3′
531 586
2210
3141
987
?
R4
531 586
2090
5188
3154
7.5-kDa (7.5)
VP1 (84)
R5
531 586
2210
5188
3034
VP1 (84)
R6
531 586
2090 2363
3225
5188
2293
7.5-kDa (7.5)
VP2 (58)
R7
531 586
2210 2363
3225
5188
2173
VP2 (58)
R8
531 586
2090 2363
4884
5188
634
7.5-kDa (7.5)
11-kDa (11)
R9
531 586
2210 2363
4884
5188
514
11-kDa (11)

Fig 1-1

Fig. 1-2. Proposed model of B19V life cycle.

B19V infects human erythroid progenitor cells. The virus first interacts with globoside (Step 1) and undergoes a conformational change that exposes VP1u which subsequently binds an unknown co-receptor (Step 1). Thereupon, the virus is endocytosed and somehow escapes the lysosomal route and enters the nucleus (Step 3). Inside the nucleus, the virion uncoats and releases the ssDNA genome (Step 4). Using the 3'OH of the left ITR, the second strand is synthesized to form a functional origin of replication (Step 5). Next, EPO and hypoxia activates and increases pSTAT5, which interacts with MCM and then binds Ori region. NS1 binding to NS1BE is critical for nicking ssDNA at trs and for helicase activity (step 6). The nicking creates a new 3' OH end to continue DNA replication that results into duplex replicative intermediate (Step 7). The dsDNA form also transcribes a single pre-mRNA that is processed into various mRNAs which are exported to cytoplasm for translation (Step 8). VP1/2 assemble into trimers to form capsids, which are transported back to the nucleus (Step 9). Through strand displacement, ssDNA is packaged into capsids, which probably requires NS1 (step 10). NS1 and 11-kDa in the cytoplasm induce apoptosis (Step 11). After multiplication, the virions are released though cell lysis.

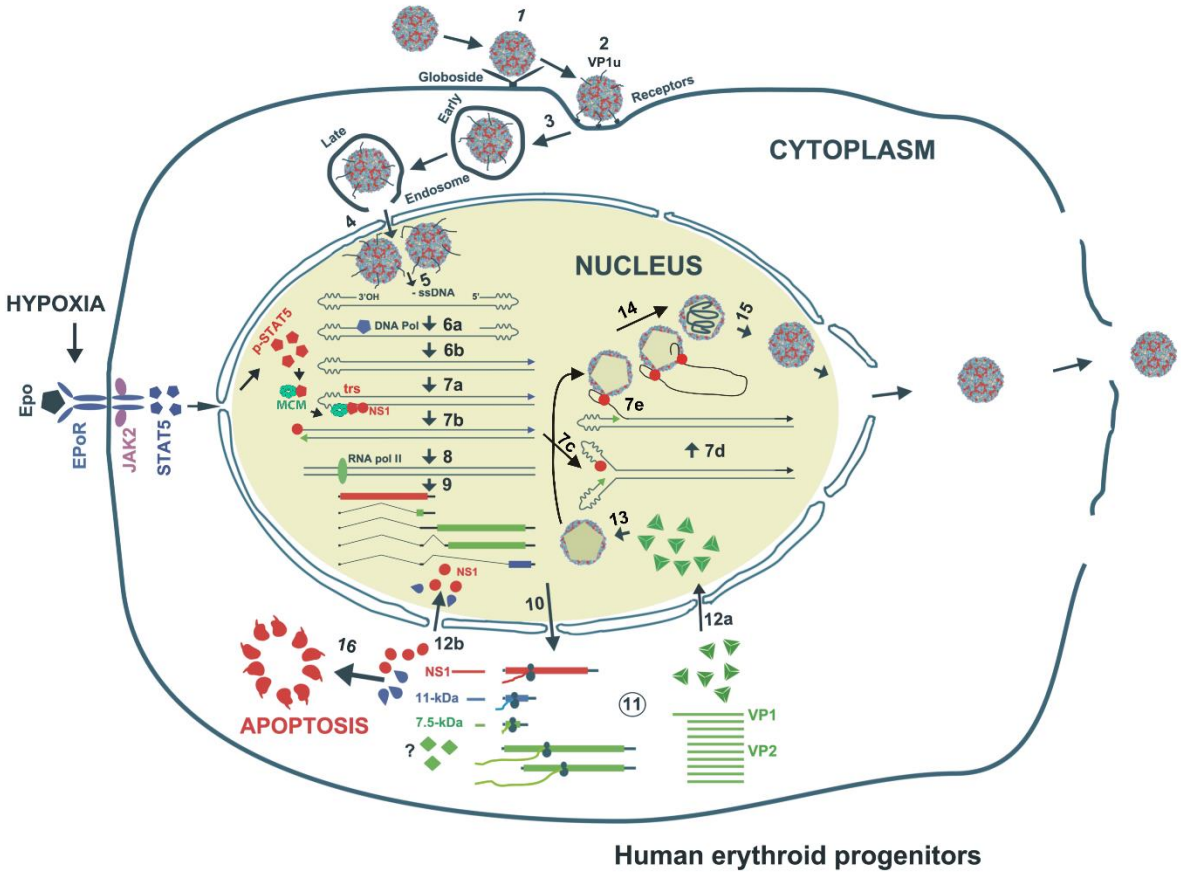
1
2
VP1u
Globoside
Receptors
Early
3
Late
Endosome
CYTOPLASM
4
5
- ssDNA
3'OH
5'
NUCLEUS
HYPOXIA
Epo
EPoR
JAK2
STAT5
p-STAT5
MCM
trs
NS1
DNA Pol
6a
6b
7a
7b
RNA pol II
8
9
14
15
7e
7c
7d
13
10
12a
16
12b
NS1
11-kDa
7.5-kDa
?
APOPTOSIS
11
VP1
VP2
Human erythroid progenitors

Fig 1-2

Figure 1-3. A diagram of NS1 functional domains.

The N-terminus (amino acid 2-176) of NS1 possesses DNA binding and endonuclease activity. The endonuclease motif resides between amino acids 137 and 145. The central region of NS1 exhibits putative helicase activity. Transactivation activity is restricted to the C-terminus of NS1. NS1 carries two nuclear localizing signals, between amino acids 177-179 & 316-321 (NLS, in green). Three putative transactivation domains have been identified in the C-terminus of the NS1 protein: TAD1 (aa 416-424), TAD2 (aa 523-531), and TAD3 (aa 566-574). The central region also contains two NTP binding motifs between amino acids 323 to 378 and 367 to 378 (NTP binding motifs, in purple).

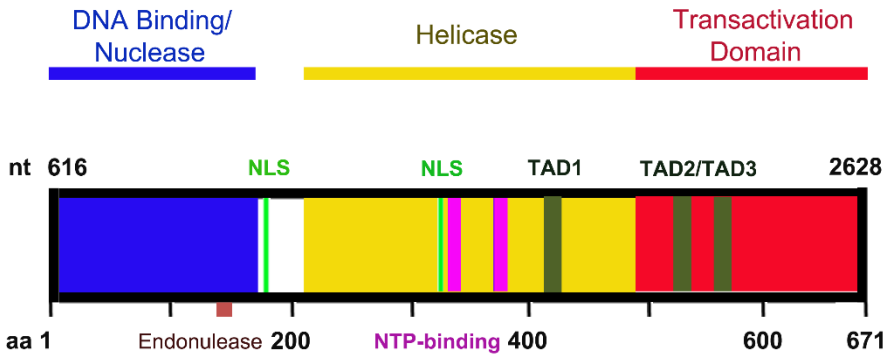
DNA Binding/
Nuclease
Helicase
Transactivation
Domain
nt 616
NLS
NLS
TAD1
TAD2/TAD3
2628
aa 1
Endonulease 200
NTP-binding 400
600
671

Fig 1-3

Figure 1-4. A diagram of the B19V minimal origin of viral DNA replication (Ori).

B19V has a 67-bp long minimum origin of DNA replication (Ori) at each end of the genome. Ori harbors two NS1 binding elements (NSBE1&2, in red), one STAT5 binding element (STAT5BE, in green), a terminal resolution site (trs, black), and two potential cellular factor binding elements (CFBE1&2). Question marks denote two unidentified host factors binding Ori.


Host factors
STAT5BE
trs
NSBE1
NSBE2
?
?
5′-AAAATTTAAAAGAAGACACCAAATCAGATGCCGCCGGTCGCCGCCGGTAGGCGGGACTTCCGGTACA-3′
3′-TTTTAAATTTTCTTCTGTGGTTTAGTCTACGGCGGCCAGCGGCGGCCATCCGCCCTGAAGGCCATGT-5′
5214
5232
5280

Fig 1-4

Figure 5. NS1 is a multi-functional protein.

The B19V NS1 multimer binds the dsDNA form of the genome at NSBE1-2 via N-terminus region (5-7), but nicks ssDNA at trs and covalently attaches to the 5’ end. NS1 induces a DNA damage response that is essential for virus replication. The virus replication process leads to the activation of ATR, ATM and DNA-PKcs. However, the activation of ATR and DNA-PKcs, but not ATM, is essential for virus replication. NS1 transactivates its P6 promoter with the assistance of Sp1/Sp3. NS1 is a global transactivator and regulates ~1,700 genes. NS1 induces apoptosis through the activation of caspases 2/6/8 and TNF-α. The central region of NS1 protein exhibits putative helicase activity.

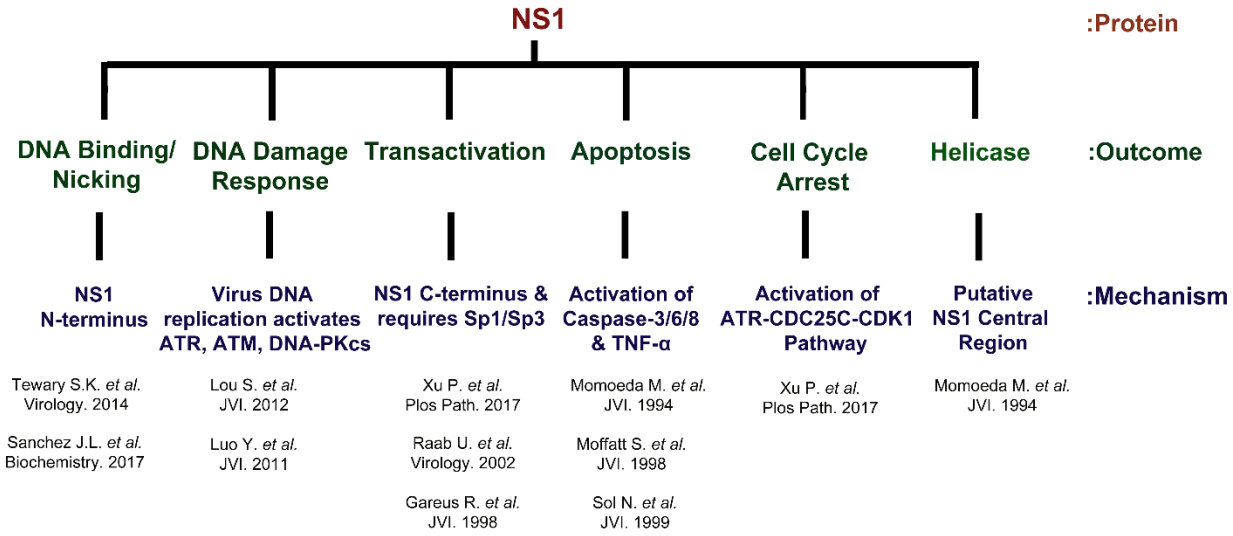
NS1
:Protein
DNA Binding/ Nicking
DNA Damage Response
Transactivation
Apoptosis
Cell Cycle Arrest
Helicase
:Outcome
NS1 N-terminus
Virus DNA replication activates ATR, ATM, DNA-PKcs
NS1 C-terminus & requires Sp1/Sp3
Activation of Caspase-3/6/8 & TNF-α
Activation of ATR-CDC25C-CDK1 Pathway
Putative NS1 Central Region
:Mechanism
Tewary S.K. et al. Virology. 2014
Sanchez J.L. et al. Biochemistry. 2017
Lou S. et al. JVI. 2012
Luo Y. et al. JVI. 2011
Xu P. et al. Plos Path. 2017
Raab U. et al. Virology. 2002
Gareus R. et al. JVI. 1998
Momoeda M. et al. JVI. 1994
Moffatt S. et al. JVI. 1998
Sol N. et al. JVI. 1999
Xu P. et al. Plos Path. 2017
Momoeda M. et al. JVI. 1994

Fig 1-5

Chapter 2:

Phosphorylated STAT5 Directly Facilitates Parvovirus B19 DNA Replication in Human Erythroid Progenitors through Interaction with the MCM Complex[2]

[2] The chapter has been previously published in PLOS Pathogens: Ganaie, S. S., Zou, W., Xu, P., Deng, X., Kleiboeker, S., and Qiu, J. (2017) Phosphorylated STAT5 directly facilitates parvovirus B19 DNA replication in human erythroid progenitors through interaction with the MCM complex. 13, e1006370. https://doi.org/10.1371/journal.ppat.1006370.

Abstract

Productive infection of human parvovirus B19 (B19V) exhibits high tropism for burst forming unit erythroid (BFU-E) and colony forming unit erythroid (CFU-E) progenitor cells in human bone marrow and fetal liver. This exclusive restriction of the virus replication to human erythroid progenitor cells is partly due to the intracellular factors that are essential for viral DNA replication, including erythropoietin signaling. Efficient B19V replication also requires hypoxic conditions, which upregulate the signal transducer and activator of transcription 5 (STAT5) pathway, and phosphorylated STAT5 is essential for virus replication. In this study, our results revealed direct involvement of STAT5 in B19V DNA replication. Consensus STAT5-binding element was identified adjacent to the NS1-binding element within the minimal origins of viral DNA replication in the B19V genome. Phosphorylated STAT5 specifically interacted with viral DNA replication origins both *in vivo* and *in vitro*, and was actively recruited within the viral DNA replication centers. Notably, STAT5 interacted with minichromosome maintenance (MCM) complex, suggesting that STAT5 directly facilitates viral DNA replication by recruiting the helicase complex of the cellular DNA replication machinery to viral DNA replication centers. The FDA-approved drug pimozide dephosphorylates STAT5, and it inhibited B19V replication in *ex vivo* expanded human erythroid progenitors. Our results demonstrated that pimozide could be a promising antiviral drug for treatment of B19V-related diseases.

Introduction

Human parvovirus B19 is a small, non-enveloped parvovirus with a single-stranded (ss) DNA genome of 5.6 kb. It belongs to the genus *Erythroparvovirus* of the *Parvoviridae* family (140). The B19V genome is flanked by identical inverted terminal repeats (ITRs) at both ends (141). B19V is pathogenic to humans and causes a myriad of pathologies, including fifth disease in children, transient aplastic crisis, persistent anemia in immune-compromised patients, hydrops fetalis in pregnant women, and arthropathy (1,142-145). B19V infects human erythroid progenitor cells through initial attachment to its primary receptor (P-antigen) (24) and interaction with co-receptors, resulting in virus internalization (27,31). Virus replication and assembly take place in the nuclei of infected cells. The B19V double-stranded (ds) replicative form (RF) genome expresses the large non-structural NS1 protein, two small non-structural proteins (the 11-kDa and 7.5-kDa proteins), and two capsid proteins (VP1 and VP2) (43,46,47)

B19V infects human EPCs during the late stages of maturation, particularly burst forming unit-erythroid (BFU-E) cells and colony forming unit-erythroid (CFU-E) cells (3-5,115). B19V also infects non-erythroid tissues (21-23), but the infection of these tissues is non-productive, as virus replication is not fully supported (19,21,96). Erythropoietin (EPO), a hormone secreted by renal tissue in response to hypoxia, is essential for survival, differentiation, and development of EPCs during the late maturation stages (87). In addition to the role in survivability of EPCs, EPO/EPO receptor (EPO-R) signaling is essential to B19V replication (17). EPO binding to EPO-R activates Janus kinase 2 (JAK2)-signal transducer and activator of transcription 5 (STAT5), phosphoinositide 3-kinase (PI3K), and extracellular signal-regulated kinase (ERK) pathways. The JAK2-STAT5 pathway positively regulates B19V replication, the ERK pathway negatively regulates B19V replication, and the PI3K pathway is dispensable to B19V replication

(18) . Expression of STAT5A is upregulated during hypoxia, and replication of B19V in human EPCs is facilitated by hypoxic conditions (18). JAK2 predominantly phosphorylates STAT5A in the cells of erythroid lineage (89), and thus STAT5A is largely involved in facilitating B19V replication of EPCs under hypoxic conditions (18). The disease outcomes of hematological disorders caused by B19V infections result from the death of infected human EPCs. B19V infection inhibits erythropoiesis by inducing cell-cycle arrest (57,60,70), and eventually results in apoptosis (65,71,116,146).

The results of this study confirmed that phosphorylation of STAT5 is essential for B19V DNA replication. Mechanistically, the B19V RF DNA genome harbors STAT5-binding element (STAT5BE) within the minimal origins of DNA replication (*Ori*), located to the ITRs at each end of the viral genome. The binding site specifically binds phosphorylated STAT5 (pSTAT5). Moreover, our experiments revealed a novel interaction between STAT5 and minichromosome maintenance (MCM) complex; B19V exploits this interaction to recruit MCM complex to the viral replication centers for initiation of B19V DNA replication.

Materials and Methods

Ethics statement.

We purchased $CD34^+$ hematopoietic stem cells, which were isolated from bone marrow of a healthy human donor, from AllCells LLC (Alameda, CA) without any identification information on the cells, and, therefore, an institutional review board (IRB) review was waived.

Primary cells and cell lines.

Primary human $CD36^+$ EPCs were expanded *ex vivo* from $CD34^+$ hematopoietic stem cells as previously described (17,18,147). Briefly, hematopoietic $CD34^+$ stem cells, purchased from AllCells, LLC (Alameda, CA), were grown in Wong medium under normoxia up to Day 4 and frozen in liquid nitrogen (18). In each experiment, Day 4 cells were thawed and grown under normoxia in an atmosphere containing 5% CO_2 and 21% O_2 at 37ºC for 2-3 days, prior to incubation under hypoxia at 5% CO_2 and 1% O_2.

The megakaryoblastoid cell line, UT7/Epo-S1, was cultured in Dulbecco's modified Eagle's medium with 10% fetal bovine serum and 2 U/ml of EPO (Amgen, Thousand Oaks, CA) in 5% CO_2 and 21% O_2 at 37ºC (14,77). A UT7/Epo-S1 cell line expressing B19V NS1 protein (NS1-S1) was cultured under the same conditions, except that 5 µg/ml doxycycline was used to induce NS1 expression when needed (70).

Virus and infection.

Plasma samples containing B19V at ~1×10^{12} viral genomic copies per ml (vgc/ml) were obtained from ViraCor Eurofins Laboratories (Lee's Summit, MO). After 2 days of hypoxia, $CD36^+$ EPCs were infected with B19V at a multiplicity of infection (MOI) of ~1,000 vgc per cell. At 48 h post-infection, the infected cells were analyzed.

Chemical inhibitors.

STAT5-SH2 Inhibitor (STAT5-SH2i, CAS 285986-31-4; catalog number (cat#) 573108), a cell-permeable compound that selectively targets the SH2 domain of STAT5 (148), and STAT5 Inhibitor III, pimozide (CAS 2062-78-4, cat# 573110), which dephosphorylates STAT5 (149), were purchased from EMD Millipore (Billerica, MA). Both chemicals were dissolved in DMSO to produce stock solutions (at 100mM) that were kept at -80 ºC.

Proximity ligation assay.

Duo link In-Situ Red Mouse/Rabbit kit (cat# DUO92101) was purchased from MilliporeSigma (St Louis, MO). Proximity ligation assay was performed following the manufacturer's instructions, as described previously (150).

Immunofluorescence assay and confocal imaging.

Immunofluorescence assay was carried out as described previously (18,68). Briefly, infected EPCs were deposited on slides by cytospinning, fixed with 3.7% paraformaldehyde for 30 min, and permeabilized with phosphate-buffered saline (PBS, pH7.2) containing 0.5% Triton X-100 (PBS-T) for 5 min at room temperature. Non-specific interactions were blocked with 3% bovine serum albumin (BSA) before subsequent incubation with primary and fluorescence-labelled secondary antibodies. The slides were visualized with a Nikon confocal microscope, and images were taken at 100 × magnification.

Plasmid construction.

pM20 contains the full-length B19V replicative from (RF) genome (nt 1-5596), and pN8 contains a half-ITR deleted B19 RF genome (nt 199-5410) (77,151). They are diagramed in **Fig 2-2A**. pN8^{mOriL} and pN8^{mOriR} were constructed by mutating the STAT5BE of the *Ori* in the left and right half ITRs of the pN8, respectively. Both STAT5BE were mutated in pM20 and pN8

resulted in $pM20^{mOri}$ and $pN8^{mOri}$, respectively, which are diagramed with *mOri* shown, and the sequence of mutated *Ori* in the half right ITR is depicted (**Fig 2-6A**).

Transfection.

UT7/Epo-S1 cells were electroporated in V solution using Amaxa Nucleofector (Lonza, Basel, Switzerland), as described previously (18). Briefly, B19V infectious clone pM20 or mutants were enzymatically digested with *Sal* I. The linearized DNA was gel-purified. 2 μg of DNA was used for electroporation of 2×10^6 cells. After transfection, UT7/Epo-S1 cells were cultured under hypoxia of 1% O_2.

Flow cytometry and cell-cycle analysis.

B19V-infected $CD36^+$ EPCs were examined for virus infection by flow cytometry analysis with an anti-B19V capsid antibody, as described previously (18,68). For cell-cycle analysis, a bromodeoxyuridine (BrdU) incorporation assay was used, as described previously (68).

Southern blot analysis.

Lower molecular DNA (Hirt DNA) was extracted from either B19V-infected $CD36^+$ EPCs or transfected UT7/Epo-S1 cells by a Hirt extraction method, as described previously (49). Hirt DNA extracted from UT7/Epo-S1 cells was further digested with *Dpn* I to remove non-replicated plasmid DNA input. Southern blot analysis was performed as reported previously (49,60). B19V RF DNA M20 excised from pM20 with *Sal* I was used as a probe.

Phosphorylated STAT5 protein purification.

A biotinylated dsDNA probe (152), 5'-Bio-GAT ACT AGT TTC GTG GAA TCG TGG CAC TAT GAA CCA-3', containing a STAT5BE (underlined), was synthesized by IDT (Coralville, IA) and used to purify pSTAT5, following a published protocol (153) with some

modifications. Briefly, UT7/Epo-S1 cells grown in 14 dishes of 145 mm diameter were collected, washed with PBS, and resuspended in(70) Lysis Buffer-1 (10 mM HEPES, pH 7.6, 0.1 mM EDTA, 1 mM DTT, 0.5% NP-40, 10 mM KCl, 0.5 mM PMSF, and protease inhibitor cocktail (PIC, MillopreSigma) for 5 min on ice. After vortexing, the lysate was centrifuged at 500 × g for 5 min at 4ºC, and the nuclear pellet was washed with Lysis Buffer-1 without NP-40. The pellet was resuspended again in Lysis Buffer-2 (50 mM Tris, pH 7.6, 150 mM NaCl, 1 mM EDTA, 1% Triton X-100, 1 mM DTT, and 1 mM PMSF, and PIC), vortexed, and kept on ice for 30 min. The nuclear lysate was sonicated, centrifuged at 12,000 × g for 20 min, and then passed through a 0.45 µm filter before being mixed with streptavidin beads pre-bound with the biotin-dsDNA probe and incubated for several hours. The beads were then washed in Wash Buffer (50 mM Tris-HCl, pH 7.6, 150 mM NaCl, 3-4 µg/ml poly dI-dC (MilliporeSigma), 1 mM PMSF, and PIC). Bound proteins were eluted in Wash Buffer with increasing salt concentrations (0.3 – 1 M NaCl). The fractions containing pSTAT5 were identified by Western blotting.

Electrophoretic mobility shift assay (EMSA).

Electrophoretic mobility shift assay (EMSA) was performed as previously reported (154). Complementary forward and reverse oligonucleotides (synthesized at IDT, Coralville, IA) were annealed to form dsDNA probes, wt-Ori-39 and mut-Ori-39 that had the STAT5BE mutated (152) (**Fig 2-2B**). The probes were 5' end labeled with ^{32}P using [γ-^{32}P] ATP. Each 20 µl binding reaction contained 3 µg/ml of poly dI-dC (MilliporeSigma).

Chromatin immunoprecipitation (ChIP) assay.

Chromatin immunoprecipitation (ChIP) assay was performed essentially as described previously (155,156) with modifications. Cells were fixed in 1% formaldehyde for 10 min at room temperature and then quenched in 125 mM glycine. Fixed cells were washed with PBS,

and then lysed in 400 µl of Lysis Buffer (10 mM Tris-HCl, pH 8.0, 10 mM NaCl, 0.2 % NP-40, 1 mM PMSF, and PIC) and incubated for 10 min on ice. After centrifugation at 2,500 rpm for 5 min at 4ºC, the nuclear pellet was resuspended in 100 µl of Nuclear Lysis Buffer (50 mM Tris-HCl, pH 8.1,10 mM EDTA, 1% SDS, and PIC) for 10 min on ice. One ml IP Dilution Buffer (20 mM Tris-HCl, pH 8.1, 2 mM EDTA, 150 mM NaCl, 1% Triton X-100, and 0.01% SDS) was added, and chromatin was sheared by sonication at 80% power for 10 cycles of 15 s pulse and 1 min rest. Sonicated samples were centrifuged to remove debris, and the supernatant was split aliquots. Antibody (2.5 µg) was added to each aliquot, and the mixtures were incubated overnight at 4°C. For each sample, 10 µg of yeast tRNA was added to 40 µl of cold PBS-prewashed Protein A/G beads (Gold BioTechnology, Inc., St Louis, MO), and this mixture was added to the sample containing antibody and incubated with rocking for 6 h. Beads were collected by centrifugation and washed with IP Wash-1 (20 mM Tris, pH 8.1, 2 mM EDTA, 50 mM/500mM NaCl, 1% Triton X-100, 0.1% SDS) three times (first at low salt of 50 mM and then twice at 500 mM) for 10 min each at 4°C, followed by one wash with IP Wash-2 (10 mM Tris, pH 8.1, 1 mM EDTA, 0.25 M LiCl, 1% NP-40, and 1% deoxycholic acid) for 10 min at 4°C. The beads were then washed with cold TE, and protein-DNA complexes were eluted twice using 200 µl of Elution Buffer (100 mM sodium bicarbonate and 1% SDS) for 10 min at room temperature. Crosslinking was reversed by addition of 16 µl of 5 M NaCl and incubation at 65°C. DNA was purified with a Qiagen PCR purification kit (Qiagen, Hilden, Germany), and ChIP product was recovered in 50 µl of H_2O, and used for PCR or quantitative PCR (qPCR) analysis.

PCR or qPCR analysis.

Immunoprecipitated viral DNA from ChIP assay was subjected to PCR analysis using either F1 and R1 or F1 and R2 primers spanning the viral origin region: F1 (nt 5036-5053), 5’-

CCT GCC CCC TCC TAT ACC-3', R1 (nt 5308-5285), 5'-CAG GAA ATG ACG TAA TTG TCC GCC-3', and R2 (nt 5393-5376), 5'-ACG TCA ACC CCA AGC GCT-3'. q-PCR analysis was done as described previously (17), using the following primers: F (nt 353-378), 5'-GCA TCT GAT TTG GTG TCT TCT TTT AA-3', R (421-403), 5'-TGG CTG CCC ATT TGC ATA A-3, and probe (nt 386-401), 5' FAM-CGG GCT TTT TTC CCG C/IABkFQ-3'.

Colony formation assay.

The colony formation assay was performed with methyl cellulose-based medium (R&D Systems, Minneapolis, MN) according to the manufacturer's instructions, with modifications**.** Briefly, $CD36^+$ EPCs were cultured in Wong expansion medium and were treated with pimozide at various concentrations on Day 7. After 48 hours, $\geq 3 \times 10^4$ cells from each well were cultured in semi-solid methyl cellulose-based medium for 10-12 days, at which time colony counts were assessed by someone who was blinded to the experimental conditions.

Immunoprecipitation assay and Western blotting.

Co-immunoprecipitation (Co-IP) assay was performed as previously described (154,157). Briefly, UT7/Epo-S1 cells were collected, washed with PBS, and lysed in radioimmunoprecipitation assay (RIPA) buffer. After centrifugation at 12,000 rpm for 20 min at 4°C, supernatant was taken and split into aliquots. Each aliquot was incubated with 3 µg of an antibody of interest overnight at 4°C, and then 40 µl of Protein A/G beads (washed with ice-cold PBS three times beforehand) was added, followed by incubation for 6 h. The beads were collected by centrifugation and washed three to five times with 1 × PBS, and then resuspended in 1 × Laemmli sample buffer. Samples were boiled for 10 min and run on 10% SDS-polyacrylamide gels for Western blot analysis, which was performed as described previously

(18,68,158). Pull-down assay was performed similarly to Co-IP, except that anti-Flag-conjugated beads or control beads were used.

Antibodies.

The following primary antibodies were purchased: mouse anti-STAT5 (cat# sc-74442), rabbit anti-STAT5 (cat# sc-835), anti-STAT5A (cat# sc-271542) and anti-STAT5B (cat# sc-1656), anti-BrdU (IIB5) (cat# sc-32323) were from Santa Cruz (Dallas, TX); anti-MCM2 (cat# 12079), and anti-pSTAT5(Y694) (cat# 4322) were from Cell Signaling (Danvers, MA); anti-STAT5a/b pan-specific antibody (cat # AF2168) and normal IgG rabbit (cat# AB-105-C) were from R&D Systems Inc (Minneapolis, MN); anti-MCM5 antibody (cat# 2380-1) was from Epitomics (Burlingame, CA); anti-B19V capsid (cat# Mab8293) was from Millipore (Billerica, MA); anti-BrdU (clone B44) was from BD (Franklin Lakes, NJ); and anti-β-actin (cat# A5441) was from Sigma; anti-MCM3 (cat# A300-124A), anti-MCM5 (cat# A300-195A; for ChIP), and MCM7(cat#A300-128A) were from Bethyl Laboratories (Montgomery, TX); anti-ATM(pS1981) (cat#ab81292) were from Abcam (Cambridge, MA); and anti-ATR(pT1989) (cat#GTX128145) from GeneTex (Irvine, CA). Rat anti-NS1 polyclonal antibody was prepared in our lab as previously reported (18).

Horseradish peroxidase (HRP)-conjugated anti-mouse and anti-rabbit secondary antibodies were purchased from Sigma, and fluorescein isothiocyanate (FITC)-, Texas Red-, and Dylight405-conjugated anti-mouse, anti-rat, and anti-rabbit secondary antibodies were all purchased from Jackson ImmunoResearch (West Grove, PA).

Statistics.

Statistical analysis was performed using GraphPad Prism Version 7.0. Statistical significance was determined by using 1-way ANOVA analysis, followed by Tukey-Kramer post-

test for comparison of three or more groups and unpaired (Student) t-test for comparison of two groups. Error bars show mean and standard deviation (Mean ± SD) unless otherwise specified

Results

Inhibition of STAT5 phosphorylation completely inhibited B19V DNA replication.

Our results previously demonstrated that pSTAT5A has a critical role in B19V infection of human EPCs cultured under hypoxic conditions (18), leading us to consider in this study whether specific inhibition of STAT5 phosphorylation affects B19V replication. This possibility was tested by treating cells with a specific inhibitor of STAT5 phosphorylation, pimozide (149). At a final concentration of 15 μM, pimozide abolished >90% of the STAT5 phosphorylation in $CD36^+$ EPCs, without altering the total expression of STAT5 (**Fig 2-1A**, lane 4). $CD36^+$ EPCs were incubated with pimozide 6 h prior to infection, and, at 48 h post-infection, numbers of B19V-infected (capsid-expressing) cells were reduced by 4.7-fold and 18.5-fold at 15 μM and 25 μM pimozide, respectively, compared with DMSO-treated cells (**Fig 2-1B**). Pimozide abolished viral DNA replication at both concentrations (**Fig 2-1C**). STAT5 dephosphorylation was confirmed in pimozide-applied infected cells (**Fig 2-1D**). These results suggested that inhibition of STAT5 phosphorylation abolishes viral DNA replication in B19V-infected $CD36^+$ EPCs. Notably, treatment with pimozide at 15 μM did not significantly inhibit cell proliferation, as assessed by the BrdU incorporation assay (**Fig 2-1E&F**).

Pimozide treatment, at a concentration as low as 10 μM, also abolished DNA replication of the B19V RF genome M20 in transfected UT7/Epo-S1 cells (**Fig 2-10A**, lane 3), and inhibited STAT5 phosphorylation (**Fig 2-10B**, lane 3). As controls, at 10 or 20 μM pimozide, cell proliferation was not significantly affected (**2-10C&D Fig**). Taken together, our results suggested that phosphorylation of STAT5 is essential for viral DNA replication.

Phosphorylated STAT5 interacts with a consensus STAT5-binding element in the B19V minimal replication origin (*Ori*).

The requirement of pSTAT5 for B19V DNA replication suggested that there might be a direct involvement of pSTAT5 in viral DNA replication. *In silico* analysis of the B19V genome demonstrated the presence of several consensus STAT5-binding elements (STAT5BEs) throughout the genome. STAT transcription factor binds a GAS or GAS-like motif with a consensus sequence of TTCN3GAA, TTCN3TAA, or TTAN3GAA (159). TTCN3TAA binds STAT5 (160) and is one of the top ten STAT5BEs identified in a genome wide analysis by ChIP-seq (161). A consensus STAT5BE is located within the previously identified 67-nt *Ori* in the B19V genome (**Fig 2-2A**) (77).

Binding of pSTAT5 from nuclear lysates of UT7/Epo-S1 cells to the STAT5BE in the *Ori* was confirmed by EMSA. A shifted band, indicating binding of protein to the probe, was observed in the presence of wild-type (wt) *Ori*-derived probe wt-Ori-39, but not the mut-Ori-39 that has the STAT5BE mutated (**Fig 2-2B**, and **Fig 2-2C**, lanes 2 vs 3). On incubation with an anti-pSTAT5 antibody, the level of shifted band was dramatically decreased (**Fig 2-2D**, lane 3). Because the EMSA was performed in the presence of excess amounts of non-specific competitor poly dI-dC, these results indicated specific binding of pSTAT5 to the B19V *Ori*.

pSTAT5 was purified from UT7/Epo-S1 cells by the use of beads conjugated with high affinity STAT5-binding DNA oligonucleotides (**Fig 2-2E**). EMSA was repeated with the purified pSTAT5, which shifted the labeled wt-Ori-39, but not the mut-Ori-39 (**Fig 2-2F**, lanes 2 vs 3). Shifting of wt-Ori-39 was abolished by addition of the STAT5-SH2 inhibitor, STAT5-SH2i, in a dose-dependent manner (**Fig 2-2G**, lanes 4-6). These binding assays confirm that pSTAT5 specifically binds to the STAT5BE of B19V *Ori in vitro*.

Phosphorylated STAT5 is associated with replicating viral DNA in the viral DNA replication centers of B19V-infected EPCs.

The association of STAT5 with B19V NS1 and the viral capsid was demonstrated by immunofluorescence assays (**Fig 2-3A&B**). STAT5 colocalized with NS1 and the viral capsid in the nucleus of B19V-infected $CD36^+$ EPCs. The association of STAT5 with viral capsid was confirmed by the observation of fluorescent foci in B19V-infected cells in a proximity ligation assay (**Fig 2-3C**), which produces an amplified signal when two labeled molecules are within 20 nm of one another (162).

Proximity ligation assay (**Fig 2-3D**) and confocal microscopy (**Fig 2-3F**) both demonstrated that STAT5 colocalized with replicating viral DNA that was pulse-labelled with BrdU in B19V-infected $CD36^+$ EPCs, which are parvovirus replication centers (163,164) as shown by proximity ligation assay using anti-BrdU and anti-capsid antibodies (**Fig. 2-3E**). Interaction of pSTAT5 with the viral genome in cells was confirmed by ChIP assays in B19V-infected $CD36^+$ EPCs and M20-transfected UT7/Epo-S1 cells. The pSTAT5-DNA complexes were pulled down with anti-pSTAT5(Y694) antibody, and bound viral *Ori* was detected by PCR. In the ChIP assay, cellular DNA was sheared to < 500 bp by sonication (**Fig 2-4A**). A specific PCR band was amplified in samples from B19V-infected or M20-transfected cells pulled down by anti-pSTAT5(Y694) (**Fig 2-4B**, lane 4). Moreover, in UT7/Epo-S1 cells transfected with the B19V RF genome (M20), we observed that application of pimozide significantly decreased the amount of the *Ori*-containing fragments of the M20, as assessed by the quantitative ChIP assay targeting *Ori* (**Fig 2-13C**, Pimozide). Thus, these results confirmed the association of pSTAT5 with B19V *Ori* in B19V-infected $CD36^+$ EPCs and M20-transfected UT7/Epo-S1 cells.

Disruption of the interaction between STAT5 and viral *Ori* inhibits viral DNA replication.

A small molecule STAT5-SH2 inhibitor (STAT5-SH2i, CAS no. 285986-31-4) specifically targets the SH2 domain of STAT5 and inhibits STAT5 binding to DNA (148). EMSA was performed to determine whether STAT5-SH2i disrupts the interaction between the STAT5 and B19V *Ori*. Incubation of either UT7/Epo-S1 nuclear lysates or purified pSTAT5 with increasing concentrations of the inhibitor showed that the STAT5-SH2i prevented formation of the STAT5-DNA formation in a dose-dependent manner (**Fig 2-5A and Fig 2-2G**). To examine the effect of the inhibitor on virus replication, $CD36^+$ EPCs were pretreated with STAT5-SH2i 6 h prior to infection with B19V. The results showed that, at a final concentration of 500 μM, the inhibitor significantly decreased the virus-infected cell population by 10.7-fold (**Fig 2-5B**), and the level of viral RF DNA by ~10-fold (**Fig 2-5C**), but not the expression level of pSTAT5 (**Fig. 2-5D**), compared with the cells with DMSO treatment. Cell proliferation was not significantly affected by this level of inhibitor in mock-infected $CD36^+$ EPCs (**Fig 2-5E&F**). The inhibition of viral DNA replication by STAT5-SH2i was also demonstrated in M20-transfected UT7/Epo-S1 cells (**Fig 2-11**), and STAT5-SH2i significantly disrupted the interaction of pSTAT5 with the *Ori* of the B19V RF genome (M20) *in vivo* as shown by a ChIP assay (**Fig 2-13C**, STAT5-SH2i).

Derivatives of B19V replicative form genome with mutated STAT5-binding elements do not replicate in UT7/Epo-S1 cells.

The effect of mutation of the STAT5BE of the viral *Ori* on replication of the B19V RF genome was determined. The viral genome has an *Ori* sequence adjacent to each ITR, and the STAT5BE was mutated in either the left ITR ($N8^{mOriL}$) or right ITR ($N8^{mOriR}$) or both ITRs ($N8^{mOri}$) of the N8 replicating RF DNA that has half ITRs at both ends, as shown in **Fig 2-6A**.

The replication capability of these mutated RF genomes was examined in UT7/Epo-S1 cells. Although the N8 RF DNA replicated well, much less replication occurred with $N8^{mOriL}$ and $N8^{mOriR}$, and no replication was observed with $N8^{mOri}$ (**Fig 2-6B**). The mutations in the STAT5BEs were then introduced into both ITRs of M20 RF genome, to make the $M20^{mOri}$ mutant. No viral DNA replication was observed in $M20^{mOri}$-transfected cells (**Fig 2-6C**, lane 2). Although both M20 and $M20^{mOri}$ RF genomes expressed NS1, viral capsid (a hallmark of B19V DNA replication (49) was present only in M20-transfected cells (**Fig 2-6D**).

pSTAT5 interacts with the MCM complex of the pre-initiation complex of cellular DNA replication.

During initiation of cellular DNA replication, the origin recognition complex (ORC) binds to autonomously replicating sequence sites and recruits cell division control protein (CDC6) and DNA replication factor CDT1 to replication origins (165). CDT1 recruits the MCM complex and primes replication initiation (166). Although viral DNA replicates independently of ORC/CDC6/CDT1, DNA viruses may require the MCM complex to initiate viral DNA replication (167). In the parvovirus adeno-associated virus (AAV), MCM complex is required for *in vitro* reconstitution of viral DNA replication (168). In the case of B19V, we previously found that MCM complex is associated with the viral DNA replication centers and has a role in B19V replication (68).

Initially, to determine whether the viral NS1 protein has a role in recruitment of the MCM complex to the viral replication origin, we performed pull-down assays using lysates from NS1-expressing UT7/Epo-S1 cells. With pull-down of NS1, MCM and pSTAT5 were not detected (**Fig 2-7A**, lane 3), but the positive control transcription factor E2F5 [which interacts with B19V NS1 (57)] was detected, which suggested that NS1 has no role in recruitment of the

MCM complex. By contrast, co-immunoprecipitation (Co-IP) with an anti-pSTAT5 antibody pulled down MCM5 protein of the MCM complex from lysates of UT7/Epo-S1 cells (**Fig 2-7B**). Similarly, Co-IP with an anti-MCM5 antibody pulled down pSTAT5, in addition to MCM2 (**Fig 2-7C**). The interaction between pSTAT5 and the MCM complex was DNA-independent, as DNase treatment of the lysate did not disrupt the interaction (**Fig 2-7D**, lane 4). Also, we show that MCM2, MCM3, MCM5 and MCM7 were associated with viral *Ori* in M20-transfected UT7/Epo-S1 cells, as confirmed by ChIP analyses **(Fig 2-13A).**

STAT5 and the MCM complex colocalized in $CD36^+$ EPCs, irrespective of whether the cells were infected (**Fig 2-7E**). An association of the MCM complex with STAT5 was confirmed in both B19V- and mock-infected cells by the proximity ligation assay (**Fig 2-7F**). This association was blocked by treatment of pimozide in $CD36^+$ EPCs (**Fig 2-7G**). Immunofluorescence detection of the viral capsid demonstrated that, following B19V infection, most of the cells were infected **(Fig 2-7H).**

pSTAT5 recruits MCM complex to B19V *Ori* to facilitate initiation of viral DNA replication.

Our demonstration that pSTAT5 interacts with viral *Ori* as well as the MCM complex suggested that B19V might exploit these interactions to initiate viral DNA replication. To test this hypothesis, we infected $CD36^+$ EPCs with B19V, and at 36 h post-infection (when B19V DNA replication was at its peak), we treated the cells with STAT5-SH2i (**Fig 2-8A**). At 6 h post-treatment, the cells were collected for ChIP assay with anti-MCM2 antibody, which showed that MCM abundance on viral *Ori* decreased significantly in the presence of STAT5-SH2i, compared with untreated control cells (**Fig 2-8B**). Results with three-color confocal imaging demonstrated that MCM2 and STAT5 colocalized in mock-infected cells (in the absence of viral NS1) (**Fig 2-**

8C, Mock). In infected cells, viral NS1 (which binds viral *Ori*) colocalized with both STAT5 and MCM, indicating that they were localized at the viral DNA replication centers (**Fig 2-8C**, B19V). These results suggested that B19V utilizes viral *Ori*-STAT5 and STAT5-MCM interactions to recruit the MCM complex to viral DNA replication origins, to initiate viral DNA replication.

Pimozide is a promising candidate for the treatment of B19V infection.

To confirm the efficacy of pimozide as a drug, we treated primary $CD36^+$ EPCs with pimozide at various concentrations, and infected them with B19V. The cells were collected 48 h post-infection for quantification of viral DNA replication (RF DNA) by Southern blot analysis, which demonstrated that the IC_{50} of pimozide for inhibition of viral DNA replication (the concentration at which 50% of viral DNA replication was inhibited) was 2.7 ± 0.69 μM (mean ± standard error) (**Fig 2-9A**). To examine the effect of pimozide on colony formation in the absence of virus infection, $CD36^+$ EPCs were incubated with pimozide at increasing concentrations on Day 7 for 2 days, and then cultured in methyl cellulose-based medium for colony formation. After 10 days, numbers of colonies were counted (**Fig 2-9B**). Pimozide only moderately reduced the numbers of colonies at higher concentrations (10-25 μM), but it did not affect the size or morphology of the colonies formed **(Fig 2-9C**).

Discussion

We have now demonstrated that STAT5 is directly involved in B19V DNA replication. Importantly, STAT5 specifically interacts with the MCM complex, the eukaryotic DNA helicase complex that is required for the formation and elongation of the cellular DNA replication fork (169). We therefore propose a novel model of B19V DNA replication in human EPCs, in which STAT5 functions as a mediator protein that brings the MCM complex to the viral DNA replication origins. Our results also identify pSTAT5 as a target for inhibition of B19V infection. In addition, as the STAT5-MCM interaction is independent of infection, we envisage an important role of this interaction in the context of cellular replication and transcription in human EPCs, which warrants further investigation.

Phosphorylated STAT5A is directly involved in B19V replication.

STAT5 is phosphorylated at a single conserved tyrosine residue (Tyr694 in STAT5A and Tyr699 in STAT5B), and these phosphotyrosine motifs, upon intermolecular interaction, enable formation of either homodimers or heterodimers of STAT5A/B (170,171). These dimers accumulate in the nucleus and bind DNA, to transactivate target genes (170). EPO-activated JAK2 phosphorylates STAT5 in human EPCs (172). We examined the relative expression of STAT5A and STAT5B in UT7/Epo-S1 and $CD36^{+}$ EPC lysates with a STAT5A/B pan-specific antibody, and found that STAT5A was predominantly expressed in both cell types (**Fig. 2-12A**). This result agrees with the observations that JAK2 kinase predominantly phosphorylates STAT5A in cells of erythroid lineage (89), and a constitutively phosphorylated STAT5A (1*6) variant enhances virus replication, whereas knockdown of *STAT5A* inhibits virus replication in B19V-infected EPCs (18).

STAT5B promotes viral DNA replication, but, during replication of human papillomavirus 16 (HPV16), STAT5B enhances viral DNA replication indirectly via regulation of *TopBP1* expression, leading to the activation of ATR kinase (173). In a proof-of-concept experiment, fusion of STAT5BEs to the DNA replication origin of polyomavirus replicon DNA improved replication efficiency in transfected mouse lymphoid BA/F3 cells, corroborating the direct role of STAT5 in viral DNA replication (174). $CD36^+$ EPCs have to be cultured in the presence of EPO for proliferation and differentiation (17), which dominantly leads activation of STAT5A (**Fig. 2-12A**) through the EPO-JAK2-STAT5 pathway (18); however, a DDR or activation of ATR is not observed in normal (uninfected) $CD36^+$ EPCs (67,70) (**Fig. 2-14A**). Furthermore, in hydroxyurea-treated $CD36^+$ EPCs, both ATR and ATM were activated; however, application of pimozide did not change the level of phosphorylated ATR or ATM (**Fig.2-14A**). As ATR activation enhances B19V replication (67), these lines of evidence suggest that pSTAT5 does not utilize the STAT5-ATR pathway to facilitate B19V replication in $CD36^+$ EPCs. Moreover, B19V infection *per se* did not affect STAT5 phosphorylation (**Fig. 2-14B**). Of note, the binding of pSTAT5 to the *Ori*, which locates in front of the B19V P6 promoter, did not obviously transactivate the P6 promoter (**Fig. 2-15**). Thus, our results provide the first evidence that an authentic virus, B19V, depends on direct binding of pSTAT5 to its replication origin (*Ori*) for viral DNA replication.

Phosphorylated STAT5 interacts with the MCM complex and recruits it to viral replication origins during DNA replication initiation.

B19V infection induces late S-phase arrest in human EPCs, and S-phase factors are fully utilized by the virus to replicate its genome (68). During cellular DNA replication, ORC-CDC6-CDT1 binding to the replication origin is a priming event that takes place in G1-phase (169).

Furthermore, CDT1 recruits the MCM complex and subsequently the whole replisome via formation of the MCM-CDC45 complex (169). Notably, no such priming takes place during S-phase, so that chromosomes are not replicated multiple times (165). However, viruses have evolved different mechanisms to initiate viral DNA replication. For examples, SV40 has the large T antigen that binds SV40 DNA replication origin and has helicase activity, and also recruits the replication machinery by interacting with DNA replication factors, such as replication factor A, DNA polymerase α and topoisomerase I (175). Parvoviruses use the large non-structural protein NS1, which binds directly to the viral origin and has helicase and nickase activities that facilitate viral DNA replication (176). In parvovirus AAV, the MCM complex is essential to AAV2 DNA replication *in vitro* (168)**,** and is probably recruited by interaction with Rep78, the large viral non-structural protein (177).

In the case of B19V, the MCM complex is localized to the viral DNA replication centers and is required for viral DNA replication (68). However, we did not observe any interaction between the B19V NS1 protein and the MCM complex, suggesting that the complex is recruited to the viral DNA replication centers by an alternative mechanism. Here, our results provided evidence that STAT5 interacts with the MCM complex in human EPCs, without involvement of viral or cellular DNA. These cells express STAT5A more abundantly than STAT5B (**Fig. 2-12A**), but both STAT5A and STAT5B proteins interact with the MCM complex (**Fig. 2-12C**).

During B19V infection, STAT5 is recruited to the viral DNA replication origin by direct interaction with STAT5BEs in the *Ori* sequences of the viral genome, thereby bringing the MCM complex to the viral *Ori*. Outside of the *Ori*, there are additional 6 putative STAT5BEs, and we tested that two of them in the capsid proteins-coding region also bound pSTAT5 (**Fig. 2-13D**). Since there is no putative terminal resolution site (trs) and NS1-binding sites outside of the

Ori, we speculate that these STAT5BEs outside of the *Ori* do not contribute to B19V DNA replication. We hypothesize that MCM complex recruited by pSTAT5 at *Ori* may contribute to virus replication through its helicase activity or the recruitment of other DNA replication factors to the viral origin (169). Notably, PIF (parvovirus initiation factor), a member of the KDWK family of transcription factors, has been shown to bind two adjacent "ACGT" motifs in front of the NS1 binding site of left-hand replication origin ($OriL_{TC}$) of the *Protoparvoviurs* minute virus of mice (MVM) (178,179). PIF stabilizes the binding of NS1 to the *Ori*, which is critical for the activation of NS1 nickase (180). In B19V, at least in an *in vitro* nicking assay, B19V NS1 is sufficient to cleave the *Ori* (62). However, whether the binding of STAT5 to B19V *Ori* or the recruited MCM complex also involves in NS1 nickase activity of the *Ori* at trs (**Fig 2-2A**) warrants further investigation.

Pimozide, an FDA-approved drug, shows promise for the treatment of B19V infection.

To date, no specific treatment (either anti-viral or vaccine-based) exists for B19V infection. We have now demonstrated that pimozide, an FDA-approved anti-psychotic drug that is used in the treatment of a wide range of diseases (181) and could be potentially used to treat chronic myeloid leukemia, in which it specifically targets cancer cells, without affecting $CD34^+$ hematopoietic stem cells (149). Pimozide specifically inhibits STAT5 phosphorylation without affecting JAK2 activation or JAK2-derived signaling pathways; however, the underlying mechanism is unknown yet (182). The pSTAT5 is presumably required for recruitment of the MCM complex to the viral *Ori*, and facilitates B19V replication in human EPCs. Pimozide is a potent inhibitor of B19V replication, with an IC_{50} of ~2.7 μM. At 15 μM, pimozide does not have a significant effect on proliferation of human EPCs expanded *ex vivo*, and has only moderate effect (~15% reduction) on colony formation of EPCs. As STAT5A phosphorylation

plays a key in B19V replication in human EPCs under hypoxic conditions (18), these lines of evidence suggest that the inhibition of B19V replication in $CD36^{+}$ EPCs is not a side-effect of the pimozide. Antivirals such as cidofovir and ribavirin are used in the treatment of adenovirus infection, and have IC_{50} values of 15 μM for cidofovir and 25 μM for ribavirin (183). Importantly, when we applied both pimozide and STAT5-SH2i (at 15 and 250 μM, respectively), a significant synergistic inhibition of B19V infection was observed (**Fig. 2-16**). Therefore, we expect that a clinical trial should be conducted to examine pimozide as a treatment for B19V infection of patients with sickle-cell disease and immunocompromised patients and as anti-viral prophylaxis of transplant recipients.

Fig 2-1. Pimozide abolishes B19V replication in primary CD36$^+$ erythroid progenitor cells (EPCs).

(A) Inhibition of phosphorylation of STAT5 by pimozide. CD36$^+$ EPCs were treated with dimethyl sulfoxide (DMSO) vehicle or pimozide at various concentrations. At 48 h post-treatment, cells were collected, washed and lysed for Western blotting with detection of pSTAT5 by anti-pSTAT5(Y694) antibody. The blot was reprobed for total STAT5 using a mouse anti-STAT5 antibody and for β-actin as a loading control. **(B-D)** Inhibition of B19V DNA replication by pimozide. CD36$^+$ EPCs were pre-incubated with DMSO or pimozide at a final concentration of 15 μM or 25 μM 6 h prior to B19V infection. At 48 h post-infection, cells were subjected to **(B)** flow cytometry analysis for the B19V-infected cell population with an anti-B19V capsid antibody, **(C)** Hirt DNA extraction, followed by Southern blot analysis with a B19V M20 DNA probe, or **(D)** Western blotting with an anti-pSTAT5(Y694) antibody, and reprobing with an anti-β-actin antibody. (E&F) Evaluation of the effect of pimozide on cell proliferation. CD36$^+$ EPCs were treated with either DMSO or pimozide (15 μM or 25 μM). After 48 h, treated cells were incubated with bromodeoxyuridine (BrdU) for 1 h to analyze cell-cycle progression by a BrdU incorporation assay. **(E)** Results of a representative cell-cycle analysis experiment. **(F)** Relative fold change in the S phase cell population of each group is shown, with means and standard deviations of three independent experiments. P values are calculated using one-way and Tukey-Kramer post-test, compared with DMSO control. * denotes $P<0.05$; **** denotes $P<0.0001$; and n.s. ($P>0.05$) denotes no statistical significance.

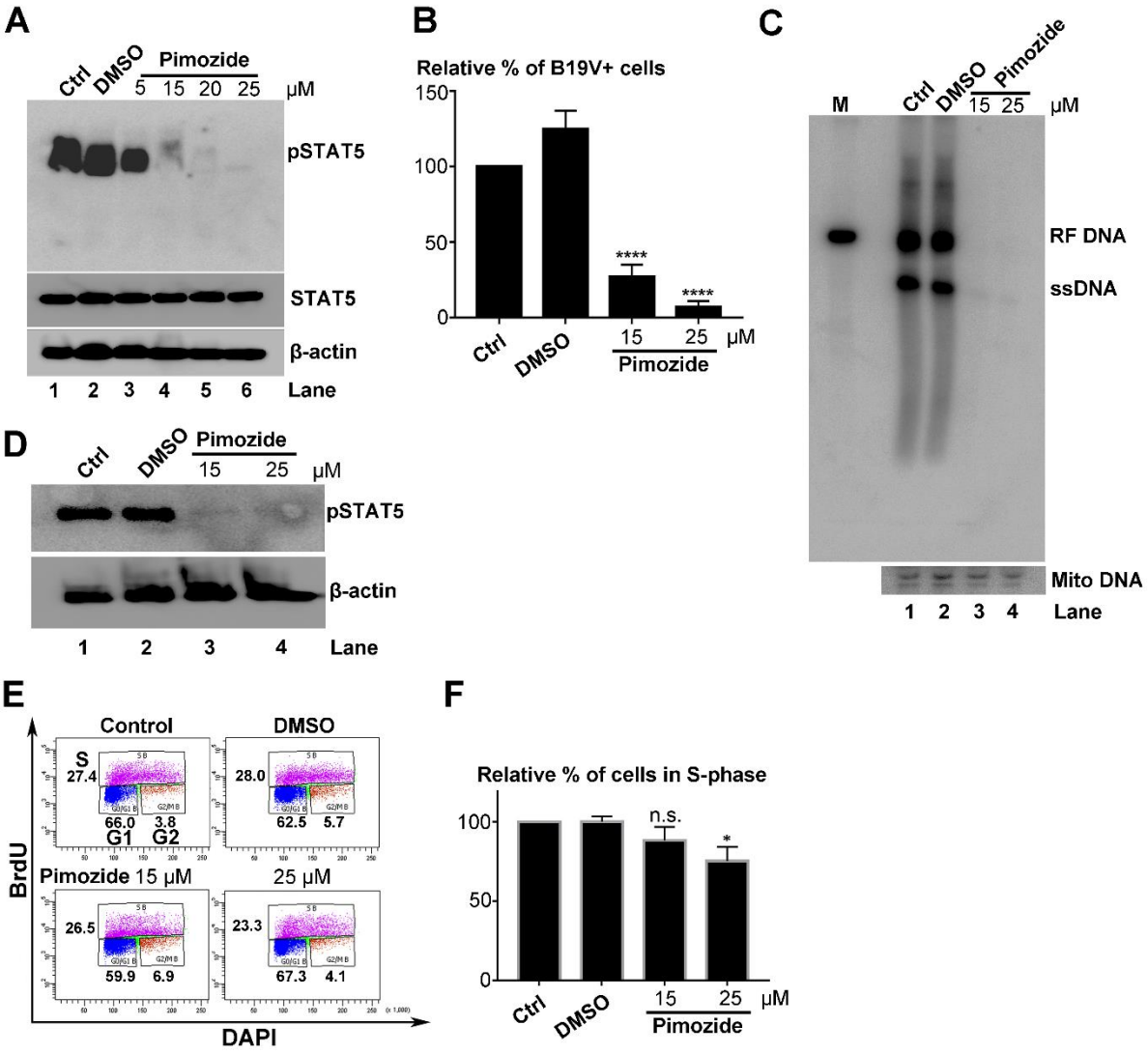
A
Ctrl
DMSO
Pimozide
5 15 20 25 μM
pSTAT5
STAT5
β-actin
1 2 3 4 5 6 Lane
B
Relative % of B19V+ cells
150
100
50
0
****
****
Ctrl
DMSO
15 25 μM
Pimozide
C
M
Ctrl
DMSO
Pimozide
15 25 μM
RF DNA
ssDNA
Mito DNA
1 2 3 4 Lane
D
Ctrl
DMSO
Pimozide
15 25 μM
pSTAT5
β-actin
1 2 3 4 Lane
E
Control
DMSO
S
27.4
66.0
G1
3.8
G2
28.0
62.5
5.7
Pimozide 15 μM
25 μM
26.5
59.9
6.9
23.3
67.3
4.1
BrdU
DAPI
F
Relative % of cells in S-phase
100
50
0
n.s.
*
Ctrl
DMSO
15 25 μM
Pimozide

Fig 2-1

Fig 2-2. STAT5 interacts with B19V replication origins (*Ori*) *in vitro*.

(A) Diagram of the B19V ssDNA and replicative form (RF) DNA genome. B19V genomes of the single-stranded (ss) DNA form and full-length replicative form (RF) are depicted, along with the sequence of viral *Ori* that contains a consensus STAT5-binding element (STAT5BE), terminal resolution site (trs), two NS1-binding elements (NSBE1 and NSBE2), and two putative cellular factor-binding elements (CFBE) (58,62,77). (B) Probes used in electrophoretic mobility shift assay (EMSA). Sequences of two 39-nt probes, wt-Ori-39 and mut-Ori-39, are shown with the consensus STAT5BE and the mutated STAT5BE (mSTAT5BE) highlighted. **(C&D)** EMSA. **(C)** ^{32}P-labeled *Ori* probes wt-Ori-39 (lane 2) and mut-Ori-39 (lane 3) were incubated with UT7/Epo-S1 nuclear lysate (NL) in the presence of non-specific competitor poly dI-dC. Products were subjected to non-denaturing 5% polyacrylamide gel electrophoresis (PAGE). Gels were dried and exposed to a phosphor screen. **(D)** Similarly, EMSA was performed with ^{32}P-labeled wt-*Ori* probes and 5 μg of NL in the presence of 5 μg of anti-pSTAT5(Y694) or IgG control antibody. **(E)** PAGE analysis of purified pSTAT5. 20 μl of pSTAT5 was analyzed by SDS-10% PAGE. Gels were either stained with Coomassie **b**rilliant blue (left panel/CBB staining), or transferred to a PVDF membrane for Western blotting with an anti-pSTAT5(Y694) antibody (right panel/Western blot). **(F&G)** EMSA with purified pSTAT5. **(F)** ^{32}P-labeled wt-Ori-39 (lane 2) and mut-Ori-39 (lane 3) probes were incubated with purified pSTAT5 in the presence of poly dI-dC. Samples were run on 5% non-denaturing PAGE, dried, and exposed to a phosphor screen. **(G)** EMSA with wt-Ori-39 in the absence (lanes 2&3) or presence of STAT5-SH2i at 0.3 mM (lane 4), 0.5 mM (lane 5), and 0.8 mM (lane 6). Lane 1, wt-Ori-39 probe only.

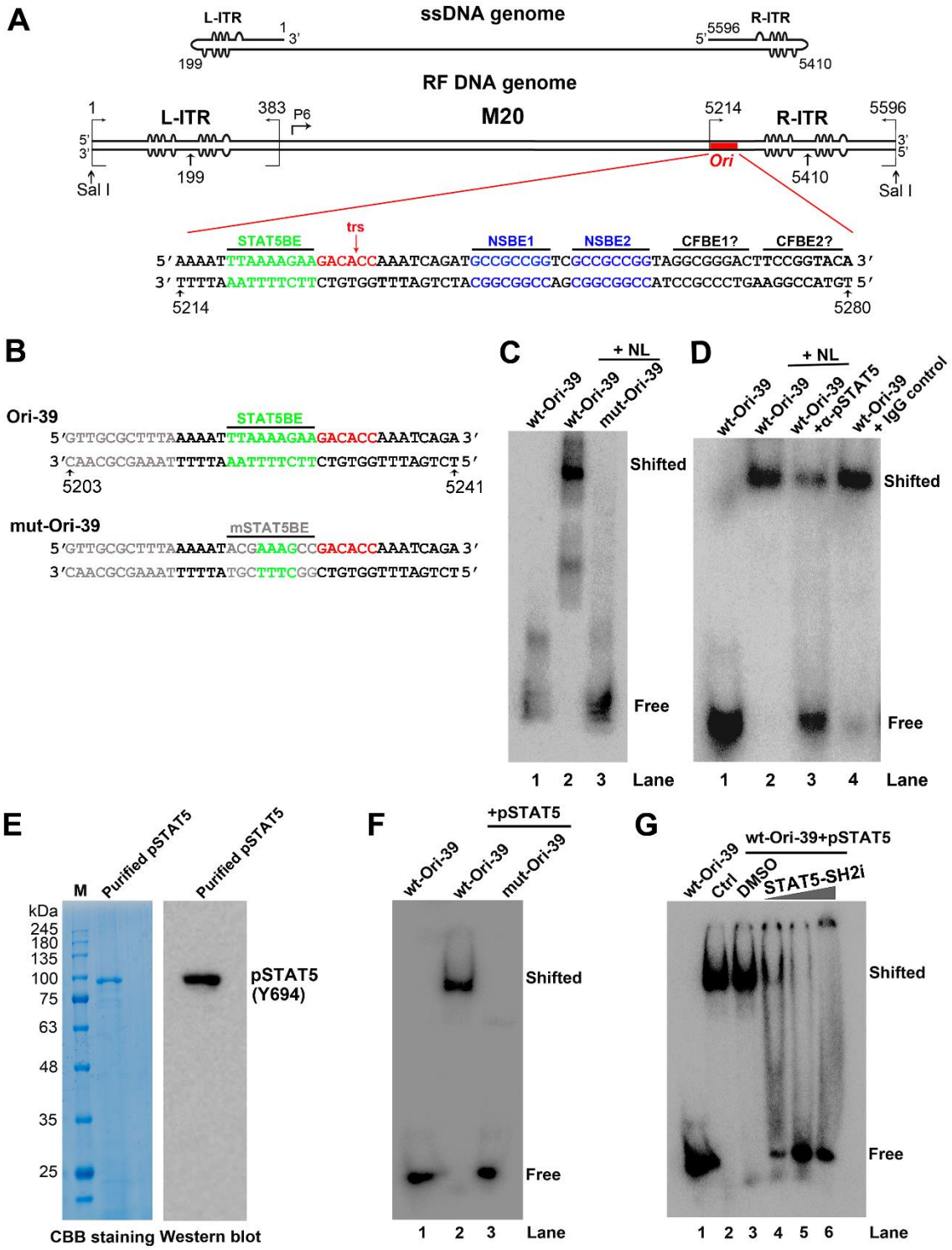
A
L-ITR
ssDNA genome
R-ITR
RF DNA genome
M20
Ori
Sal I
STAT5BE
trs
NSBE1
NSBE2
CFBE1?
CFBE2?
B
Ori-39
mut-Ori-39
mSTAT5BE
C
+ NL
wt-Ori-39
mut-Ori-39
Shifted
Free
Lane
D
+α-pSTAT5
+ IgG control
E
M
Purified pSTAT5
kDa
pSTAT5 (Y694)
CBB staining Western blot
F
+pSTAT5
G
wt-Ori-39+pSTAT5
Ctrl
DMSO
STAT5-SH2i

Fig 2-2

Fig 2-3. STAT5 colocalizes with B19V NS1, capsids, and the replicating B19V genome.

(A&B) STAT5 colocalizes with B19V NS1 and capsids. Mock- or B19V-infected $CD36^+$ EPCs were co-stained and examined with rabbit anti-STAT5 and rat anti-B19V NS1 antibodies **(A)** or with rabbit anti-STAT5 and mouse anti-B19V capsid antibodies **(B)**. (C-E) Proximity ligation assay. Infected cells were co-stained with rabbit anti-STAT5 and mouse anti-B19V capsid antibodies **(C)**, or co-stained with rabbit anti-STAT5 and mouse anti-BrdU antibodies **(D)**, or co-stained with mouse anti-B19V capsid and rabbit anti-BrdU antibodies **(E)**, followed by a proximity ligation assay, which produces amplified signal for labeled molecules in close proximity. **(F)** STAT5 colocalizes with the replicating viral genome. Mock- or B19V-infected $CD36^+$ EPCs were BrdU labeled to identify replicating viral ssDNA genomes. The treated cells were co-stained with rabbit anti-STAT5 and mouse anti-BrdU antibodies, followed by incubation with secondary antibodies. Images were taken with an Eclipse C1 Plus (Nikon) confocal microscope at 100 × magnification. Nuclei were stained with DAPI.

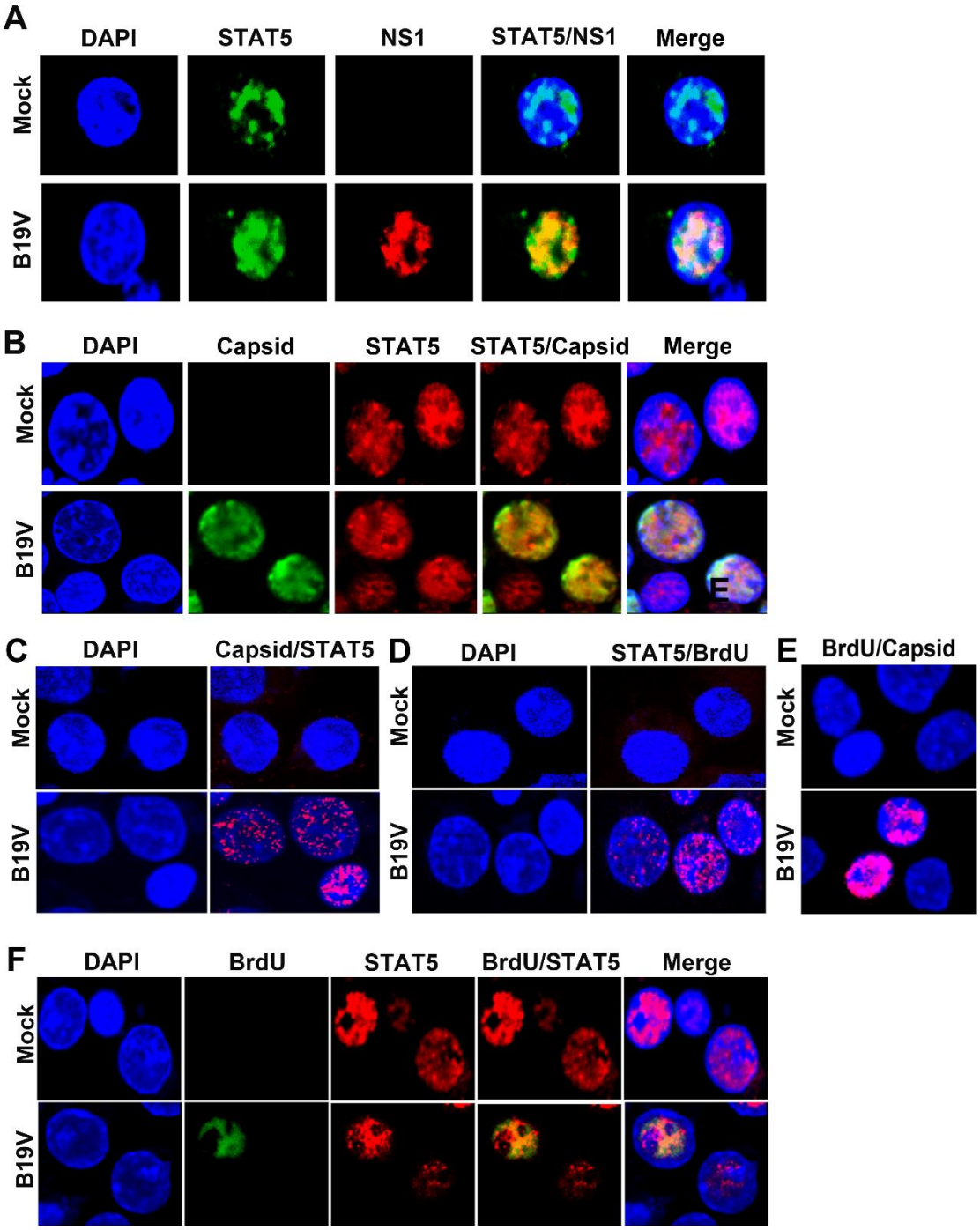
A
DAPI
STAT5
NS1
STAT5/NS1
Merge
Mock
B19V
B
DAPI
Capsid
STAT5
STAT5/Capsid
Merge
Mock
B19V
C
DAPI
Capsid/STAT5
Mock
B19V
D
DAPI
STAT5/BrdU
Mock
B19V
E
BrdU/Capsid
Mock
B19V
F
DAPI
BrdU
STAT5
BrdU/STAT5
Merge
Mock
B19V

Fig 2-3

Fig 2-4. Chromatin immunoprecipitation (ChIP) assay.

ChIP assay was performed using either infected $CD36^+$ EPCs or transfected UT7/Epo-S1 cells, as indicated. **(A)** Crosslinked chromatin was sheared by sonication to sizes of ~500 bp. **(B)** An anti-pSTAT5(Y694) antibody or negative control IgG was used to pull down DNA-protein complexes. Recovered DNA from UT7/Epo-S1 cells or $CD36^+$ EPCs was examined for viral DNA by PCR with primer sets of F1/R1 and F1/R2, respectively, which span the *Ori* sequences of the B19V genome. pM20 plasmid was used as a template for positive controls of PCR. **(C)** A diagram of the *Ori*-targeting PCR. The primers used for PCR are shown.

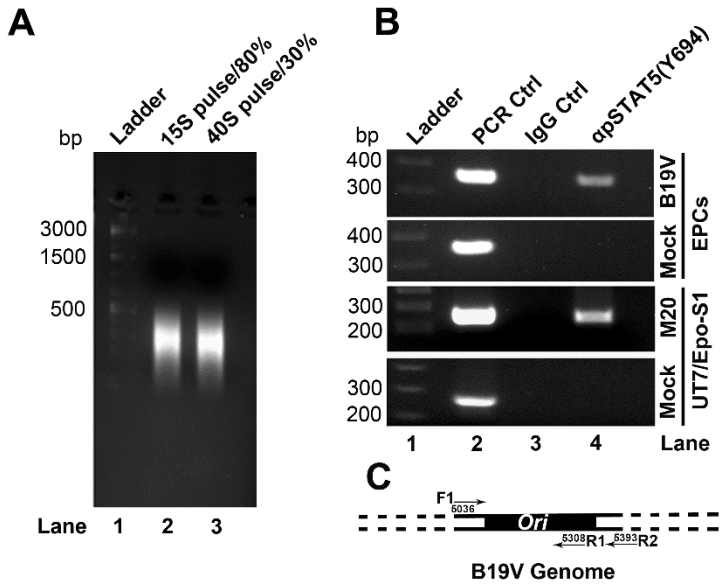
A
bp
Ladder
15S pulse/80%
40S pulse/30%
3000
1500
500
Lane 1 2 3
B
bp
Ladder
PCR Ctrl
IgG Ctrl
qpSTAT5(Y694)
400
300
400
300
300
200
300
200
B19V
Mock
EPCs
M20
Mock
UT7/Epo-S1
1 2 3 4 Lane
C
F1
5036
Ori
5308R1
5393R2
B19V Genome

Fig 2-4

Fig 2-5. Blockage of interaction between STAT5 and B19V *Ori* DNA inhibits B19V replication.

(A) STAT5-SH2 inhibitor (STAT5-SH2i) abolishes the shift of viral *Ori* in EMSA. UT7/Epo-S1 nuclear lysate (NL) was incubated with ^{32}P-labelled wt-Ori-39 probe (lanes 2-5) with the addition of DMSO (lane 3) or STAT5-SH2i at 0.4 mM (lane 4) and 0.8 mM (lane 5). **(B&D)** STAT5-SH2i significantly inhibits viral DNA replication. $CD36^+$ EPCs were incubated with either DMSO or STAT5-SH2i (250 μM or 500 μM), 6 h prior to infection. At 48 h post-infection, cells were collected and subjected either to **(B)** flow cytometry analysis for the B19V-infected (B19V+) cell population, with an anti-capsid antibody, or to **(C)** Hirt DNA extraction for Southern blot analysis with a B19V M20 DNA probe (upper panel), with mitochondrial DNA (Mito DNA) probed as a loading control (lower panel), or to **(D)** protein extraction for Western blotting with anti-pSTAT5 and anti-β-actin. **(E&F)** Effect of STAT5-SH2i on cell proliferation. $CD36^+$ EPCs were treated with either DMSO or STAT5-SH2i (250 μM or 500 μM), and were then incubated with BrdU to perform BrdU incorporation assays. **(E)** Results of a representative cell-cycle analysis. **(F)** Relative fold changes in the S-phase cell population of each group shown with means and standard deviations of three independent experiments. P values are calculated using one-way ANOVA and Tukey-Kramer post-test ($P>0.05$), compared with DMSO control. **** denotes $P<0.0001$, ** $P<0.01$, and n.s. no statistical significance.

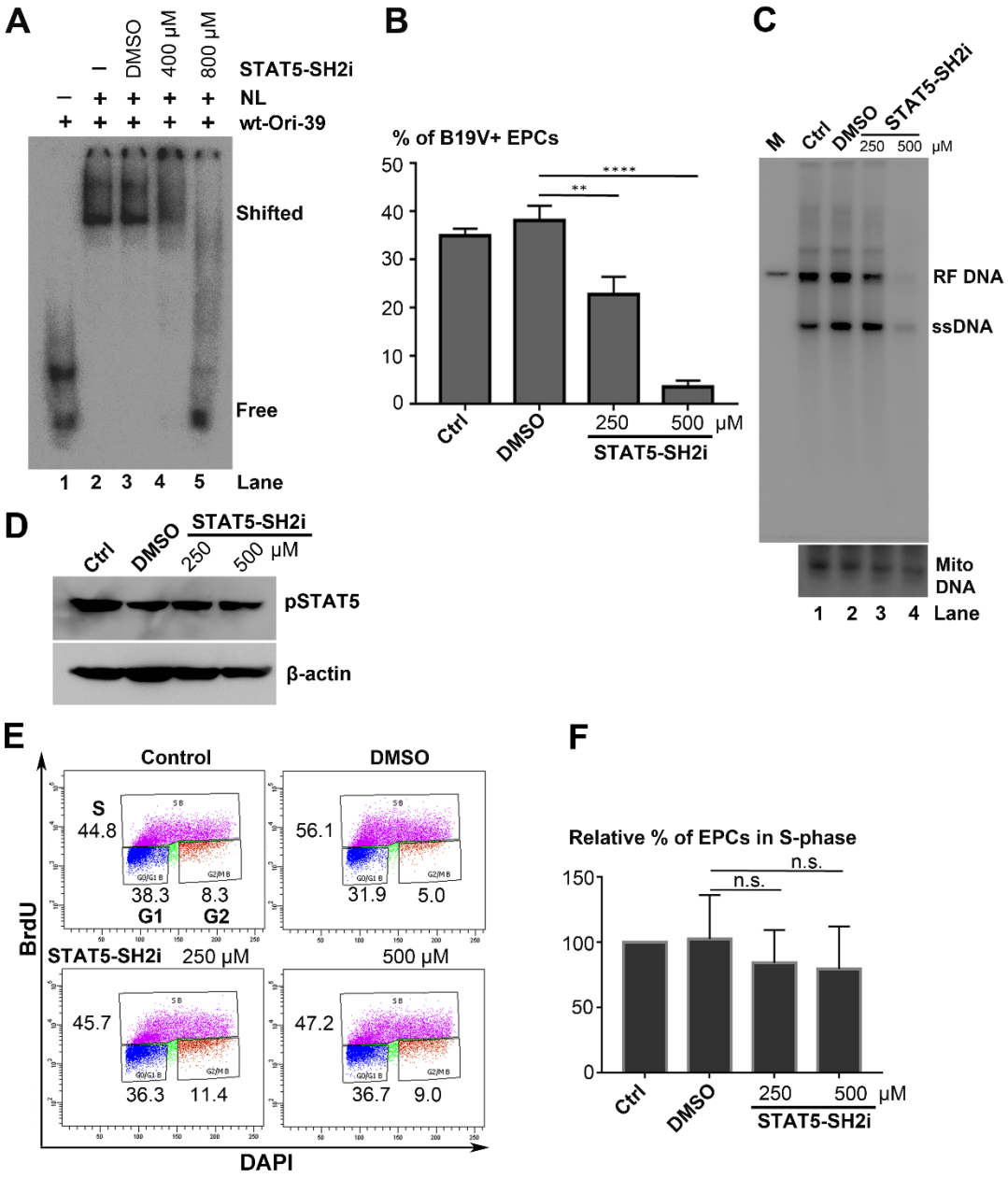
A
STAT5-SH2i
NL
wt-Ori-39
DMSO
400 μM
800 μM
Shifted
Free
1 2 3 4 5 Lane
B
% of B19V+ EPCs
****
**
Ctrl
DMSO
250
500 μM
STAT5-SH2i
C
M
Ctrl
DMSO
STAT5-SH2i
250 500 μM
RF DNA
ssDNA
Mito DNA
1 2 3 4 Lane
D
Ctrl
DMSO
STAT5-SH2i
250
500 μM
pSTAT5
β-actin
E
Control
DMSO
S
44.8
38.3
G1
8.3
G2
56.1
31.9
5.0
STAT5-SH2i
250 μM
500 μM
45.7
36.3
11.4
47.2
36.7
9.0
BrdU
DAPI
F
Relative % of EPCs in S-phase
n.s.
n.s.
Ctrl
DMSO
250
500 μM
STAT5-SH2i

Fig 2-5

Fig 2-6. Failure of B19V replicative form DNA clones with STAT5-binding element mutations in replication in transfected UT7/Epo-S1 cells.

(A) Diagram of the B19V full-length M20 RF genome and various half ITR-deleted N8 RF genomes with mutations at STAT5-binding elements (STAT5BEs). Red squares indicate the position of the *Ori* sequences at both ITRs, and grey squares indicate mutated Ori (*mOri*). The sequence of the *mOri* is shown with mutated nucleotides in grey in the STAT5BE. (B&C) Southern blot analysis. **(B)** The N8 RF DNA, or derivatives with mutations in the STAT5BE of either the left ITR ($N8^{OriL}$), right ITR ($N8^{OriR}$), or both ($N8^{mOri}$), were transfected into UT7/Epo-S1 cells. **(C)** M20, and $M20^{mOri}$, a derivative of the M20 RF DNA with STAT5BEs of both ITRs mutated, were transfected into UT7/Epo-S1 cells. At 48 h post-transfection, cells were collected for Hirt DNA extraction. And Hirt DNA samples were analyzed by Southern blotting with an M20 DNA probe. RF DNA (RF), ssDNA (ss), and Dpn I-digested DNA (shown with a line) are indicated. Mitochondrial DNA (Mito DNA) was used as a loading control (lower panels). **(D)** Viral protein expression of B19V DNA mutants. M20 or $M20^{mOri}$ transfected UT7/Epo-S1 cells were stained with anti-NS1 or anti-capsid antibodies. Confocal images were taken with an Eclipse C1 Plus (Nikon) microscope at 100 × magnification.

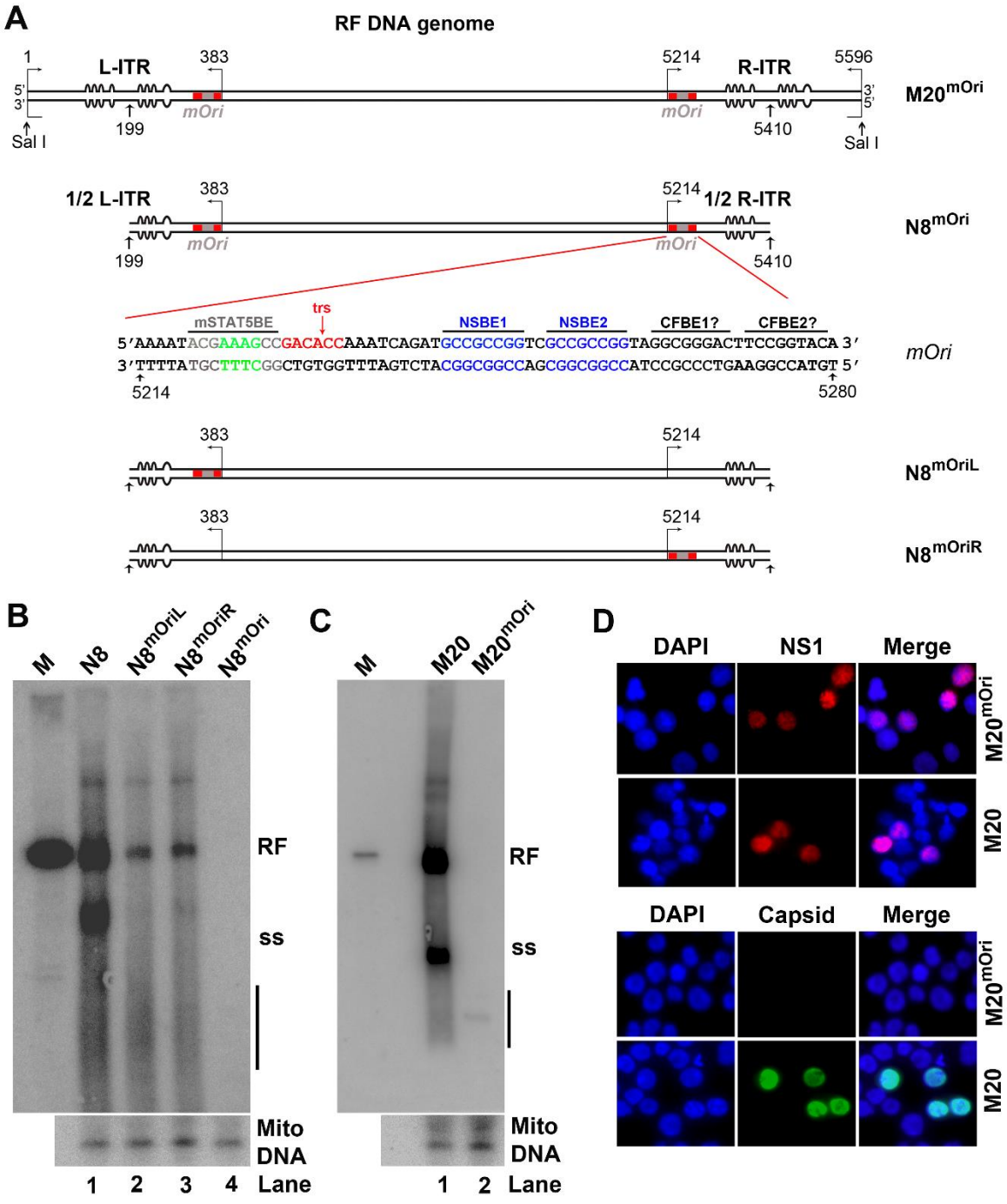
A
RF DNA genome
L-ITR
R-ITR
mOri
Sal I
M20mOri
1/2 L-ITR
1/2 R-ITR
N8mOri
mSTAT5BE
trs
NSBE1
NSBE2
CFBE1?
CFBE2?
mOri
N8mOriL
N8mOriR
B
M
N8
N8mOriL
N8mOriR
N8mOri
RF
ss
Mito DNA
Lane
C
M
M20
M20mOri
D
DAPI
NS1
Merge
Capsid

Fig 2-6

Fig 2-7. pSTAT5, but not NS1 interacts with the MCM complex.

(A) Immunoprecipitation (IP) assay. Cell lysates of $NS1^{Flag}$-expressing UT7/Epo-S1 cells were prepared for pull-down assays with either anti-Flag-conjugated beads or control beads. Immunoprecipitated proteins were examined for the presence of MCM2 by Western blotting. Blots were reprobed with rabbit anti-pSTAT5(Y694), anti-E2F5, and anti-Flag antibodies. Detection of E2F5 was used as a positive control for NS1 IP. **(B)** Co-IP assay. UT7/Epo-S1 cells were collected, washed, and lysed with RIPA buffer. After centrifugation, the supernatant was incubated with either rabbit anti-pSTAT5(Y694) or control IgG antibody. Immunoprecipitated proteins were blotted for the presence of the MCM complex with an anti-MCM5 antibody and for pSTAT5 with rabbit anti-pSTAT5(Y694). **(C)** Reverse Co-IP assay. Reverse Co-IP was performed with an anti-MCM5 antibody. Immunoprecipitated proteins were examined for pSTAT5, MCM2, and MCM5, respectively. **(D)** Co-IP of lysates treated with DNase. UT7/Epo-S1 cell lysates, either treated or untreated with DNase (750 units of Benzonase) were incubated with anti-pSTAT5(Y694) or control IgG antibodies for Co-IP assay, and immunoprecipitated proteins were examined for MCM2 by Western blot analysis. (E-H) Immunofluorescence analysis. **(E&F)** Mock- or B19V-infected $CD36^+$ EPCs were co-stained with rabbit anti-STAT5 and mouse anti-MCM2 antibodies, followed by **(E)** incubation with respective secondary antibodies, or by **(F)** proximal ligation assay, which produces amplified signal for labeled molecules in close proximity. **(G)** $CD36^+$ EPCs were incubated with either DMSO or pimozide (at 30 μM) for 2 days. And then the cells were co-stained with rabbit anti-STAT5 and mouse anti-MCM2 antibodies for proximity ligation assay. **(H)** Infected EPCs were stained with an anti-capsid antibody. Confocal images were taken with an Eclipse C1 Plus (Nikon) microscope at 100 × magnification.

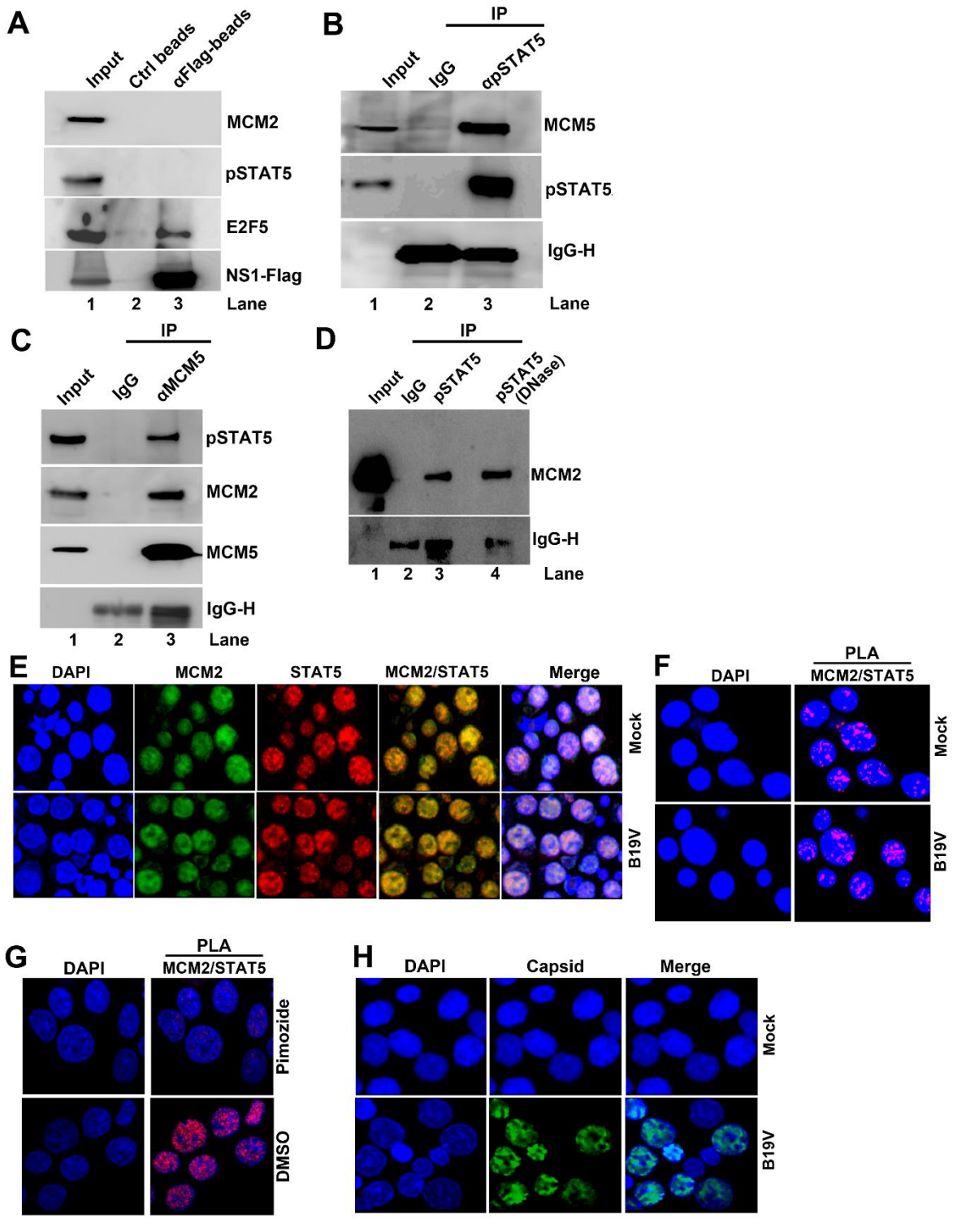
A
Input
Ctrl beads
αFlag-beads
MCM2
pSTAT5
E2F5
NS1-Flag
1 2 3 Lane
B
IP
Input
IgG
αpSTAT5
MCM5
pSTAT5
IgG-H
1 2 3 Lane
C
IP
Input
IgG
αMCM5
pSTAT5
MCM2
MCM5
IgG-H
1 2 3 Lane
D
IP
Input
IgG
pSTAT5
pSTAT5 (DNase)
MCM2
IgG-H
1 2 3 4 Lane
E
DAPI
MCM2
STAT5
MCM2/STAT5
Merge
Mock
B19V
F
DAPI
PLA
MCM2/STAT5
Mock
B19V
G
DAPI
PLA
MCM2/STAT5
Pimozide
DMSO
H
DAPI
Capsid
Merge
Mock
B19V

Fig 2-7

Fig 2-8. The MCM complex is loaded onto the viral *Ori*.

(A) Experimental strategy. The STAT5-MCM complex is depicted interacting with a DNA sequence, such as the viral *Ori*. The time line of B19V infection and treatment with the STAT5-SH2 inhibitor (STAT5-SH2i) shows time (h) post-infection or post-treatment. **(B)** ChIP assay. Cells were treated as shown in panel A. An anti-MCM2 antibody was used to pull down the STAT5-MCM-DNA complex, and the recovered ChIP DNA was subjected to qPCR with a primer set spanning the *Ori* region. Compared with the absence of the STAT5-SH2i, the relative abundance (percentage) of MCM on the viral *Ori* in the presence of the STAT5-SH2i is shown, with mean and standard deviation of three independent experiments. P values are calculated using a Student's t test, ** denotes $P<0.01$. **(C)** Three color confocal microscopy. Mock- or B19V-infected $CD36^+$ EPCs were co-stained with rabbit anti-STAT5, rat anti-NS1, and mouse anti-MCM2 antibodies, followed by staining with secondary antibodies conjugated with Dylight405, Texas Red, and FITC, respectively. Images were taken with an Eclipse C1 Plus (Nikon) confocal microscope at 100 × magnification.

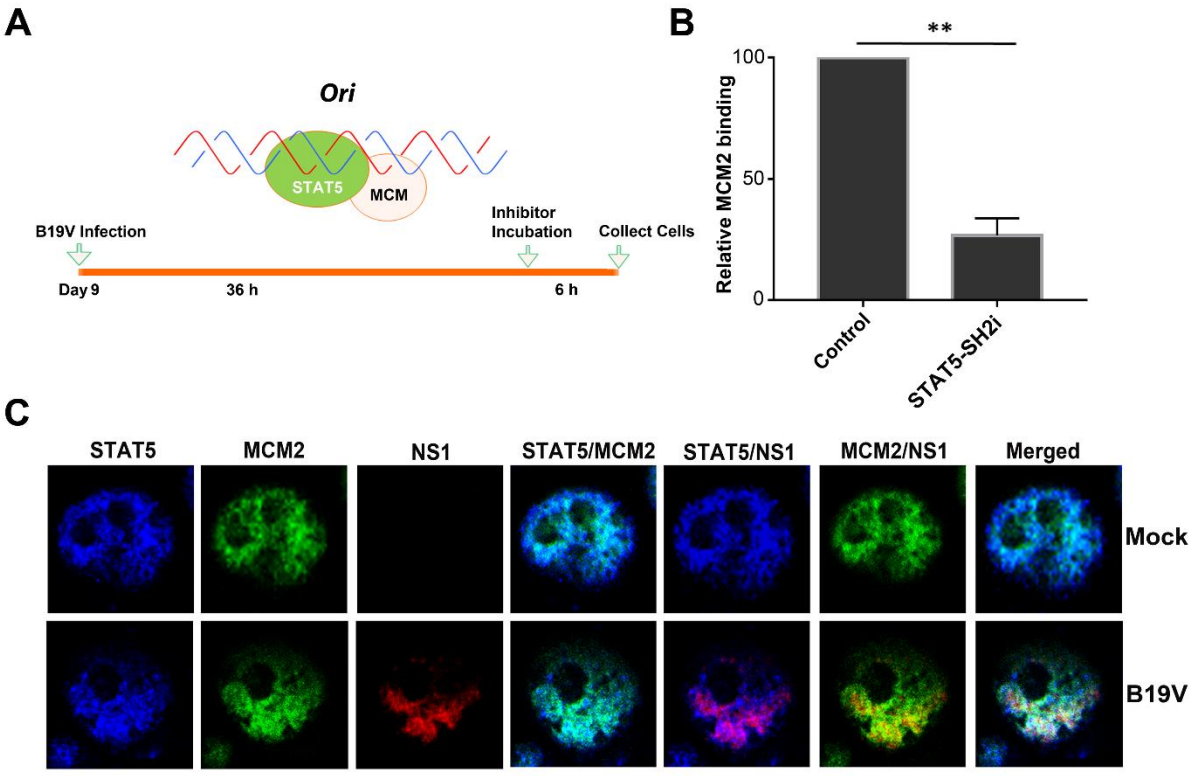
A
Ori
STAT5
MCM
B19V Infection
Inhibitor Incubation
Collect Cells
Day 9
36 h
6 h
B
**
100
50
0
Relative MCM2 binding
Control
STAT5-SH2i
C
STAT5
MCM2
NS1
STAT5/MCM2
STAT5/NS1
MCM2/NS1
Merged
Mock
B19V

Fig 2-8

Fig. 2-9. IC_{50} determination and colony formation assay.

(A) IC_{50} determination. $CD36^+$ EPCs incubated with pimozide at different concentrations were infected with B19V. After 48 h post-infection, the cells were extracted for Hirt DNA. The DNA samples were examined for B19V DNA with Southern blot analysis using a M20 RF DNA probe. Viral RF DNA was quantified. RF DNA levels with pimozide relative to levels without pimozide are plotted against the concentrations of pimozide for the calculation of the IC_{50} value with GraphPad Prism. **(B&C)** Colony formation assay. $CD36^+$ EPCs were incubated with pimozide at different concentrations for 48 h, and then cultured in methyl cellulose-containing medium. After 10 days, numbers of the colonies were counted **(B)**. P values are calculated using one-way ANOVA followed by Tukey-Kramer post-test, compared with DMSO group. ** $P<0.01$; * $P< 0.05$; n.s. ($P>0.05$) denotes no statistical significance. Images of colonies were taken with Eclipse C1 Plus (Nikon) inverted microscope at 10 × and 40 × magnifications **(C)**.

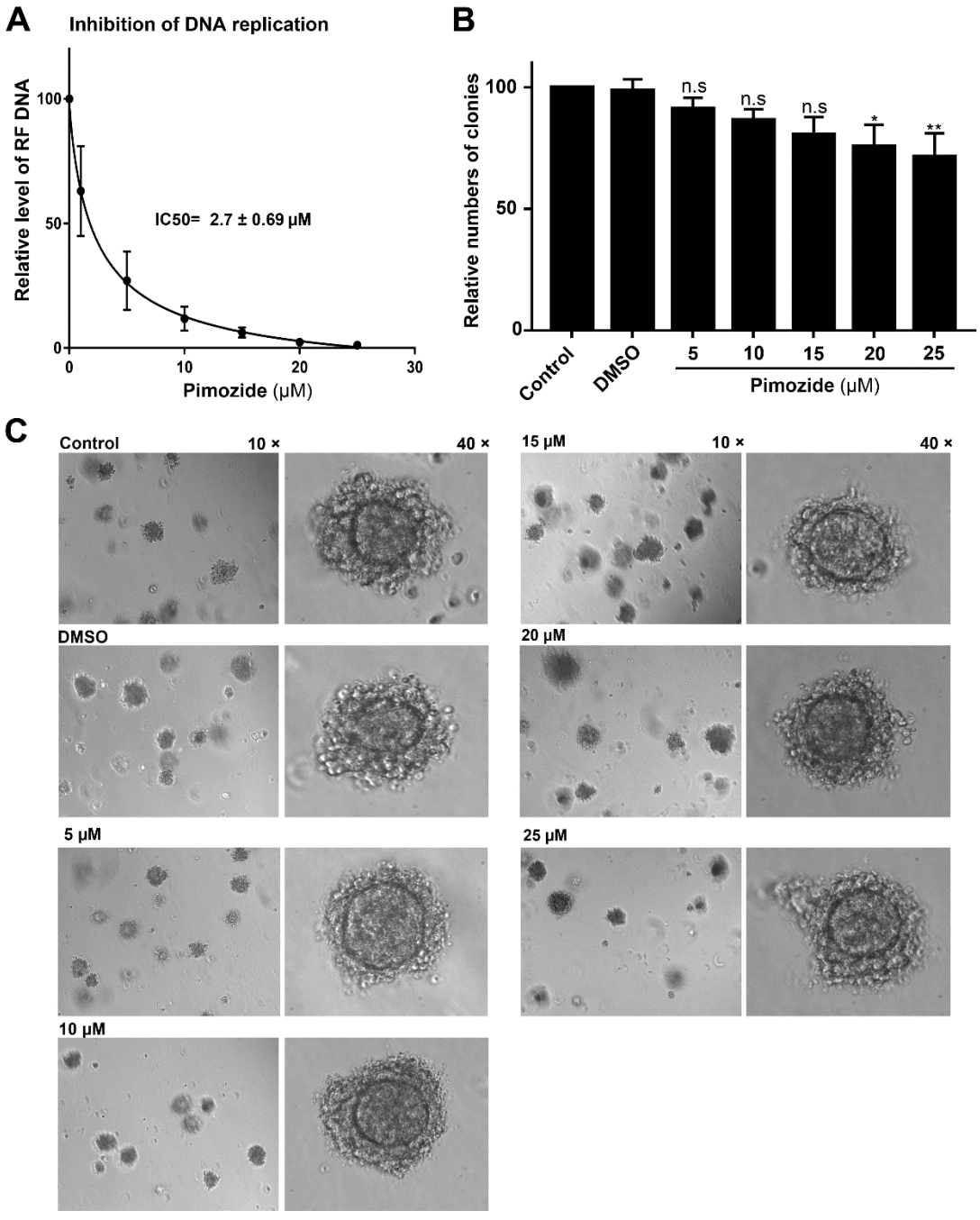
A
Inhibition of DNA replication
Relative level of RF DNA
100
50
0
IC50= 2.7 ± 0.69 μM
0
10
20
30
Pimozide (μM)
B
Relative numbers of clonies
100
50
0
n.s
n.s
n.s
*
**
Control
DMSO
5
10
15
20
25
Pimozide (μM)
C
Control
10 ×
40 ×
15 μM
10 ×
40 ×
DMSO
20 μM
5 μM
25 μM
10 μM

Fig 2-9

Fig 2-10. Pimozide abolishes B19V DNA replication in UT7/Epo-S1 cells.

(A&B) Inhibition of B19V DNA replication. UT7/Epo-S1 cells were pre-incubated with DMSO or pimozide (at a final concentration of 10 μM or 20 μM), 6 h prior to M20 transfection. Transfected cells were cultured under hypoxic conditions. **(A)** At 48 h post-transfection, cells were collected for Hirt DNA extraction. The DNA samples were subjected to Southern blotting with a B19V M20 probe (upper panel). Mitochondrial (mito) DNA was probed as a loading control (lower panel). **(B)** At 48 h post-transfection, cells were collected for Western blotting with anti-pSTAT5(Y694). The blot was reprobed for β-actin. (C&D) Evaluation of the effect of pimozide on cell proliferation. $CD36^+$ EPCs were treated with either DMSO or pimozide and then incubated with BrdU to perform a BrdU incorporation assay. **(C)** Results of a representative cell-cycle analysis. **(D)** Relative fold changes of the cell population in S-phase are shown with means and standard deviations, which were obtained from three independent experiments. P values are calculated using one-way ANOVA followed by Tukey-Kramer post-test, n.s. ($P > 0.05$) denotes no statistical significance.

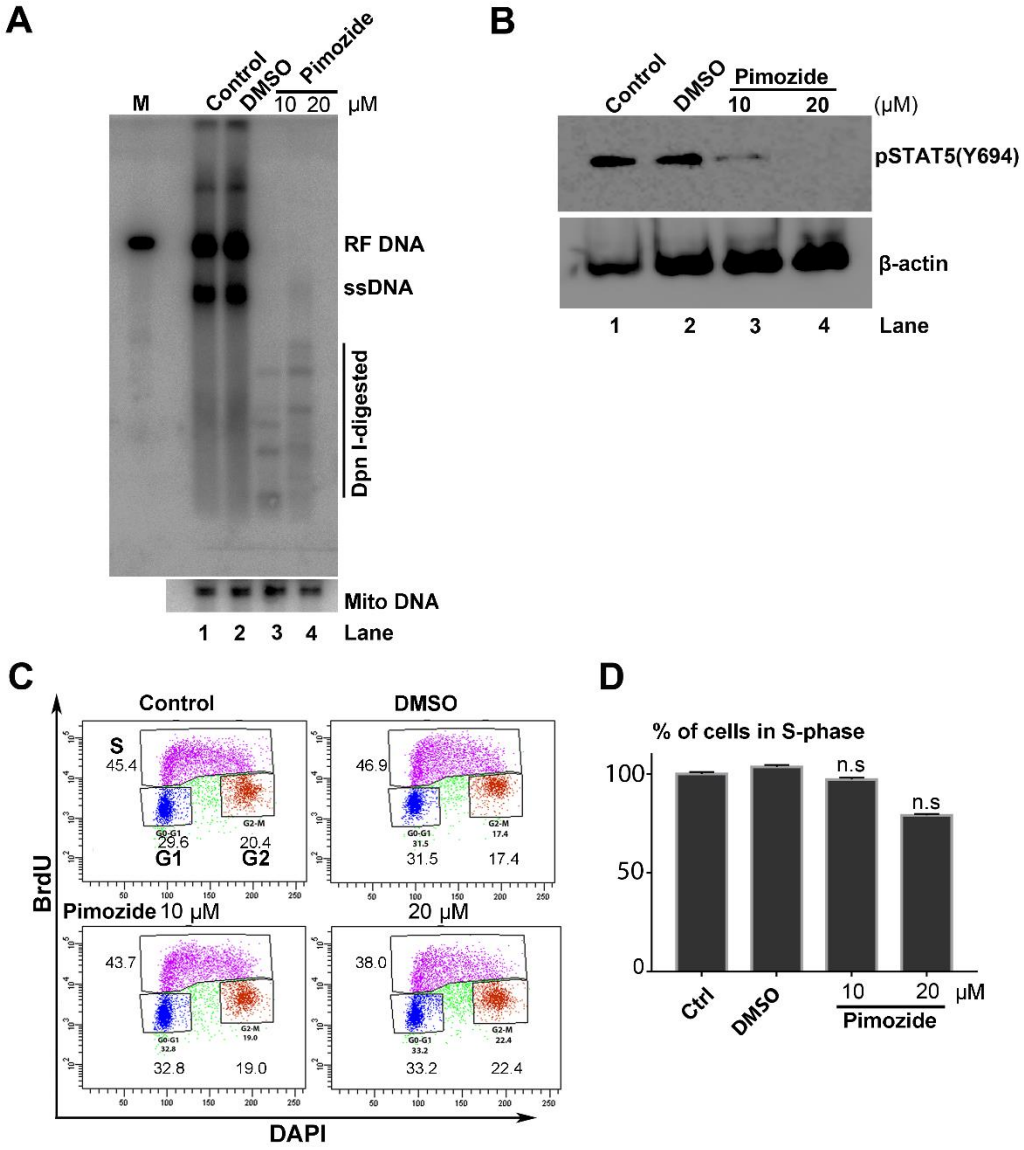
A
M
Control
DMSO
Pimozide
10 20 μM
RF DNA
ssDNA
Dpn I-digested
Mito DNA
1 2 3 4 Lane
B
Control
DMSO
Pimozide
10 20 (μM)
pSTAT5(Y694)
β-actin
1 2 3 4 Lane
C
Control
DMSO
S
45.4
46.9
G1
G2
29.6
20.4
31.5
17.4
Pimozide 10 μM
20 μM
43.7
38.0
32.8
19.0
33.2
22.4
BrdU
DAPI
D
% of cells in S-phase
100
50
0
n.s
n.s
Ctrl
DMSO
10 20 μM
Pimozide

Fig 2-10

Fig 2-11. Blockage of STAT5-DNA interaction inhibits B19V replication in UT7/Epo-S1 cells.

(A) Southern blot analysis. UT7/Epo-S1 cells were incubated with either DMSO or STAT5-SH2 inhibitor (STAT5-SH2i; 250 μM or 500 μM) at 6 h prior to transfection, and then the cells were transfected with M20 DNA and cultured under hypoxic conditions. At 48 h post-transfection, cells were collected for Hirt DNA extraction. The DNA samples were subjected to Southern blotting with an M20 DNA probe. Mitochondrial (Mito) DNA was probed as a loading control (lower panel). **(B&C)** Evaluation of the effect of STAT5 inhibitor on cell proliferation. UT7/Epo-S1 cells were treated with either DMSO or STAT5-SH2i (at 250 μM or 500 μM), and then incubated with BrdU for BrdU incorporation assays. **(B)** Results of a representative cell-cycle analysis. **(C)** Relative fold changes of the cell population in S-phase are shown, with means and standard deviations shown. P values are calculated using one-way ANOVA followed by Tukey-Kramer post-test, compared with DMSO group. *** denotes $P<0.001$ and n.s. ($P>0.05$) for no statistical significance.

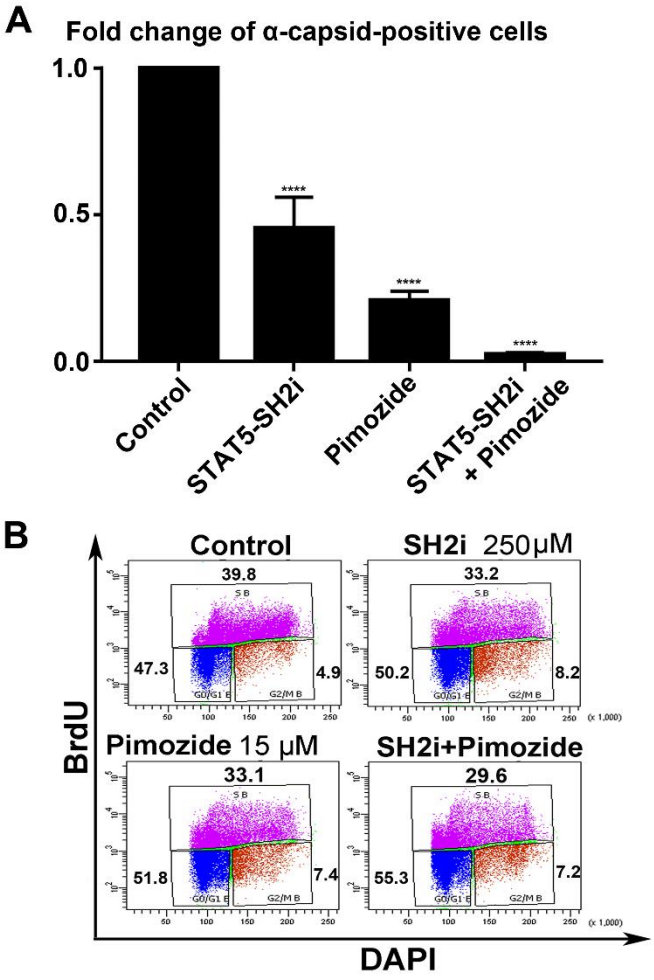
A
Fold change of α-capsid-positive cells
1.0
0.5
0.0
****
****
****
Control
STAT5-SH2i
Pimozide
STAT5-SH2i + Pimozide
B
Control
39.8
47.3
4.9
SH2i 250μM
33.2
50.2
8.2
Pimozide 15 μM
33.1
51.8
7.4
SH2i+Pimozide
29.6
55.3
7.2
BrdU
DAPI

Fig 2-11

Fig 2-12. STAT5A is the major STAT5 isoform expressed in erythroid lineage cells.

(A&B). Differential expression of STAT5A and STAT5B. **(A)** Cell lysates of UT7/Epo-S1 and EPCs were subjected to Western blotting with STAT5A/B pan-specific, STAT5A-specific, or STAT5B-specifc antibodies. Asterisks indicate dimerized or degraded or non-specific protein bands. **(B)** Purified STAT5 of UT7/Epo-S1 cells was subjected to Western blotting with a STAT5A/B pan-specific antibody. **(C)** Both STAT5A and STAT5B interact with the MCM2 complex. UT7/Epo-S1 cells were collected and lysed with RIPA buffer. The lysates were incubated with an anti-MCM2 or control IgG antibody for co-immunoprecipitation (Co-IP). Immunoprecipitated proteins were blotted for the presence of STAT5A, STAT5B, and MCM2 with anti-STAT5A, anti-STAT5B, and anti-MCM2 antibodies, respectively. The precipitated IgG heavy chain is also shown.

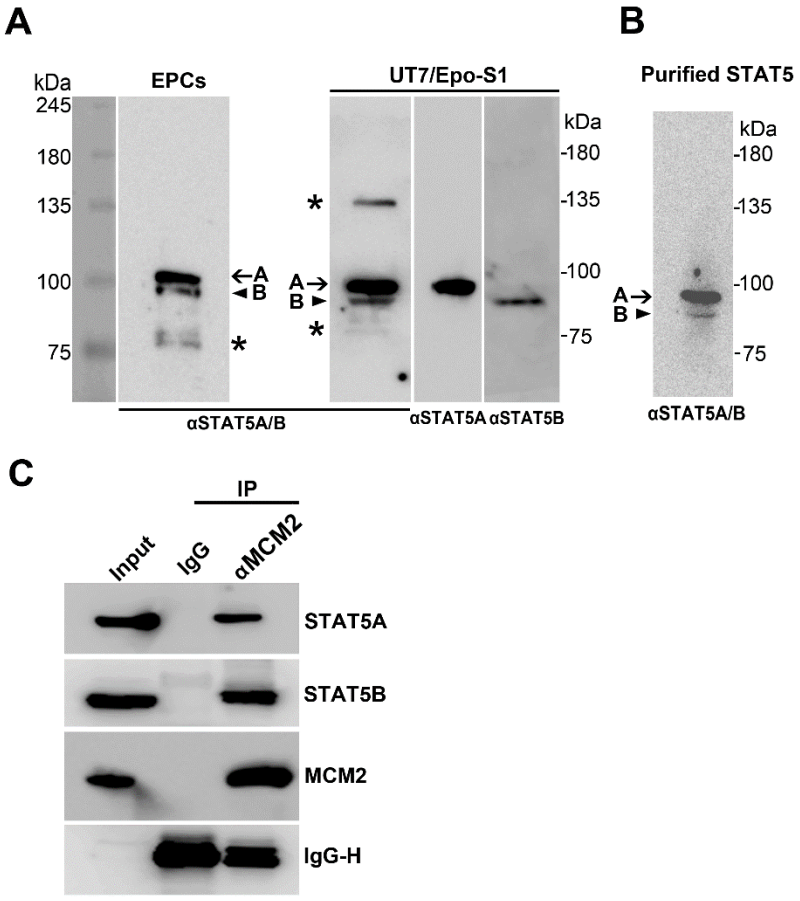
A
kDa
EPCs
245
180
135
100
75
←A
◄B
*
UT7/Epo-S1
kDa
-180
-135
-100
-75
*
A→
B►
*
αSTAT5A/B
αSTAT5A
αSTAT5B
B
Purified STAT5
kDa
-180
-135
-100
-75
A→
B►
αSTAT5A/B
C
IP
Input
IgG
αMCM2
STAT5A
STAT5B
MCM2
IgG-H

Fig 2-12

Fig 2-13. Analyses of MCM or STAT5 binding to B19V genome by ChIP assay.

(A) UT7/Epo-S1 cells were transfected with M20 and allowed to replicate for 48 h under hypoxic conditions. Cells were collected for ChIP analysis. Anti-MCM2, anti-MCM3, anti-MCM5, anti-MCM7, and control IgG antibodies were used to pull down DNA-protein complex. Recovered DNA was analyzed by qPCR targeting the viral origin (Ori-qPCR). Error bars represent standard deviations taken from at least three experiments. P values were calculated using a Student's t test, compared to the IgG control. ** $P<0.01$; * $P<0.05$. **(B)** A diagram of the Ori-qPCR amplicon targeting the viral replication origin (*Ori*) at the left ITR (L-ITR). The starting nucleotide numbers of both forward and reverse (F and R) and the location of the probe are indicated. **(C)** UT7/Epo-S1 cells were treated with either DMSO, STAT5-SH2i inhibitor (at 500 μM) or pimozide (at 25μM), as indicated in the figure, at 6h prior to transfection. Then, the cells were transfected with M20 and cultured under hypoxic conditions for 48 h. Cells were collected for ChIP analysis using an anti-STAT5 and Ori-qPCR. Error bars represent standard deviation taken from at least three experiments. P values were calculated using one-way ANOVA followed by Tukey-Kramer post-test, compared with the M20 group. **** denotes $P<0.0001$. **(D)** Mock- or M20- transfected UT7/Epo-S1 cells, cultured under hypoxic conditions for 48 h, were collected for ChIP assay using an anti-STAT5 antibody, followed by PCR using primers: forward (F, nt 3135-3156), 5'- GGA CTG TAG CAG ATG AAG AGC T-3', and reverse (R, nt 3393-3373), 5'-GTG GCC CCC TCA CTC CAC AT-3', primes as indicated in the diagram. Rabbit IgG was used as a negative control of pull-down, and M20 DNA was used as PCR positive control.

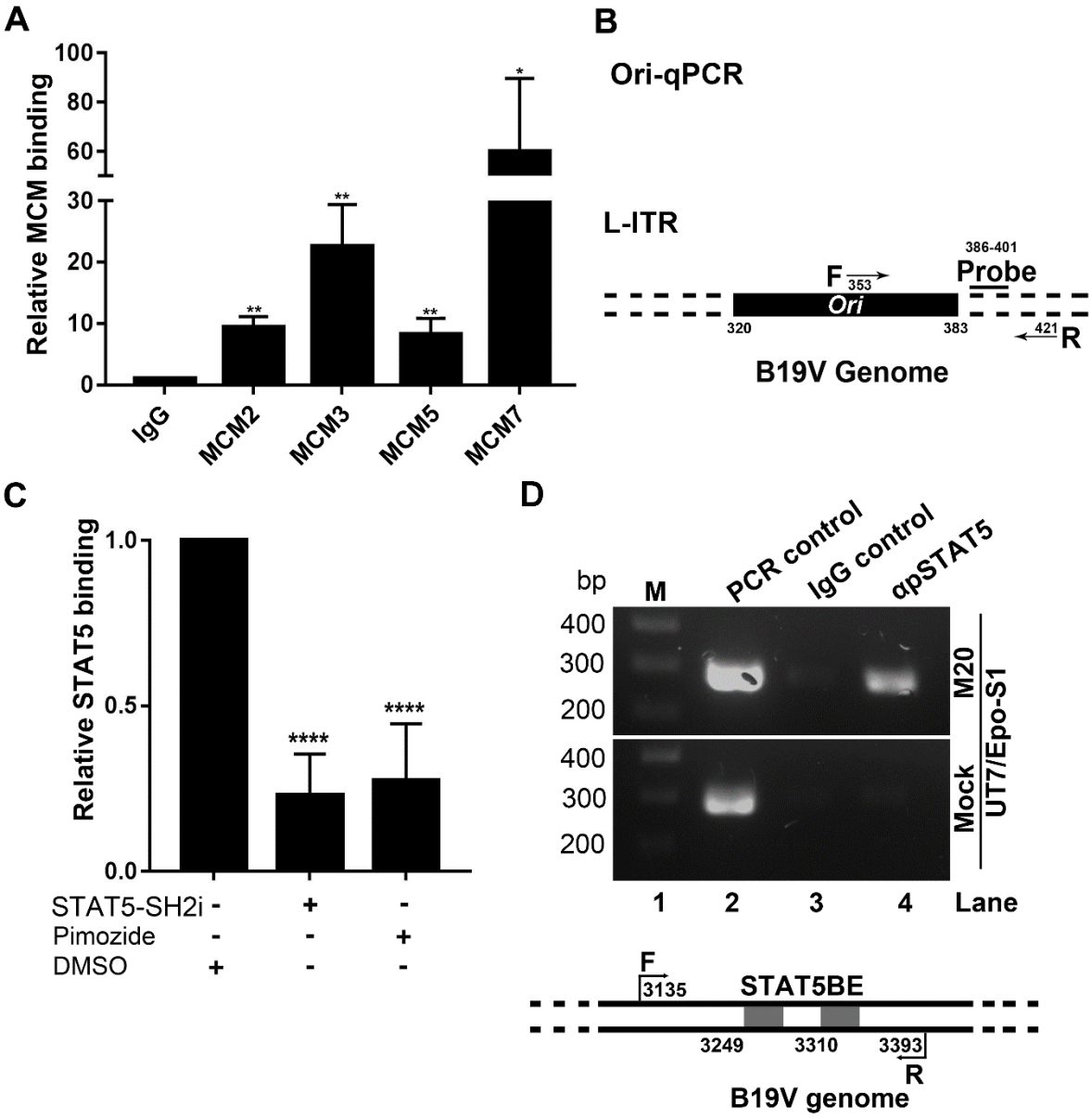
A
Relative MCM binding
100
80
60
30
20
10
0
IgG
MCM2
MCM3
MCM5
MCM7
B
Ori-qPCR
L-ITR
F 353
Ori
386-401
Probe
320
383
421
R
B19V Genome
C
Relative STAT5 binding
1.0
0.5
0.0
****
****
STAT5-SH2i - + -
Pimozide - - +
DMSO + - -
D
bp
M
PCR control
IgG control
αpSTAT5
400
300
200
M20
Mock
UT7/Epo-S1
1 2 3 4 Lane
F
3135
STAT5BE
3249
3310
3393
R
B19V genome

Fig 2-13

Fig 2-14. Pimozide did not affect hydroxyurea-induced ATR/ATM activation, and B19V infection did not alter pSTAT5 expression, in $CD36^+$ EPCs.

(A) $CD36^+$ EPCs were treated with pimozide (at 15 μM). At 3 h post-treatment, cells were incubated with hydroxyurea at 10 mM for 24 h under hypoxic conditions. Then, the same numbers of the cells were collected for Western blot analysis of proteins, as indicated, using anti-ATM(pST1981), anti-ATR(pT1989), pSTAT5, and β-actin, respectively. **(B)** Mock and B19V-infected $CD36^+$ EPCs, cultured under hypoxic conditions, were used for Western blot analysis of pSTAT5. The membrane was reprobed for β-actin.

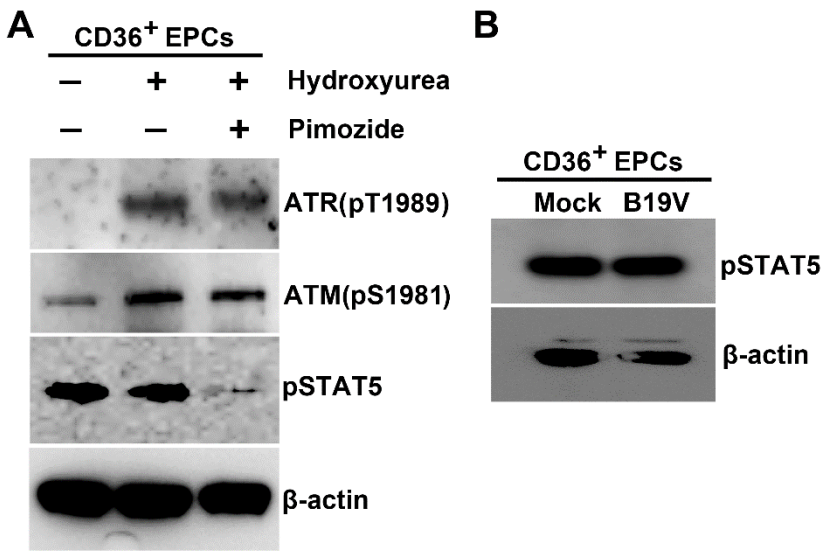
A
CD36+ EPCs
–
+
+
Hydroxyurea
–
–
+
Pimozide
ATR(pT1989)
ATM(pS1981)
pSTAT5
β-actin
B
CD36+ EPCs
Mock
B19V
pSTAT5
β-actin

Fig 2-14

Fig. 2-15. pSTAT5 did not transactivate viral P6 promoter.

(A) A diagram of lentivirus Lenti-ATF/P6-GFP. The virus was made as we reported previously (70). **(B)** UT7/Epo-S1 (S1) cells or NS1-expressing UT7/Epo-S1 (NS1-S1) cells were transduced with Lenti-ATF/P6-GFP at an MOI of 2–4 transduction units/cell and cultured under hypoxic conditions. At 24 h post-transduction, cells were incubated either with DMSO or pimozide (at a final concentration of 15 μM) for 48 h. Then, the cells were collected and subjected to flow cytometry analysis for a mean fluorescence intensity (MFI) value of GFP expression. P values are calculated using one-way ANOVA followed by Tukey-Kramer post-test, compared with DMSO group. **** denotes $P<0.0001$ and n.s. ($P>0.05$) for no statistical significance.

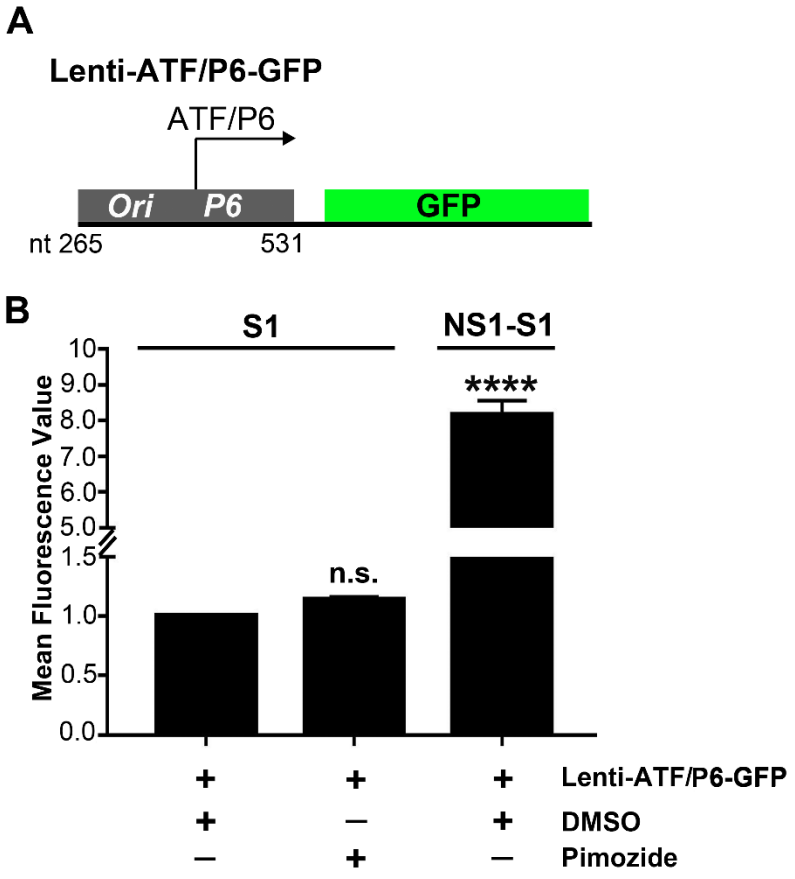
A
Lenti-ATF/P6-GFP
ATF/P6
Ori
P6
GFP
nt 265
531
B
S1
NS1-S1
****
n.s.
Mean Fluorescence Value
10
9.0
8.0
7.0
6.0
5.0
1.5
1.0
0.5
0.0
+ + + Lenti-ATF/P6-GFP
+ – + DMSO
– + – Pimozide

Fig 2-15

Fig 2-16. Pimozide and STAT5-SH2i synergistically inhibited B19V infection.

$CD36^+$ EPCs were pre-incubated with DMSO or pimozide (at 15 μM), STAT5-SH2i (at 250 μM), or pimozide plus STAT5-SH2i (at 15 and 250 μM, respectively), 6 h prior to B19V infection under hypoxic conditions. **(A)** At 48 h post-infection, cells were subjected to flow cytometry analysis using anti-B19V capsid antibody. Error bars represent standard deviation taken from at least three experiments. P values are calculated using one- way ANOVA followed by Tukey-Kramer post-test, compared with DMSO group. **** denotes $P<0.0001$. **(B)** Similarly, at 48 h post-treatment, uninfected cells were labeled with BrdU for cell cycle analysis. Numbers shown are percentages of cells at G1, S, and G2 phase, respectively.

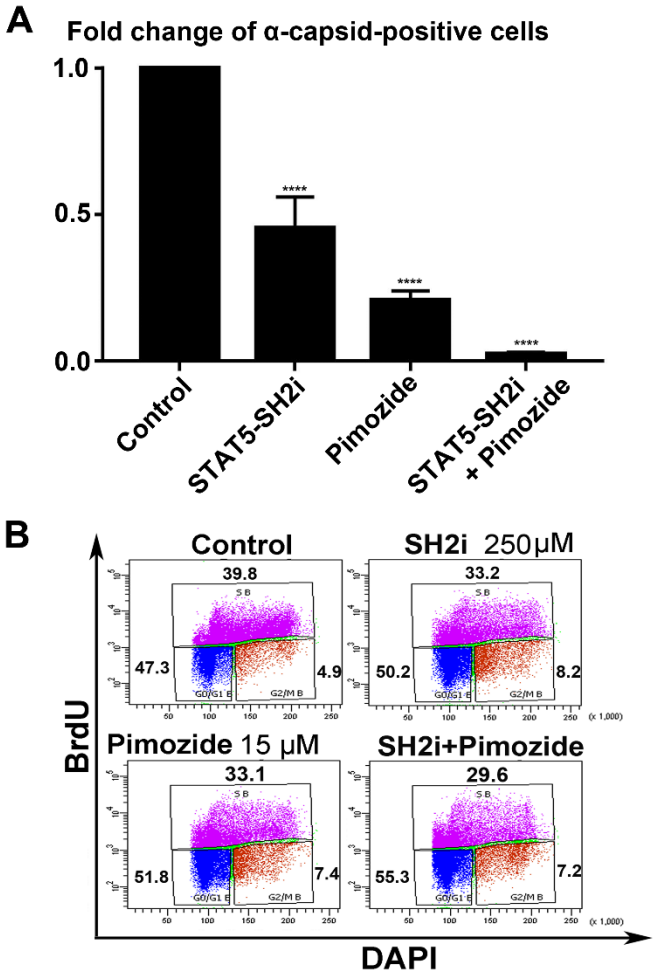
A
Fold change of α-capsid-positive cells
1.0
0.5
0.0
****
****
****
Control
STAT5-SH2i
Pimozide
STAT5-SH2i + Pimozide
B
Control
39.8
47.3
4.9
SH2i 250μM
33.2
50.2
8.2
Pimozide 15 μM
33.1
51.8
7.4
SH2i+Pimozide
29.6
55.3
7.2
BrdU
DAPI

Fig 2-16

Chapter 3:

RNA Binding Protein RBM38 Regulates Expression of the 11-kDa Protein of Parvovirus B19 which Facilitates Viral DNA Replication[3]

[3] The chapter has been previously published in Journal of Virology: Ganaie, S. S., Chen, A. Y., Huang, C., Xu, P., Kleiboeker, S., Du, A., and Qiu, J. (2018) RNA Binding Protein RBM38 Regulates Expression of the 11-Kilodalton Protein of Parvovirus B19, Which Facilitates Viral DNA Replication. *Journal of virology* **92.** https://doi.org/10.1128/JVI.02050-17.

Abstract

Human parvovirus B19 (B19V) expresses a single precursor mRNA (pre-mRNA), which undergoes alternative splicing and alternative polyadenylation to generate 12 viral mRNA transcripts that encode two structural proteins (VP1 and VP2) and three nonstructural proteins (NS1, 7.5-kDa, and 11-kDa). Splicing at the second 5' donor site (D2) of the B19V pre-mRNA is essential for the expression of VP2 and 11-kDa. We have previously identified that a *cis*-acting intronic splicing enhancer 2 (ISE2) that lies immediately after the D2 site facilitates recognition of the D2 donor for its efficient splicing. In this study, we report that ISE2 is critical for expression of the 11-kDa viral non-structural protein. We found that ISE2 harbors a consensus RNA-binding motif protein 38 (RBM38) binding sequence–5'-UGUGUG-3'. RBM38 is expressed during the middle stage of erythropoiesis. We first confirmed that the RBM38 binds specifically with the ISE2 element in vitro. Knockdown of RBM38 significantly decreases the level of the spliced mRNA at D2 that encodes 11-kDa protein and, thereafter, expression of the 11-kDa protein, but not the D2-spliced mRNA that encodes VP2. Importantly, we found that the 11-kDa protein enhances viral DNA replication and virion release. Accordingly, knockdown of RBM38 decreases virus replication *via* downregulating 11-kDa expression. Taken together, these results suggest that the 11-kDa protein facilitates B19V DNA replication, and that RBM38 is an essential host factor for B19V pre-mRNA splicing and for the expression of the 11-kDa protein

Introduction

Human parvovirus B19 (B19V) belongs to genus *Erythroparvovirus* of the *Parvoviridae* family (140). B19V productive infection displays a high tropism for burst forming unit-erythroid (BFU-E) and colony forming unit-erythroid (CFU-E) progenitor cells in human bone marrow and fetal liver (3-5,115). B19V also infects non-erythroid tissues (19); however, the infection is not productive (1). B19V infection causes human diseases, such as erythema infectiosum or fifth disease in children, transient aplastic crises in sickle cell disease patients, pure red blood aplasia in immunocompromised patients, arthropathy, cardiomyopathy in adults, and non-immune hydrops fetalis in pregnant women (1,142,144).

B19V is a small, non-enveloped virus with a single-stranded (ss) DNA genome of 5.6 kb (140). The B19V genome is flanked by two identical inverted terminal repeats (ITRs) at both ends (**Fig. 3-1A**) (141). The left portion of the genome encodes nonstructural proteins NS1 and 7.5-kDa, whereas the right side encodes structural proteins VP1 and VP2, and an additional nonstructural protein 11-kDa (**Fig. 3-1B**) (43,46,47). B19V genome has a single promoter at map unit 6 (P6), which transcribes a single precursor mRNA (pre-mRNA) (1). B19V pre-mRNA has two donor sites (D1 and D2) and four acceptor sites (A1-1, A1-2, A2-1, and A2-2), which are used for alternative splicing to generate all species (12) of the viral mRNAs (**Fig. 3-1B**). There are two internal (proximal) polyadenylation sites, (pA)p1 and (pA)p2, and one distal (pA)d site (1). NS1 and 7.5-kDa mRNAs use the (pA)p1/2 sites, and VP1, VP2, and 11-kDa mRNAs utilize the (pA)d site for polyadenylation (**Fig. 3-1B**) (44).

In absence of virus genome replication, most of the viral transcripts are polyadenylated at (pA)p sites in both B19V-permissive and non-permissive cells, the majority of which encode NS1 and 7.5-kDa proteins (48,49). However, virus genome replication overcomes the blockade

and enhances the read-through of the (pA)p sites, generating full-length transcripts that encode capsid and 11-kDa proteins (49). In the past, our group and others used a B19V replication-competent model, where a nearly full-length B19V genome was amplified by the SV40 replication origin in COS-7 cells, to analyze the B19V transcription profile (43,44,49,184,185). Using that artificial viral DNA replication system, we demonstrated that efficient splicing of the first intron promotes the polyadenylation at (pA)p (53). However, splicing within the second intron competes with polyadenylation at (pA)p and stimulates polyadenylation at (pA)d (53). We also showed that binding of small nuclear U1 RNA to splice donor site D2 is sufficient to inhibit polyadenylation at (pA)p (53). Importantly, we previously found multiple splicing enhancers that define the central exon, which spans A1-1/A1-2 to D2 sites, determine its inclusion (52). Notably, we identified an intronic splicing enhancer 2 (ISE2) after the D2 site of B19V pre-mRNA, and demonstrated that ISE2 sequence (**Fig. 3-1C**) is essential for the recognition of D2 site for splicing (52). Use of morpholino antisense oligonucleotide to ISE2 region reduced splicing at D2 site in B19V infected *ex vivo* expanded human erythroid progenitor cells (52).

In this study, we showed that RNA-binding motif protein 38 (RBM38) protein binds to B19V ISE2 element, which is essential for efficient splicing of B19V pre-mRNA at D2 site. We showed that knockdown of RBM38 reduced the level of viral mRNA transcripts encoding 11-kDa protein. Importantly, the 11-kDa protein augmented virus DNA replication and, thereafter, virion release. Overall, our results revealed that RBM38 regulates B19V DNA replication *via* enhancing B19V pre-mRNA splicing at D2 site which ensures the production of viral mRNA transcripts that encode the 11-kDa protein.

Materials and Methods

Ethics statement.

Primary human $CD133^+$ hematopoietic stem cells were isolated from bone marrow of healthy donors according to a protocol (04-H-0179) approved by the National Heart, Lung, and Blood Institute institutional review board. There was no donor information associated with samples when we received the cells.

Primary cells and cell lines.

Human $CD133^+$ hematopoietic stem cells were expanded *ex vivo* to $CD36^+$ EPCs in Wong medium, as described previously (70,78)**.** Briefly, $CD133^+$ cells were cultured in Wong medium under normoxia (5% CO_2 and 21% O_2) up to day-4 and frozen in liquid nitrogen. In each experiment, Day-4 cells were seeded under normoxia for 2-3 days, prior to incubation under hypoxia (5% CO_2 and 1% O_2) for 2 days.

UT7/Epo-S1, a human megakaryoblastoid cell line (14,77), was cultured in Dulbecco's modified Eagle's medium with 10% fetal bovine serum and erythropoietin (2 units/ml; Amgen, Thousand Oaks, CA). UT7/Epo-S1 cells were cultured at hypoxia (1% O_2) for 2-3 days post-transfection.

UT7/Epo-S1 cells were transduced with lentiviruses expressing shRBM38-1&3. The cells were further selected at increasing concentration of puromycin (1 to 5 μg/ml) and passaged for several weeks to generate the RBM38-knocked down UT7/Epo-S1 cell line.

Virus and infection.

Plasma sample no. P430 containing B19V (~1×10^{12} viral genome copies (vgc)/ml) were obtained from ViraCor Eurofins Laboratories (Lee's Summit, MO). $CD36^+$ EPCs were infected with B19V at a multiplicity of infection (MOI) of 1,000 vgc per cell. The infected cells and the

media were collected after 2-3 days post-infection for Southern/Western blot analyses and for the quantification of the virion release, respectively.

Plasmid constructions.

11-kDa knockout M20 clone ($pM20^{11KO}$): The three ATG's in 11-kDa ORF of pM20 were mutated to ACG's using overlap PCR approach, as described previously (52,53).

pLKO constructs: Lentiviral vector pLKO.1 with mCherry reporter was used to clone shRNA sequences between *Age* I and *EcoR* I sites. pLKO.1-containing scramble shRNA sequence was used as control (70). Following shRNA sequences were obtained from Sigma (St. Louis, MO) for knocking down RBM38: shRBM38-1:5'- CCG GCG GCT TCT CTT TAA TCT AGG TC TCG AGA CCT AGA TTA AAG AGA AGC CGT TTT TTG-3'; shRBM38-2: 5'-CCG GGA CGA CGA TAG TGT TTC TGT ACT CGA GTA CAG AAA CAC TAT CGT CGT CTT TTT TG-3'; shRBM38-3: 5'-CCG GCA ACG TGA ACC TGG CAT ATC TCT CGA GAG ATA TGC CAG GTT CAC GTT GTT TTT TG-3'; shRBM38-4: 5'-CCG GGA AAC CTG AAA GCA AGA AGT TCT CGA GAA CTT CTT GCT TTC AGG TTT CTT TTT TG-3'.

pLenti-11-kDa construct: pLenti vector was used to clone optimized 11-kDa ORF between the restriction sites *Xba* I and *Sal* I, as described previously (17,70).

Transfection.

UT7/Epo-S1 cells were electroporated with 2 μg of B19V DNA fragments, as reported earlier (70,78), using solution V from Amaxa Nucleofector (Lonza, Basel, Switzerland). B19V infectious clone pM20 and mutant $pM20^{11KO}$ were digested with *Sal* I to release B19V duplex genome M20 and mutant $M20^{11KO}$.

RNase protection assay.

Total RNA was extracted from infected or transfected cells, using TRIzol reagent (Invitrogen). RNase protection was performed as described previously (52,53). Both D1 and D2 probes were generated using T7 in-vitro transcription kit MAXIscript® (Ambion), following manufacturer's instructions. The images were captured by Typhoon FLA 9000 imager (GE Healthcare) and quantified using Image Quant TL software (GE Healthcare).

Reverse transcription (RT)-quantitative (q) PCR.

cDNA was synthesized by using Moloney murine leukemia virus (M-MLV) kit (Life Technologies, Carlsbad, CA). A multiplex RT-qPCR system was used to detect B19V-specific mRNAs, with β-actin mRNA serving as an internal control (77). For quantification of 11-kDa mRNA, forward primer 5'-GAA GCC TTC TAC ACA CCT TTG G-3', reverse primer, 5'-TGG CTG TCC ACA ATT CTT CAG G-3', and probe 5'-FAM-AGA CCA GTT TCG TGA ACT/CTA CAG ATG CA-BHQ-3' were used (77). For quantification of VP2 mRNA, forward primer 5'-GAC CAG TTC AGG AGA ATC AT-3', reverse primer 5'-TTC TGA GGC GTT GTA AGC-3' and probe 5'-FAM-TCG TGA ACT GTG CAG CTG CCC CTG TG-BHQ1-3' were used (77). All primers and probes were purchased from Integrated DNA Technologies (Coralville, IA). The primers and probe for quantification B19V genome were described previously (78).

RNA pulldown assay.

RNA pulldown assay was performed as described in previously published methods (186,187) with some modifications. Briefly, wild-type ISE2 (ISE2-WT) and mutant ISE2 (ISE2-mut1/2) RNA sequences were chemically synthesized by Integrated DNA Technologies (Coralville, IA) with biotinylation at 5' end. 100 µl of streptavidin slurry (Gold biotechnology

Inc., St Louis, MO) was used for each sample and washed three times with Wash buffer [20 mM Tris-HCl, pH7.5, 100 mM KCl, 2 mM EDTA, 0.5 mM DTT and 1 × protease inhibitor cocktail (Sigma)]. Beads were finally resuspended into 500 µl of Wash buffer and 10 µl of biotinylated RNA molecules (ISE2-WT or ISE2-mut1/2, 100 µM) were added to it. The mixtures were rotated for 3-4 hr at 4ºC. The beads were spun down and washed again with Wash buffer three times and resuspended into 500 µl of RNA binding buffer (20 mM Tris-HCl, pH7.5, 300 mM KCl, 0.2 mM EDTA, 0.5 mM DTT, poly I-C 6-10 µg/ml, proteinase inhibitors and RNase inhibitor) and 100 µl of nuclear lysate (at a concentration of 3-5 µg/µl) was added to each sample. UT7/Epo-S1 nuclear extract was prepared as described previously (70). The mixtures were rotated overnight, and then the beads were spun down, washed thrice with Wash buffer. The bound proteins were eluted using 60 µl of 2 × Laemmli loading buffer and boiled for 5 mins. The samples were run on SDS-PAGE either for Western blotting or Mass spectrometry.

Electrophoretic mobility shift assay.

ISE2-WT and ISE-mut1 RNA sequences were synthesized, using a T7 *in-vitro* transcription kit from MAXIscript® (Ambion), and further purified using RNA purification kit (Cat. no. R1015, Zymo Research, Irvine, CA), following the manufacturer's instructions. Glutathione S-transferase (GST) and GST-RBM38 proteins were incubated with radiolabeled ISE2-WT RNA in presence or absence of cold ISE2-WT and cold ISE2-mut1, as indicated in each experiment. Gel shift assay was as performed as reported previously (78,154,188).

Hirt DNA extraction and Southern blotting.

Hirt DNA (lower molecule DNA) was extracted from B19V-infected $CD36^+$ EPCs or B19V DNA-transfected UT7/Epo-S1 cells, as reported previously (78,189). Hirt DNA extracted from transfected cells were *Dpn* I digested before subjected to Southern blot analysis. B19V

M20 DNA was used as a temple for radioactive labeling to generate M20 probe. A mitochondrial DNA (Mito-DNA) probe was used as a control for the recovery of the Hirt DNA (190).

Western blotting.

Western blotting was performed as reported previously (68,78). Following primary antibodies were used: Anti-RBM38 antibody (#sc-365898; Santa Cruz, Dallas, TX), anti-VP1/VP2 (#MAB8293; Millipore, Billerica, MA), anti-GAPDH (#A01622; GenScript, Piscataway, NJ), anti-β-actin (#A5441; Sigma Aldrich, St. Louis, MO), and anti-BrdU (#600-401-C29; Rockland; Limerick, PA). Anti-NS1 and anti-11-kDa antibodies were produced in house, as described previously (67,71). HRP-conjugated anti-mouse IgG and anti-rabbit IgG secondary antibodies were purchased from Sigma.

Virion release and quantification.

For quantifying virions released from transfected UT7/Epo-S1 cells, M20 and $M20^{11KO}$ were electroporated with *Sal* I-linearized DNA. For quantifying virions released from B19V-infected $CD36^+$ EPCs, shRNA-transduced $CD36^+$ EPCs were infected with B19V. The cells were washed at 3 hr post-infection and cultured under hypoxia. At 3 days post-electroporation, or post-infection, 200 μl of supernatant from each cell sample was collected and treated with Benzonase® Nuclease (250 U/ml) at 37°C for 2 hr. 10 mM EDTA was added to stop the reaction, followed by proteinase K treatment. The nuclease digestion resistant viral genome was extracted using DNeasy Blood & Tissue kit (Qiagen, Germantown, MD), following the manufacturer's instructions. Finally, the recovered viral DNA was resuspended into 200 μl of DNase-free H_2O, and was quantified by qPCR for viral genome copies (vgc), as described previously (77).

Biolayer interferometry.

Biolayer interferometry was used to calculate the binding affinities of RBM38 with ISE2-WT and ISE2-mut1 RNA sequences, as reported earlier (157,158). Briefly, biotinylated RNA was mounted on Streptavidin biosensors (#18-5019, Forte Bio Inc. Fremont, CA) and then equilibrated with RNA binding buffer (20 mM Tris-HCl, pH 7.4, 80 mM NaCl), and then dipped into buffer containing RBM38 protein at different concentrations to calculate the binding parameters; K_{ass}(association rate constant), K_{diss}(dissociation rate constant) and K_D was calculated using Blitz Pro software.

Cell cycle analysis.

BrdU incorporation assay was used to determine the percentage of cell population in S-phase, followed by flow cytometry, as described previously (70,78).

Lentivirus production.

Lentiviruses were produced according to the instructions provided by Addgene (http://www.addgene.org/tools/protocols/plko) and purified as described previously (17). Cells were transduced with lentiviral vector at a MOI of ~5 transduction units/cell, as described previously (17).

Purification of GST- and 6×histine (His)-tagged RBM38 proteins.

Bacterially optimized RBM38 ORF was cloned either in pGEX-4T-3 vector with GST encoding sequence at 5' end or in pET30a (+) vector between *Nde* I and *Xho* I restriction sites to express GST-RBM38 and RBM38-His proteins, respectively. The resulting plasmids were transformed into bacterial strain BL21 (DE3) pLysS (Promega, Madison, WI). To induce the protein expression, isopropul-D-1-thiogalactopyranoside (IPTG) was added to bacterial culture at OD_{600} = 0.6 at a final concentration of 0.5 mM and the culture was grown for another 2-3 hr at

37ºC. GST-RBM38 protein was purified as described previously (191). For the purification of RBM38-His, the cells were pelleted down and resuspended into lysis buffer (50 mM Tris, pH 7.4, 150 mM NaCl, 2 mM dithiothriotol [DTT], 5mM CHAPS, 1% Triton-X100 and 1X-protease inhibitor cocktail [Sigma]). The lysate was further sonicated, centrifuged and passed through 0.45 μM filter (Thermo). The cleared lysate was mixed with Ni-NTA beads (Qiagen) and loaded onto a column. The beads were equilibrated with lysis buffer and then washed with lysis buffer, followed by three washes of lysis buffer containing imidazole at 20, 30, and 40 mM. During all washing steps, NaCl concentration was raised to 500 mM. The bound protein was eluted with elution buffer (50 mM Tris, 500 mM NaCl, 0.05% Triton X-100 and 250 mM imidazole). The eluted protein was dialyzed against Tris buffer (20 mM Tris pH 7.4, 100 mM NaCl), concentrated, quantified, aliquoted and stored at -80ºC.

Statistics.

Statistical analysis was done using Graphpad Prism Version 7.0. Error bars represent mean and standard deviation (Mean ± SD) and statistical significance (P values) were determined by using student t test. $p>0.05$, no statistical significance (n.s.); ** denotes $p<0.01$, *** denotes $p<0.001$, **** denotes $p< 0.0001$.

Results

Intronic splicing enhancer 2 (ISE2) specifically interacts with RBM38 protein.

Our previously published results demonstrated that intronic splicing enhancer 2 is critical for the recognition of D2 site for splicing (52). In an *in-silico* analysis of the B19V ISE2 RNA sequence, we found that ISE2 harbors a 5'-UGUGUG-3' motif, a consensus sequence that binds SUP12, an RBM38 ortholog in *C. elegans* (192-194). We then asked whether RBM38 interacts with ISE2 element of the B19V pre-mRNA. We synthesized WT ISE2 (ISE2-WT) RNA and a mutant ISE2 (ISE2-mut1) RNA that is identical to the ISEm3 mutation sequence and has been shown to abolish splicing of B19V pre-mRNA at D2 donor site (52) (**Fig. 3-2A**) and labeled them with biotin at their 5' ends. Upon incubation of the two RNA molecules with UT7/Epo-S1 nuclear lysates in presence of poly-I: C, we performed a pulldown assay, using streptavidin-coated beads that bound biotinylated RNA molecules. Upon several washings, the pulled down proteins were run on SDS-PAGE for Western blotting. We found that ISE2-WT pulled down RBM38, whereas ISE2-mut1 didn't (**Fig. 3-2B**, upper panel). Similarly, we mutated only the RBM38 binding motif within ISE2 (ISE2-mut2) (**Fig. 3-2A)** and performed a pull-down assay. Like ISE2-mut1, ISE2-mut2 also didn't pull down RBM38 (**Fig. 3-2B**, lower panel). Next, we purified GST-tagged RBM38 for *in vitro* binding assays. ISE2-WT RNA was synthesized *in vitro* and radio-labelled with ^{32}P. ^{32}P-labelled hot RNA was incubated with either GST (**Fig. 3-2C**, lane 2) or increasing concentrations of the GST-RBM38 (**Fig. 3-2C**, lane 3-7), and the mixtures were run on native gel for gel shift assay. It is evident that RBM38 bound ISE2-WT (**Fig. 3-2C**). In order to confirm whether the interaction is specific, we co-incubated GST-RBM38 and hot ISE2-WT either with molar excess of cold ISE2-WT or cold ISE2-mut1. Our results showed that only ISE2-WT, but not ISE2-mut1, competed with hot-ISE2 WT (**Fig. 3-2C,**

lane 11 *vs* 12). Further on, to determine the binding affinity of RBM38 with ISE2, we purified 6×histine(His)-tagged RBM38 (**Fig. 3-2D**). We synthesized biotinylated ISE2-WT or ISE2-mut1, and performed *in vitro* binding assay using biolayer interferometry. The sensograms showed the binding kinetics of RBM38 with ISE2-WT at different protein concentrations (**Fig. 3-2E**). Upon comparing binding affinities of RBM38 with either WT or mutant ISE2, the results showed that ISE2-WT bound RBM38 with a high affinity (91.5 ± 5.15 nM) as compared to ISE2-mut1 (597.8 ± 5.23 nM) (**Fig. 3-2F**). Values for association and dissociation kinetics are also provided (**Fig. 2G**). In conclusion, our results demonstrated that RBM38 binds specifically with the ISE2 sequence of B19V pre-mRNA, but not the ISE2-mutated sequence (ISEm3 or ISE2-mut1) that did not facilitate B19V pre-mRNA splicing at D2 donor site in cells (52).

RBM38 is expressed during the middle stage of erythroid progenitor development and knockdown of RBM38 significantly decreases splicing of B19V pre-mRNA at the D2 donor.

It has been reported earlier that RBM38 regulates splicing during erythroid differentiation process (195). We then looked into the expression levels of RBM38 during erythroid developmental stages. Hematopoietic stem cells were cultured from day-4 until day-14, and the cells were collected each day for Western blot analysis of RBM38. As shown in **Fig. 3-3A**, RBM38 expression increased from day-5 through day-12, which is highly coordinated and consistent with the time course of B19V infection during erythropoiesis (147).

Next, using lentiviral system, we knocked down RBM38 in UT7/Epo-S1 cells using RBM38 shRNA (shRBM38-1, 2, 3, or 4) expressing lentiviruses, and in $CD36^{+}$ EPCs using shRBM38-1&3 expressing lentiviruses (**Fig. 3-3B**). RBM38 was successfully knocked down (>90% reduction) in both types of cells. Since B19V replication is dependent on the cellular DNA replication machinery (68,96), we asked whether knockdown of RBM38 has any impact on

cell cycle progression. Using BrdU incorporation assay, we determined the percentage population of cells in S-phase. Our results demonstrated that RBM38 knockdown didn't obviously alter the cell proliferation of $CD36^+$ EPCs (**Fig. 3-3C&E**) and UT7/Epo-S1 cells (**Fig. 3-3D&F**).

As RBM38 binds ISE2 under *in vitro* conditions, we next asked whether RBM38 knockdown affects the splicing efficiency at D2 site. UT7/Epo-S1 and RBM38-knocked down UT7/Epo-$S1^{RBM38KD}$ cells were transfected with M20 B19V infectious DNA, and the cells were collected after 48 hr post-transfection for total RNA extraction, followed by RNase protection assay. Radiolabeled 234-nt long D2 probe was generated and used to detect unspliced and spliced RNAs at D2 site (**Fig. 3-4A**). The result showed that RBM38 knockdown decreased the efficiency of B19V pre-mRNA splicing at D2 donor site (**Fig. 3-4B**, lane 3). Splicing events at D2 decreased by 61.1% (**Fig. 3-4C**), while unspliced RNA remained unaffected (**Fig. 3-4D**). Since D1 donor site isn't flanked by any RBM38 binding motif, as a control, we performed an additional RNase protection assay using D1 probe **(Fig. 3-4E)** to confirm that RBM38 knockdown didn't affect splicing at D1 **(Fig. 3-4F).** In conclusion, our results demonstrated that RBM38 is one of the *trans*-acting factors required for efficient splicing of B19V pre-mRNA at D2 site.

RBM38 determines 11-kDa expression during B19V replication.

Splicing of B19V pre-mRNA at D2 site is essential for generation of both viral mRNA transcripts encoding VP2 and 11-kDa proteins (**Fig. 3-1B**). As RBM38 knockdown decreased splicing efficiency of B19V pre-mRNA at D2 site, we asked whether such a decrease affects VP2 and/or 11-kDa expression at the protein or the mRNA level. To this end, $CD36^+$ EPCs were infected with B19V, and UT7/Epo-S1 cells were transfected with M20 infectious clone. The

cells were collected at 48 hr post-infection or transfection for Western blot analysis. The result showed that 11-kDa, but not VP1 and VP2, was significantly decreased in both B19V-infected $CD36^+$ EPCs and M20-transfected UT7/Epo-S1 cells upon RBM38 knockdown (**Fig. 3-5A**, left and right panels, respectively). We then followed up to analyze viral RNAs extracted as total RNA samples at 48 hr post-transfection, using reverse-transcription (RT)-qPCR that were specifically designed to detect 11-kDa and VP2 mRNAs **(Fig. 3-5B),** as reported earlier (77). The RT-qPCR analyses showed that knockdown of RBM38 in UT7/Epo-S1 cells significantly decreased 11-kDa mRNA levels by 6.6-fold (**Fig. 3-5C**) but the level of VP2 mRNA remained unaffected (**Fig. 3-5D**). Also, there was no obvious change in the levels of NS1-encoding and VP2-encoding mRNAs (**Fig. 3-5E&F**). RT-qPCR analyses of viral RNA samples extracted from B19V-infected cells revealed similar results (data not shown).

RBM38 knockdown decreases B19V DNA replication and the virion release.

Next, we asked whether RBM38 knockdown affects virus replication. To this end, $CD36^+$ EPCs were transduced with scramble shRNA (shScram) and shRBM38-expressing lentiviruses, and were infected with B19V at 48 hr post-transduction. The cells were collected at 48 hr post-infection for determining viral DNA replication and virion release. Surprisingly, our results showed that RBM38 knockdown significantly decreased both viral DNA replication (**Fig. 3-6A&B**) and virion production (**Fig. 3-6C**). Similarly, M20-transfected RBM38 knockdown cells also showed a decrease in virion production (**Fig. 3-8A**, compare groups 1&4) and virus DNA replication (**Fig. 3-8B**, compare lanes 1&4), as compared to those from WT M20-transfected control UT7/Epo-S1 cells.

Thus, our results demonstrated that RBM38 plays an important role in viral DNA replication and virion release during B19V infection of $CD36^+$ EPCs as well as in transfection of the B19V duplex genome in UT7/Epo-S1 cells.

11-kDa protein enhances B19V DNA replication and the virion release.

As knockdown of RBM38 decreases 11-kDa expression, we investigated the role of 11-kDa in viral DNA replication and virion release. We first constructed an 11-kDa-null M20 mutant ($M20^{11KO}$) by silently mutating the three potential AUG sites in the ORF of 11-kDa (**Fig. 3-7A**). We confirmed that $M20^{11KO}$ didn't affect the expression of NS1, VP1, and VP2 (**Fig. 3-7B**).

To determine whether 11-kDa expression has an impact on virus replication, M20 and $M20^{11KO}$ clones were transfected into UT7/Epo-S1 cells. At 48 hr post-transfection, cells were collected for extraction of Hirt DNA samples which were subsequently subjected to Southern blot analysis. As shown in **Fig. 3-7C&D**, replication of $M20^{11KO}$ is significantly poor than that of the WT M20. At 72 hr post-transfection, the media of the transfected cells were collected, subjected to DNase I treatment, and further used to quantify the released virions. As shown in **Fig. 3-7E**, $M20^{11KO}$-transfected cells had a significant decrease in the released virions, compared with these WT M20-transfected cells. Collectively, these results strongly supported that 11-kDa augments B19V DNA replication and virion release.

Decreased 11-kDa protein expression in RBM38 knocked down cells contributes to the reduced viral DNA replication and virion release.

In order to confirm whether RBM38 knockdown decreased viral DNA replication *via* 11-kDa inhibition, we generated 11-kDa expressing lentivirus to transduce UT7/Epo-S1 cells. UT7/Epo-S1 cells were transfected with M20 and $M20^{11KO}$, and 11-kDa-expressing UT7/Epo-S1

cells were transfected with $M20^{11KO}$. At 72 hr post-transfection, supernatant and cells were collected and examined for virion release and DNA replication, respectively. The results show that 11-kDa complementation to $M20^{11KO}$-transfected cells significantly enhanced virion release (**Fig. 3-8A**, compare groups 2&3) and virus DNA replication (**Fig. 3-8B**, compare lanes 2&3). Similarly, RBM38 knocked down UT7/Epo-$S1^{RBM38KD}$ cells and 11-kDa-expressing UT7/Epo-$S1^{RBM38KD}$ cells were transfected with M20. At 72 hr post-transfection, supernatants and cells were collected and examined for virion release and virus DNA replication, respectively. Obviously, we observed that both virion release (**Fig. 3-8A**, compare groups 4&5) and virus DNA replication (**Fig. 3-8B**, compare lanes 4&5) were significantly higher in 11-kDa-expressing UT7/Epo-$S1^{RBM38KD}$ cells than those in non-11-kDa-expressing UT7/Epo-$S1^{RBM38KD}$ cells. Overall, the complementation of 11-kDa in UT7/Epo-$S1^{RBM38KD}$ cells recovered ~60% of the function of 11-kDa in virion release and viral DNA replication during transfection of the M20 clone.

Taken together, these results confirmed that RBM38 plays an important role in B19V viral DNA replication and virion release through regulation of the 11-kDa expression.

Discussion

Parvoviruses with the limited genome size use alternative splicing and alternate polyadenylation to maximize the coding capacity of their genome. B19V pre-mRNA splicing at the D2 donor site is critical for the production of VP2- and 11-kDa encoding mRNAs (52). However, the remained unspliced mRNAs constitute NS1, 7.5-kDa and VP1 encoding mRNAs. B19V tightly regulates pre-mRNA splicing at D2 to maintain the variable expression levels of all the five viral proteins. Alternative splicing of pre-mRNA is regulated by both *cis*-acting elements and *trans*-acting factors that regulate splicing both positively and negatively (196). In the case of B19V pre-mRNA splicing at D2, we have earlier identified an ISE2, a *cis*-acting element that facilitates the recognition of D2 donor for splicing (52). In this study, we show that ISE2 is essential for the expression of viral 11-kDa protein. A cellular *trans*-acting factor, RBM38, binds ISE2 and regulates splicing at D2 site. Knockdown of RBM38 decreased splicing of B19V pre-mRNA at D2, which particularly affects the splicing from D2 donor to A2-2 acceptor sites that decreases level of mRNAs for encoding 11-kDa protein (**Fig. 3-1B**, R8&R9). Importantly, we show that 11-kDa protein augments viral DNA replication and virion release and that RBM38 promotes B19V replication *via* the 11-kDa regulation.

RBM38 binds to ISE2 and regulates splicing at D2 site and therefore 11-kDa expression.

During alternative splicing, the splice donor sites are usually weak, and are regulated by the interplay of positive and negative *cis*-acting elements and *trans*-acting factors (196). Splicing of B19V pre-mRNA at D2 generates either VP2 or 11-kDa encoding mRNAs, while as unspliced mRNAs at D2 encode NS1, VP1, and 7.5-kDa proteins (**Fig. 3-1**, R1, R2, R4&R5). It is obvious that D2 splicing needs to be regulated in such a way that expression of all the five proteins is maintained at an optimal ratio. We identified at least two *cis*-elements: exon splicing enhancer 3

(ESE3) and ISE2 that regulate D2 splicing (52). While looking for other *trans*-acting factors, we observed that ISE2 carries a 5'-UGUGUG-3' motif that binds SUP12, an RBM38 ortholog in *C. elegans* (192-194). RBM38 is expressed during middle stage of erythroid differentiation which coincides with the time course of B19V infection **(Fig. 3-3)**. Using RNA pulldown assay, gel shift assay and biolayer interferometry (**Fig. 3-2**), our results showed that RBM38 specifically binds to ISE2 RNA under *in vitro* conditions, and the ISE2-mutated sequence (ISEm3 or ISE2-mut1), which did not facilitate splicing of B19V pre-mRNA at D2 donor site (52), also did not specifically bind RBM38. Knockdown of RBM38 in M20-transfected UT7/Epo-S1 cells decreased splicing efficiency at D2 site. Surprisingly, the decrease in D2 splicing affected only mRNAs encoding 11-kDa, but not VP2-encoding mRNAs (**Fig. 3-5**), which implies that RBM38 promotes the splicing of the second intron from D2 to A2-2 sites. It is possible that other ESE3- or ISE2-binding factor(s) might be responsible for the splicing of the second intron from D2 to A2-1 sites, which remains further investigation in the future. The complex interplay between *cis*-acting elements surrounding D2 site and *trans*-acting factors, at least the RBM38, determine the splicing of the second intron and eventually the production of VP2, and 11-kDa proteins. Of note, there are at least other five 5'-UGUGUG-3' motifs in B19V pre-mRNA sequence, among which two sites follow the D2' cryptic donor. We have previously reported that B19V uses a cryptic donor D2', when D2 site is mutated (52). The cryptic donors might also need RBM38, since it is followed by similar two 5'-UGUGUG-3' motifs.

11-kDa protein enhances B19V DNA replication and the virion release from infected cells.

It has been reported that 11-kDa helps in capsid production and viral infectivity (61). We asked whether 11-kDa plays any other roles in virus replication. Our results show that 11-kDa augments viral DNA replication and virion release (by ~7-10-fold). We have previously reported

that erythropoietin (EPO) signaling is essential for B19V replication (17). EPO binds EPO receptor, activates JAK2-STAT5 and MEK/ERK pathways (89). We also have demonstrated that ERK pathway negatively regulates B19V replication (18), whereas STAT5 phosphorylation is critical for viral DNA replication (78). 11-kDa protein has been shown to interact with growth factor receptor-bound protein 2 (Grb2) *via* its proline rich region, a Src homology-3 (SH3)-like ligand (90). Grb2 is an adaptor protein that interacts with Ras guanine exchange factor-SOS *via* its SH3 domain, thereby activates MAPK/ERK signal transduction pathway (197). Since MEK/ERK pathway impedes B19V replication (18), we speculate that B19V uses 11-kDa interaction with Grb2 to disrupt MEK/ERK signaling to promote virus replication. On the other hand, during B19V infection, viral DNA replication (136), NS1 (65) and 11-kDa (71) induce death of erythroid progenitors. In this study, we examined the role of RBM38 in 11-kDa production and its outcomes in context of virus replication. It is possible that the contribution of 11-kDa to B19V induced cell death can also be modulated *via* RBM38 regulation. Whether 11-kDa mediated cell death plays any role in virion release, needs further investigation.

RBM38 functions as an essential host factor for B19V infection.

RBM38 is an RNA recognition motif (RRM)-containing RNA binding protein, a largest family of RNA binding proteins (198,199). Diverse roles have been attributed to RBM38 ranging from RNA stability (200), mRNA translation (201,202) to regulation of splicing during erythroid differentiation (195). In case of B19V, we didn't observe any change in the expression levels of NS1, VP1 and VP2 upon knockdown of RBM38 (**Fig. 3-5**), therefore, it is less likely that RBM38 regulates viral mRNA stability and translation during virus infection. The RBM38 ortholog SUP12 regulates splicing of various genes in *C. elegans* (192-194). Here we identified RBM38 as one of the *trans*-acting factors that binds to ISE2, promoting splicing of the second

intron from D2 to A2-2 sites that favors the expression of 11-kDa. We show mechanistically how B19V uses cellular host factor (RBM38) for its efficient replication. The RBM38 expression during the stages when the cells are highly susceptible to B19V infection renders it as one of the determinants of B19V tropism. Our hypothetical model for D2 splicing of B19V pre-mRNA is that RBM38 binding to ISE2 activates the recognition of the D2 site with the A2-2 acceptor site (**Fig. 3-9**). Since U2 small nuclear ribonucleoprotein (snRNP) recognizes both A2-1 and A2-2 sites, we speculate that after binding ISE2 element, RBM38 interacts with A2-2 acceptor site *via* an unknown mediator M3 that specifically binds A2-2 acceptor site (**Fig. 3-9**, M3). We further investigated other host factors that bind ISE2 region. Our mass spectrometry analysis showed that ISE2 interacts with at least 20 other splicing-related factors **(**data not shown**).** These candidates need further to be investigated for their role in B19V pre-mRNA splicing. Our overall hypothesis is that the two *cis*-acting elements flanking D2 site, i.e., ESE3 and ISE2, with the help of *trans*-acting factors regulate the expression of at least two viral proteins (VP2 and 11-kDa) during B19V replication. Identification of such *trans*-acting factors will eventually reveal the entire scenario of how the D2 donor plays the central role in the processing of B19V pre-mRNA, which will identify new targets to check B19V infection.

Fig. 3-1. B19V transcription map.

(A) B19V genome. Linear single-stranded B19V genome is shown in negative sense with unpaired or mismatched bases diagramed as bulges and bubbles. ITR, inverted terminal repeat. **(B) Transcription profile**. B19V duplex genome is shown at the top. P6 represents viral promoter, D1 and D2 denote splice donor sites, and A1-1, A1-2, A2-1, and A2-2 denote splice acceptor sites. Different open reading frames are shown by different colors (Red, Green, and Blue). (pA)p and (pA)d represent polyadenylation sites at proximal and distal ends, respectively. At bottom, twelve major RNAs are shown encoding different viral proteins, as indicated. Question marks indicate whether the protein is expressed from the species of mRNA is unknown. **(C) ESE3, D2 and ISE2 elements.** Donor 2 site (D2) of the B19V pre-mRNA is flanked by exon splicing enhancer 3 (ESE3) on left and intronic splicing enhancer 2 (ISE2) on right. They act as *cis*-acting elements for splicing at D2 site.

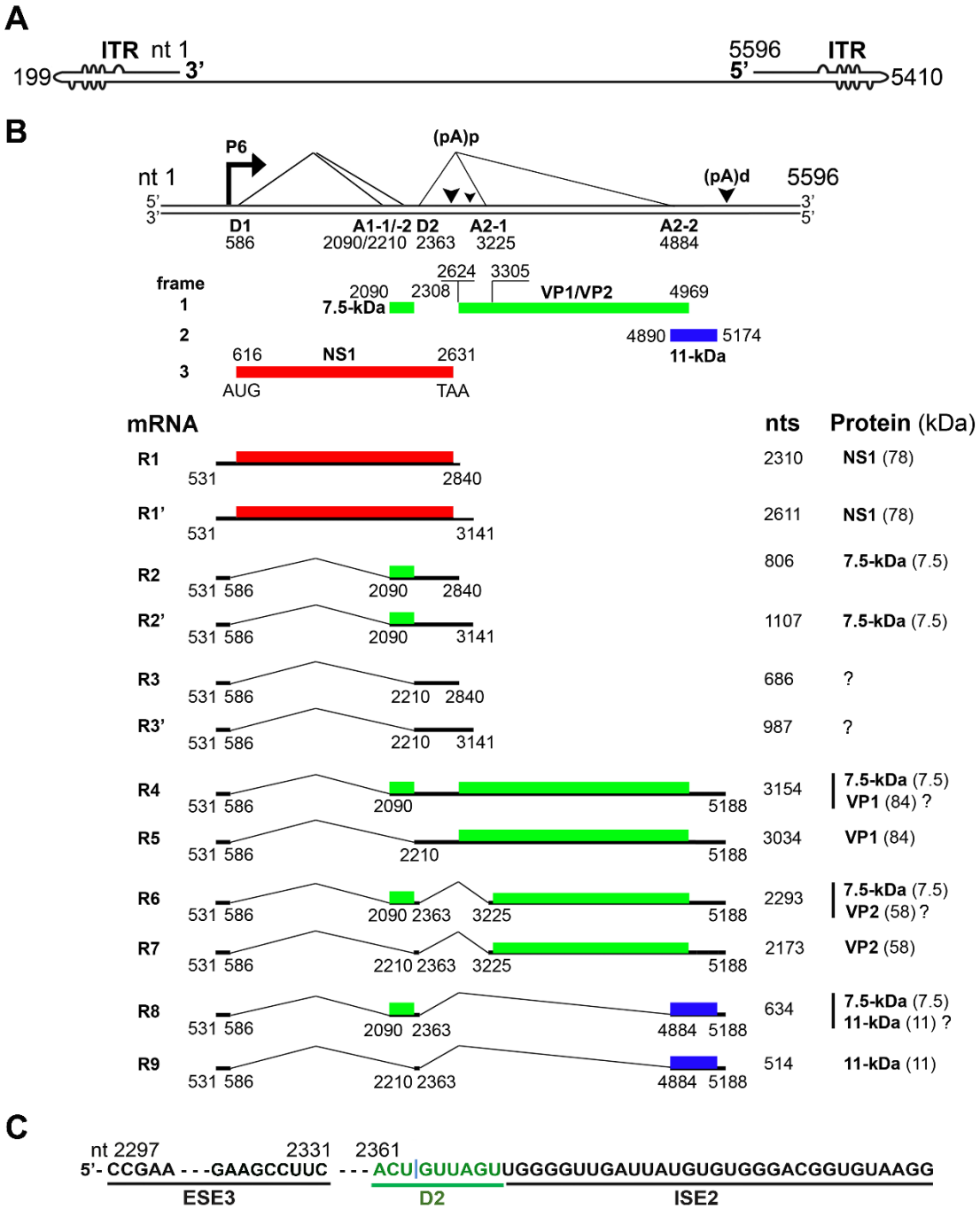
A
ITR nt 1
199
3'
5596
ITR
5'
5410
B
P6
(pA)p
nt 1
(pA)d
5596
5'
3'
3'
5'
D1
586
A1-1/-2 D2
2090/2210 2363
A2-1
3225
A2-2
4884
frame
2624
3305
2090
2308
VP1/VP2
4969
1
7.5-kDa
2
4890
5174
11-kDa
3
616
NS1
2631
AUG
TAA
mRNA
nts
Protein (kDa)
R1
531
2840
2310
NS1 (78)
R1'
531
3141
2611
NS1 (78)
R2
531 586
2090
2840
806
7.5-kDa (7.5)
R2'
531 586
2090
3141
1107
7.5-kDa (7.5)
R3
531 586
2210
2840
686
?
R3'
531 586
2210
3141
987
?
R4
531 586
2090
5188
3154
7.5-kDa (7.5)
VP1 (84) ?
R5
531 586
2210
5188
3034
VP1 (84)
R6
531 586
2090 2363
3225
5188
2293
7.5-kDa (7.5)
VP2 (58) ?
R7
531 586
2210 2363
3225
5188
2173
VP2 (58)
R8
531 586
2090 2363
4884 5188
634
7.5-kDa (7.5)
11-kDa (11) ?
R9
531 586
2210 2363
4884 5188
514
11-kDa (11)
C
nt 2297
2331
2361
5'- CCGAA - - -GAAGCCUUC - - - ACU|GUUAGUUGGGGUUGAUUAUGUGUGGGACGGUGUAAGG
ESE3
D2
ISE2

Fig 3-1

Fig. 3-2. ISE2 specifically binds RBM38 protein under *in vitro* conditions.

(A) ISE2 wild-type (ISE2-WT) and ISE2 mutants (ISE2-mut1/2) RNA sequence. These two RNAs shown were used in the following binding experiments. **(B) Pulldown assay.** Biotinylated ISE2-WT and ISE2-mut1/2 were incubated with UT7/Epo-S1 nuclear lysates in presence of poly-I:C and then pulled down using streptavidin beads followed by several washings. The RNA-bound proteins were eluted and run on SDS-PAGE for Western blotting and detected with an anti-RBM38 antibody, as indicated. UT7/Epo-S1 nuclear lysate was run in lane 1 as control. **(C) Gel shift assay.** Radioactively labelled ISE2-WT was incubated with either purified GST (lanes 2 and 9) or increasing concentrations (5, 10, 50, 100, and 300 nM) of purified GST-RBM38 (lanes 3-7, respectively) and run on native gel and then examined for shift (left panel). Similarly, GST-RBM38 was incubated with hot ISE2-WT in absence (lane 10) or presence of excess amounts of cold ISE2-WT (lane 11) and cold ISE2-mut1 (lane 12) for competition assay (right panel). Only RNA was run as controls in lanes 1 and 8) **(D) RBM38-His purification.** RBM38-His was purified, as described in Materials and Methods, and 6 μg of protein was run on SDS-10%PAGE and then stained with Coomassie brilliant blue dye. **(E-G) Biolayer Interferometry**. (E) BLI sensograms showing overtime association and dissociation of RBM38 protein with ISE2-WT at different concentrations. (F) Comparison of binding affinities of RBM38 protein (1 μM) with ISE2-WT and ISE2-mut1 RNA molecules. (G) Binding parameters to calculate K_D values (ratio of dissociation and association rate constants). Experiments were repeated at least three times for calculating the means and standard deviations.

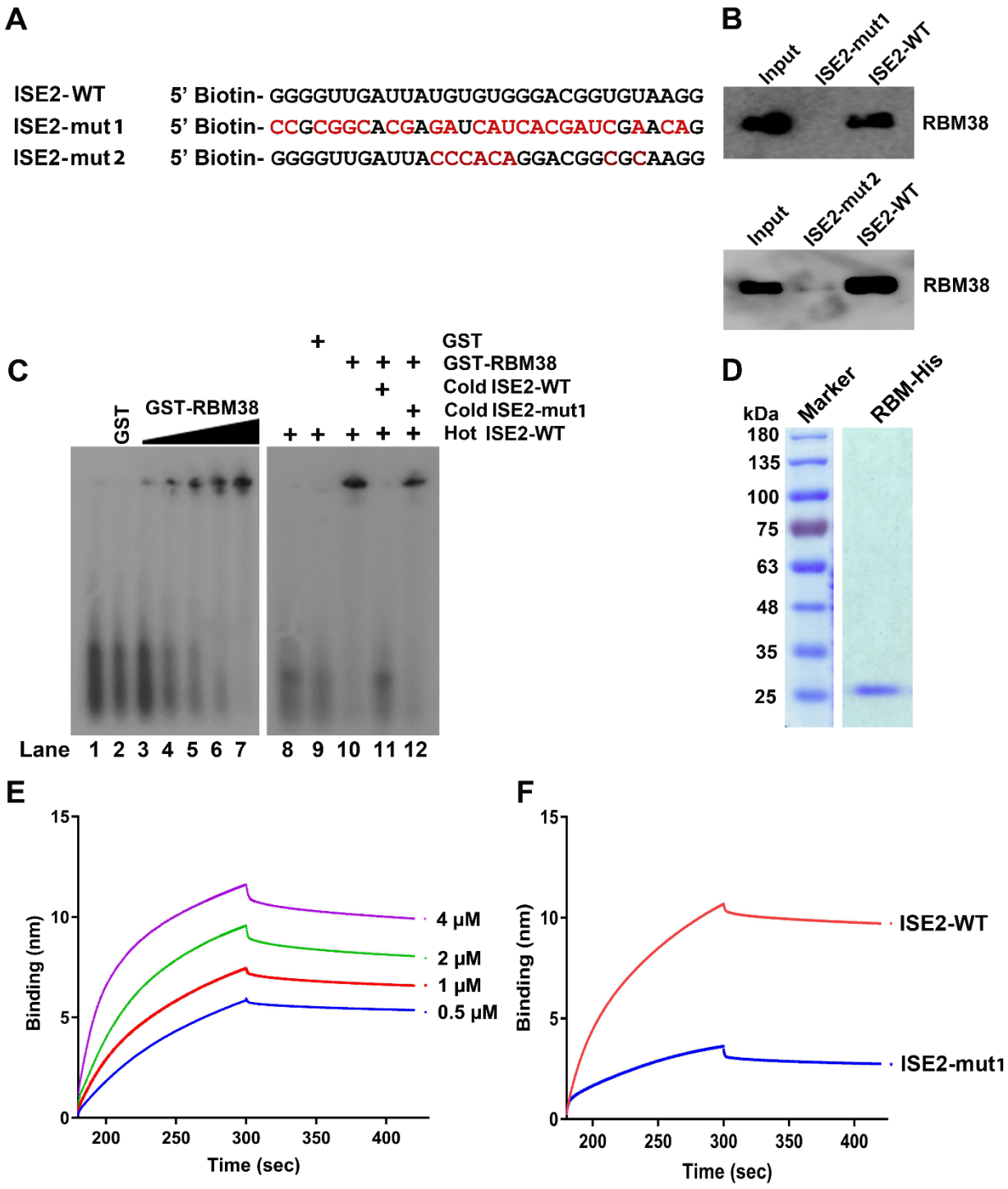

G Binding parameters for the interaction of RBM38 with ISE2 or ISE2-mut1 using BLitz

RNA-Type	RBM38	K_D (nM) ± SD	K_{ass} (M^{-1} s^{-1})	K_{diss} ($M^{-1}s^{-1}$)
ISE2-WT	1 μM	91.5 ± 5.15	1.609×10^4	1.407×10^{-3}
ISE2-mut1	1 μM	597.8 ± 5.23	6.288×10^3	3.748×10^{-3}

Fig 3-2

Fig. 3-3. RBM38 is expressed during middle phase of erythropoiesis and its knockdown doesn't alter cell cycle progression.

(A) RBM38 expression during erythroid differentiation process. Hematopoietic stem cells (HSC) were cultured from day-4 through day-14. Same numbers of cells were collected on each day, lysed and run for Western blot analysis. The blot was detected for RBM38 protein using an anti-RBM38 antibody and re-probed for β-actin. **(B) RBM38 knockdown**. Four lentiviruses expressing shRNAs against RBM38 were transduced into UT7/Epo-S1 cells. $CD36^+$ EPCs were transduced with shRBM38-1&3. At 3 days post-transduction, the cells were lysed for Western blot analysis using an anti-RBM38 antibody. Blots were reprobed for β-actin. **(C-F) Cell cycle analysis.** Lentiviruses expressing shRBM38-1&3 were used to generate RBM38 knocked down UT7/Epo-S1 cell line (UT7/Epo-$S1^{RBM38KD}$). $CD36^+$ EPCs were transduced with shScram or shRBM38-1&3. BrdU incorporation assay was used to track *de novo* DNA synthesis as described in Materials and Methods. The cells were processed and analyzed for cell cycle progression using flow cytometry. Representative diagrams showing cell cycle analysis in control and RBM38 knockdown $CD36^+$ EPCs **(C)** or UT7/Epo-S1 and UT7/Epo-$S1^{RBM38KD}$ cells **(D).** Relative fold change of cell population in S phase were calculated for both $CD36^+$ EPCs **(E)** and UT7/Epo-S1 cells **(F).** Each experiment was repeated three times for the calculation of means and standard deviations.

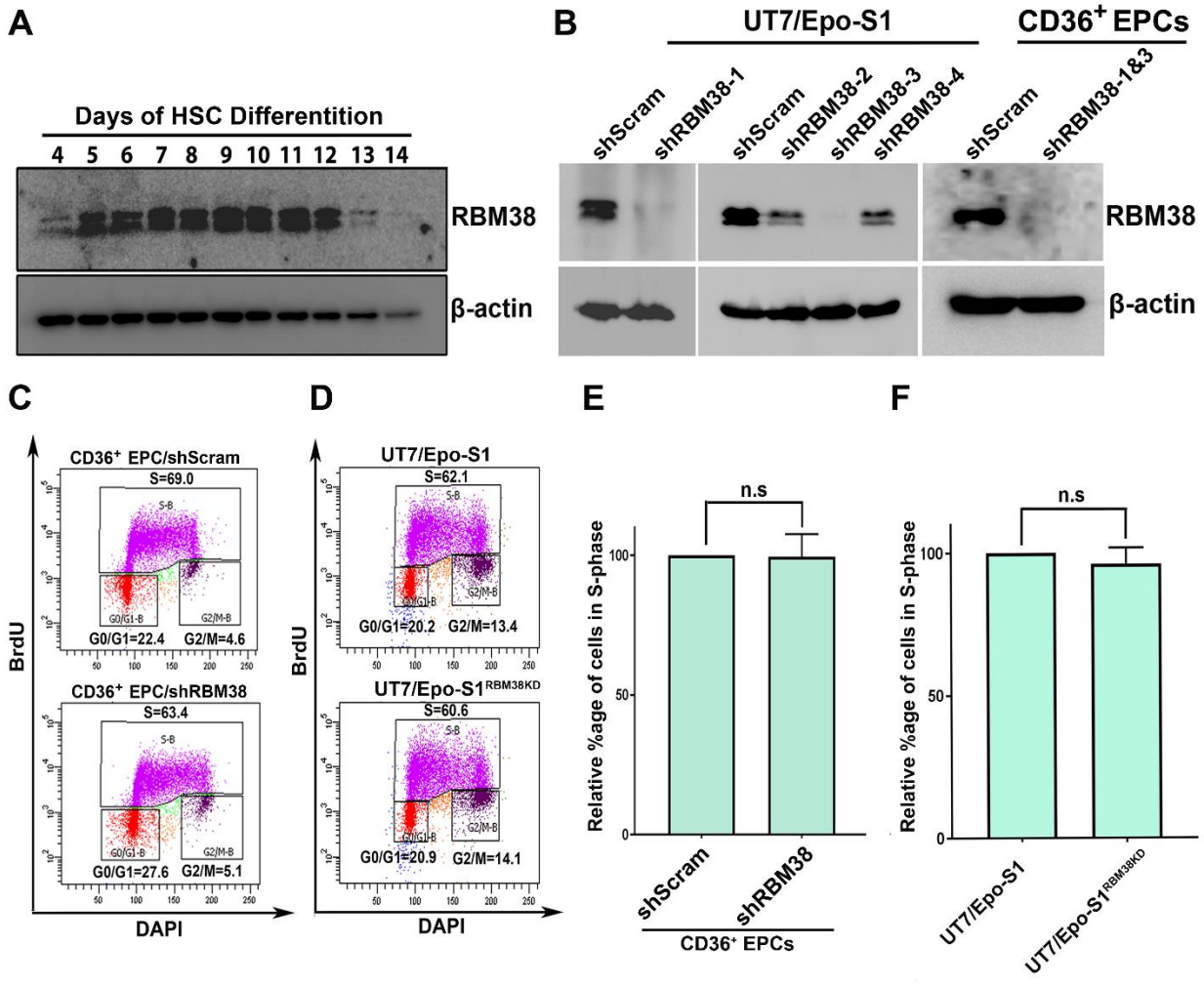
A
Days of HSC Differentition
4 5 6 7 8 9 10 11 12 13 14
RBM38
β-actin
B
UT7/Epo-S1
CD36+ EPCs
shScram
shRBM38-1
shScram
shRBM38-2
shRBM38-3
shRBM38-4
shScram
shRBM38-1&3
RBM38
β-actin
C
CD36+ EPC/shScram
S=69.0
G0/G1=22.4 G2/M=4.6
CD36+ EPC/shRBM38
S=63.4
G0/G1=27.6 G2/M=5.1
BrdU
DAPI
D
UT7/Epo-S1
S=62.1
G0/G1=20.2 G2/M=13.4
UT7/Epo-S1RBM38KD
S=60.6
G0/G1=20.9 G2/M=14.1
BrdU
DAPI
E
n.s
Relative %age of cells in S-phase
shScram
shRBM38
CD36+ EPCs
F
n.s
Relative %age of cells in S-phase
UT7/Epo-S1
UT7/Epo-S1RBM38KD

Fig 3-3

Fig. 3-4. RBM38 promotes splicing at D2 donor site.

(A) Probe designing. Schematic representation of D2 probe showing the spliced and unspliced RNA species generated upon RNase protection assay. **(B) RNase protection assay.** Normal UT7/Epo-S1 cells and RBM38 knocked down cells (UT7/Epo-S1^{RBM38KD}) were transfected with M20. At 2 days post-transfection, the cells were collected for extraction of total RNA. RNA samples were analyzed by RNase protection assay using the D2 probe which was designed to detect spliced/unspliced RNAs from the D2 site of B19V pre-mRNA, as indicated. RNase protection assay was performed as described in Materials and Methods. **(C-D) Quantification.** The detected spliced (C) and unspliced (D) RNA bands at D2 site were quantified in RBM38 knocked down cell samples and compared to normal cell samples (arbitrarily set as 100%). The experiment was repeated at least three times to calculate their means and standard deviations. **(E-F) D1 splicing.** Schematic representation of D1 probe showing the spliced and unspliced RNA species generated upon RNase protection assay (E). As described above, RNA samples were subjected to RNase protection assay using D1 probe to detect spliced/unspliced RNAs from D1 donor site (F).

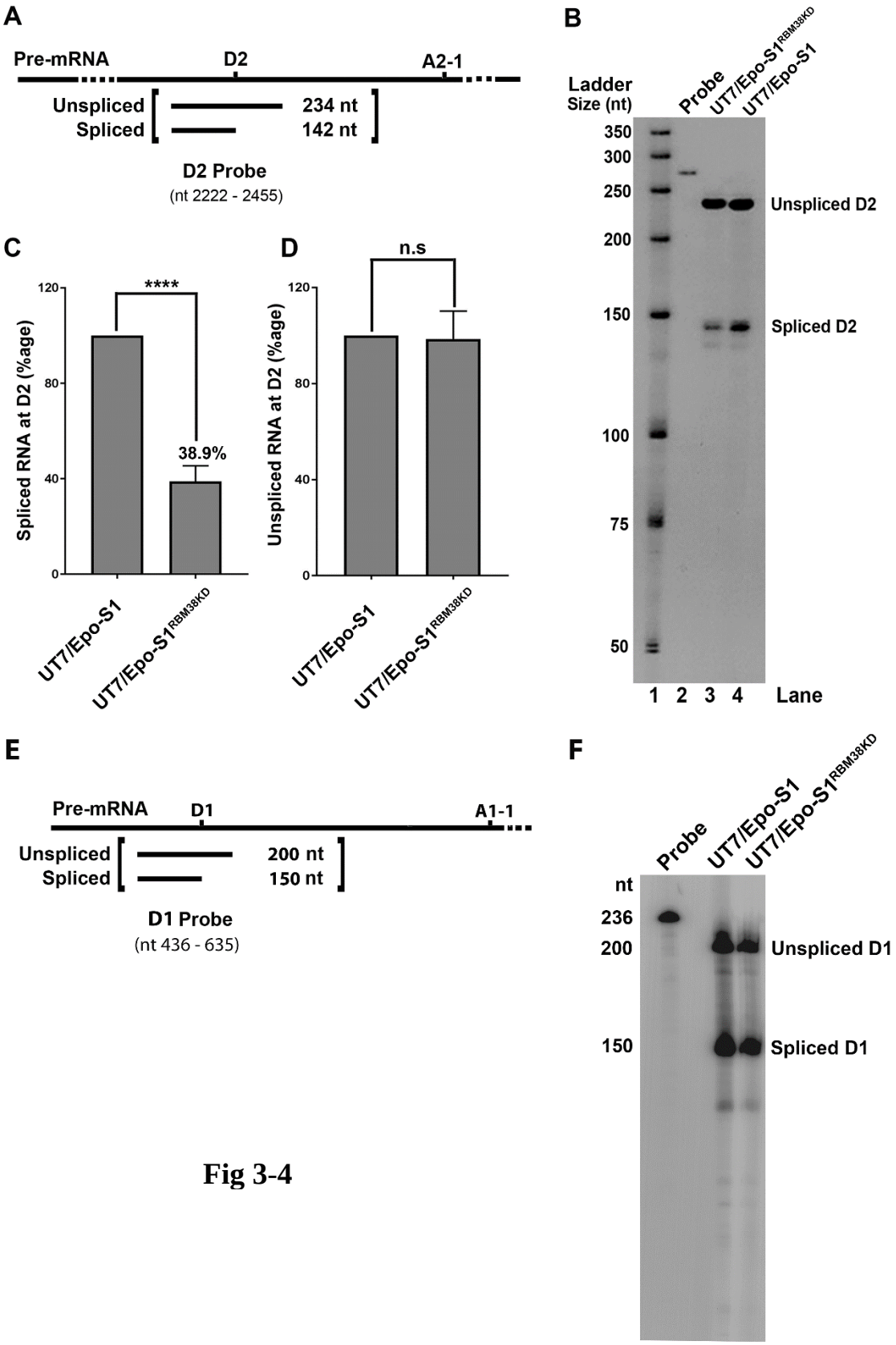
A
Pre-mRNA
D2
A2-1
Unspliced
Spliced
234 nt
142 nt
D2 Probe
(nt 2222 - 2455)
B
Ladder
Size (nt)
Probe
UT7/Epo-S1RBM38KD
UT7/Epo-S1
350
300
250
200
150
100
75
50
Unspliced D2
Spliced D2
1 2 3 4
Lane
C
Spliced RNA at D2 (%age)
****
38.9%
120
80
40
0
UT7/Epo-S1
UT7/Epo-S1RBM38KD
D
Unspliced RNA at D2 (%age)
n.s
120
80
40
0
UT7/Epo-S1
UT7/Epo-S1RBM38KD
E
Pre-mRNA
D1
A1-1
Unspliced
Spliced
200 nt
150 nt
D1 Probe
(nt 436 - 635)
F
Probe
UT7/Epo-S1
UT7/Epo-S1RBM38KD
nt
236
200
150
Unspliced D1
Spliced D1

Fig 3-4

Fig. 3-5. RBM38 regulates 11-kDa expression.

$CD36^{+}$ EPCs transduced with a scramble shRNA (shScram) and shRBM38-1&3 (shRBM38)-expressing lentiviruses were infected with B19V at 2 days post-transduction. UT7/Epo-S1 and UT7/Epo-$S1^{RBM38KD}$ cells were transfected with M20. **(A) Western blotting.** The cells were collected at 2 days post-infection or post-transfection, lysed and run for Western blotting. Immunoblots were probed for NS1, VP1/2 and 11-kDa proteins, using their respective antibodies. Blots were re-probed for GAPDH, as a loading control. **(B) Reverse Transcription (RT)-qPCR.** Specific primers and probes detecting VP2 or 11-kDa mRNA, as diagramed, were used for qPCR analysis. **(C-F) Detection of 11-kDa, VP2, NS1 and VP1 mRNAs by RT-qPCR.** At 2 days post-transfection, total RNA was extracted from UT7/Epo-S1 and UT7/Epo-$S1^{RBM38KD}$ cells. The RNA was further used to generate cDNA for the quantification of 11-kDa (C), VP2 (D), NS1 (E), and VP1 (F) mRNAs, using the RT-qPCR approach. Quantified viral mRNAs were normalized to β-actin mRNA, and mRNAs extracted from M20-transfected control UT7/Epo-S1 cells were used as controls and arbitrarily set as 1.

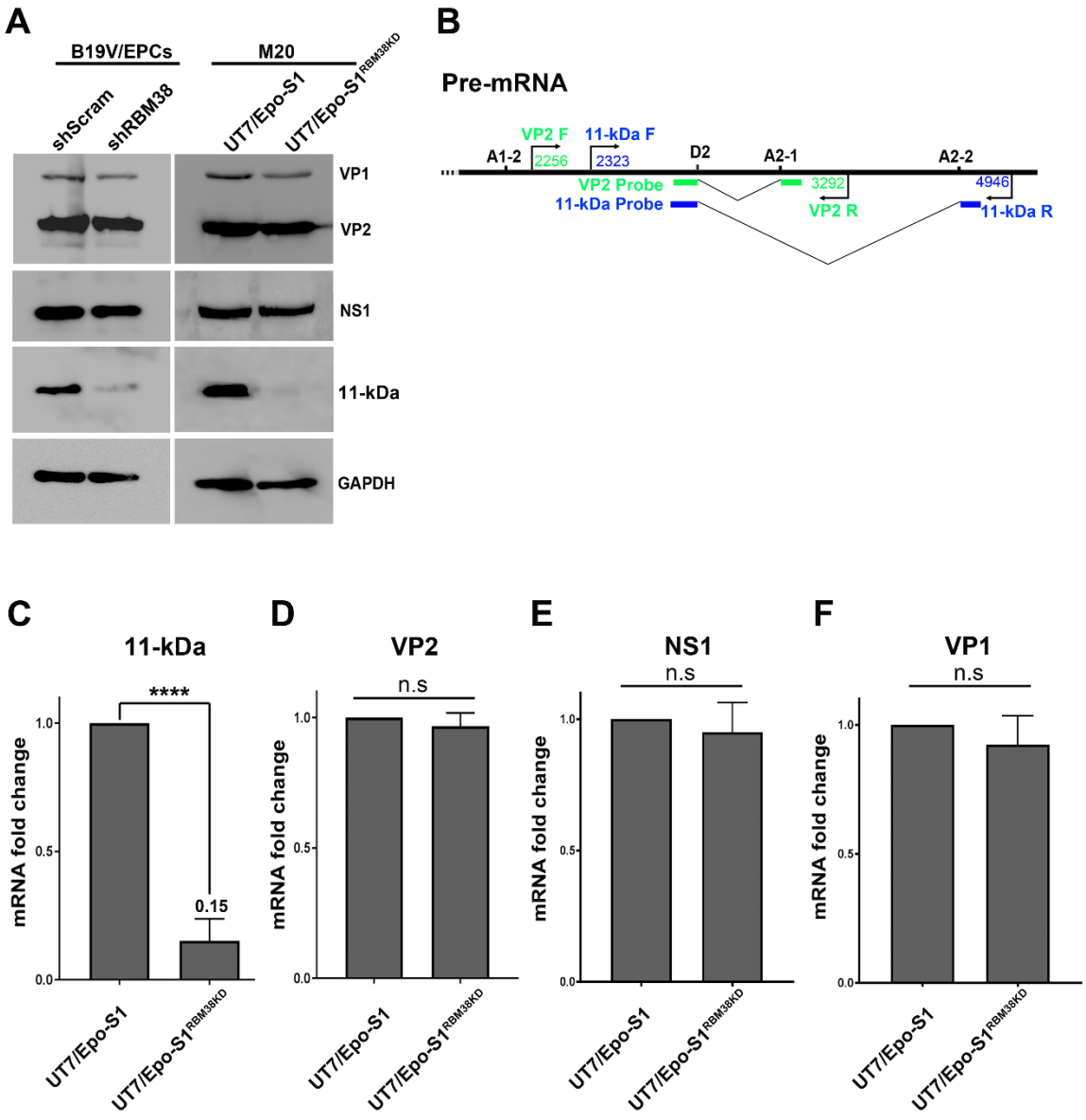
A
B19V/EPCs
M20
shScram
shRBM38
UT7/Epo-S1
UT7/Epo-S1RBM38KD
VP1
VP2
NS1
11-kDa
GAPDH
B
Pre-mRNA
VP2 F
11-kDa F
A1-2
2256
2323
D2
A2-1
A2-2
VP2 Probe
11-kDa Probe
3292
VP2 R
4946
11-kDa R
C
11-kDa
****
0.15
D
VP2
n.s
E
NS1
n.s
F
VP1
n.s
mRNA fold change
1.0
0.5
0.0
UT7/Epo-S1
UT7/Epo-S1RBM38KD

Fig. 3-5

Fig. 3-6. RBM38 knockdown decreases viral DNA replication and virion release.

$CD36^+$ EPCs were transduced with scramble shRNA (shScram) and shRBM38-1&3 (shRBM38) lentiviruses. At 2 days post-transduction, the cells were infected with B19V. **(A&B) Southern blotting.** At 2 days post-infection, the cells were collected for Southern blot analysis. (A) The blots were probed with M20 probe (upper panel) and mitochondrial DNA probe (Mito-DNA) (lower panel), respectively. dRF and mRF, double and monomer replicative forms, respectively; ssDNA, single-stranded DNA. (B) The replicated (mRF) DNA bands were quantified and plotted. **(C) Virion release.** At 3 days post-infection, the supernatants of infected cells were collected for quantification of virion released using qPCR. Results shown were average and standard deviations which were obtained from at least three independent experiments (B&C).

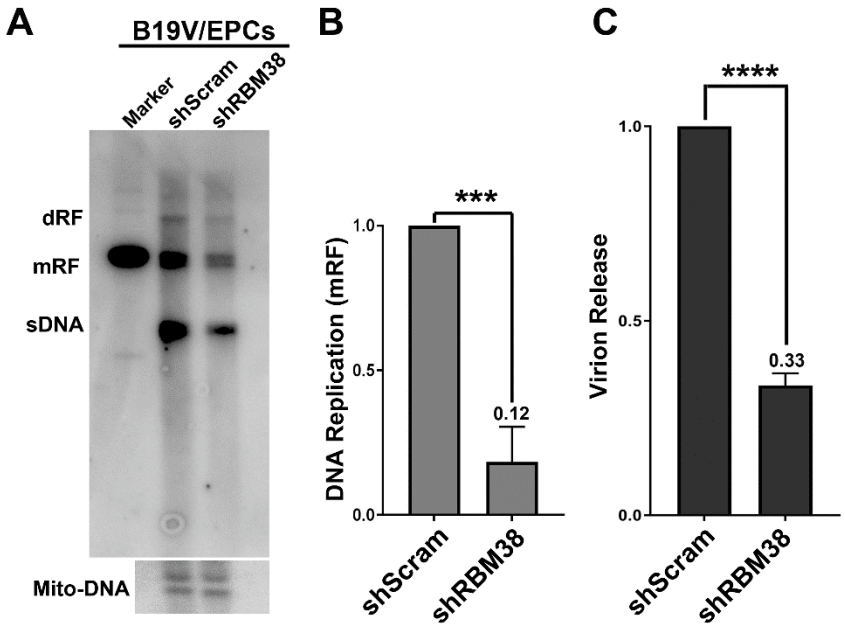
A
B19V/EPCs
Marker
shScram
shRBM38
dRF
mRF
sDNA
Mito-DNA
B
***
1.0
0.5
0.0
0.12
DNA Replication (mRF)
shScram
shRBM38
C
****
1.0
0.5
0.0
0.33
Virion Release
shScram
shRBM38

Fig. 3-6

Fig. 3-7. 11-kDa protein enhances B19V DNA replication and virion release.

(A) Diagram of M20^{11KO}. 11-kDa knockout M20 clone (M20^{11KO}) is diagramed and shown with mutations of three translation initiation codons from ATG to ACG. **(B) Western blotting**. UT7/Epo-S1 cells were transfected with M20 and M20^{11KO}, respectively. At 2 days post-transfection, cells were collected, lysed and run for Western blot analysis. The blots were detected with anti-VP1/2, NS1, 11-kDa, and GAPDH antibodies. **(C&D) Southern blotting**. UT7/Epo-S1 cells were transfected with M20 and M20^{11KO}. At 2 days post-transfection, Hirt DNA samples were extracted from transfected cells and subjected to Southern blotting. (C) The blots were probed using M20 probe (upper panel) and mitochondrial DNA (Mito-DNA) probe (lower panel), respectively. mRF, monomer replicative form DNA; ssDNA, single-stranded DNA. (D) mRF DNA bands were quantified, and the means and standard deviations was calculated from three independent experiments. **(E) Virion release.** At 3 days post-transfection, the supernatants from the transfected cells were collected and used for the quantification of virions. Virions released from M20-transfected cells were arbitrarily set as 1.

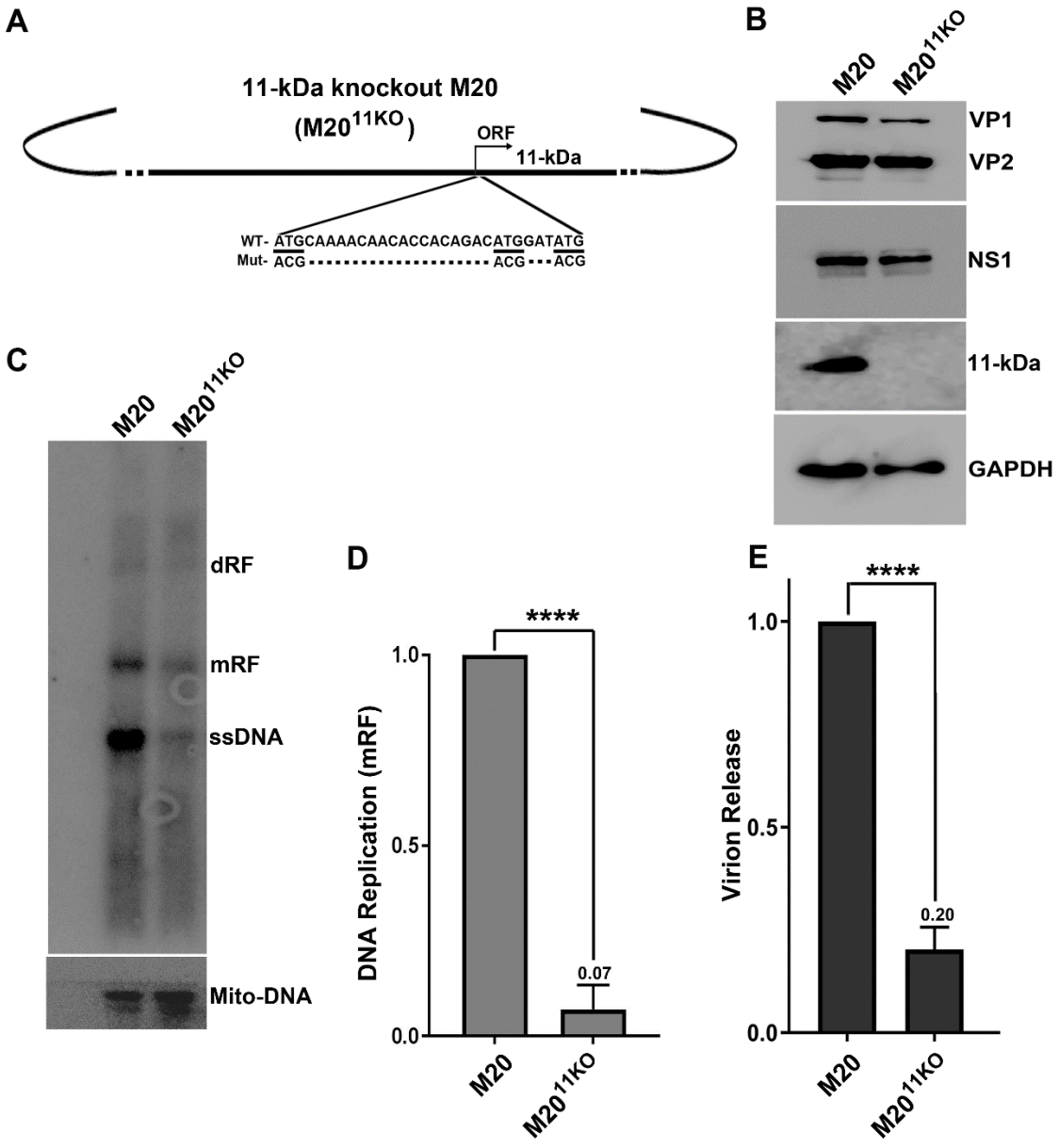
A
11-kDa knockout M20
(M20^11KO)
ORF
11-kDa
WT- ATGCAAAACAACACCACAGACATGGATATG
Mut- ACG ACG ACG
B
M20
M20^11KO
VP1
VP2
NS1
11-kDa
GAPDH
C
M20
M20^11KO
dRF
mRF
ssDNA
Mito-DNA
D
****
1.0
0.5
0.0
DNA Replication (mRF)
0.07
M20
M20^11KO
E
****
1.0
0.5
0.0
Virion Release
0.20
M20
M20^11KO

Fig. 3-7

Fig. 3-8. RBM38 knockdown deceases viral DNA replication and virion release *via* reducing 11-kDa expression.

UT7/Epo-S1 cells were transfected with M20 or $M20^{11KO}$, and 11-kDa-expressing UT7/Epo-S1 cells were transfected with $M20^{11KO}$, as indicated. UT7/Epo-$S1^{RBM38KD}$ cells or 11-kDa-expressing UT7/Epo-$S1^{RBM38KD}$ cells were transfected with M20. **(A) Virion release.** At 3 days post-transfection, the supernatant from each transfected sample were collected and used for virion quantification by qPCR. **(B) Southern blot analysis.** At 3 days post-transfection, cells were collected for Hirt DNA extraction. Hirt DNA samples were subjected to Southern blotting using M20 and Mito-DNA probes, respectively. dRF and mRF, double and monomer replicative forms, respectively; ssDNA, single-stranded DNA.

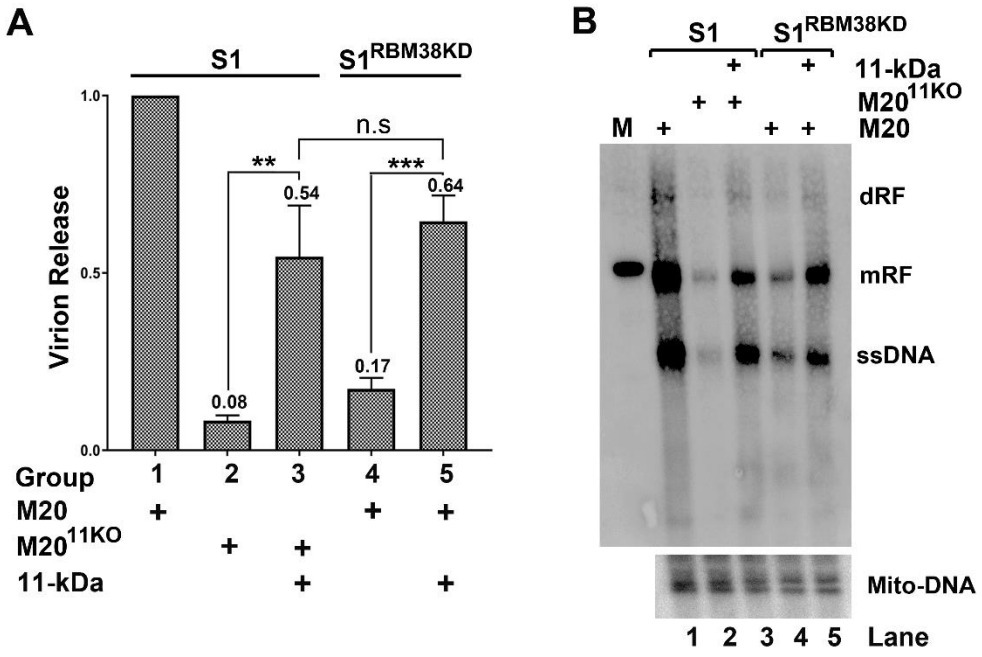
A
S1
S1RBM38KD
1.0
0.5
0.0
Virion Release
n.s
**
***
0.54
0.64
0.17
0.08
Group 1 2 3 4 5
M20 + + +
M20^11KO + +
11-kDa + +
B
S1
S1RBM38KD
11-kDa
M20^11KO
M + + + M20
dRF
mRF
ssDNA
Mito-DNA
1 2 3 4 5 Lane

Fig. 3-8

Fig. 3-9. Proposed model for the role of RBM38 in B19V pre-mRNA processing.

U1 and U2 represent U1- and U2-small nuclear ribonucleoprotein (snRNP) complexes, and M represents protein mediators associated with U1- and U2-snRNPs. RBM38 and ISE2-binding proteins (ISE2-BPs) interact with ISE2 sequence, whereas ESE3-binding proteins (ESE3-BPs) interact with ESE3 region of the B19V pre-mRNA. Both ISE2 and ESE3 and their associated *trans*-acting factors help in the recognition of D2 site, as shown by arrows. RBM38 interaction with ISE2 promotes splicing from D2 to A2-2 intron. Question marks indicate unknown factors.

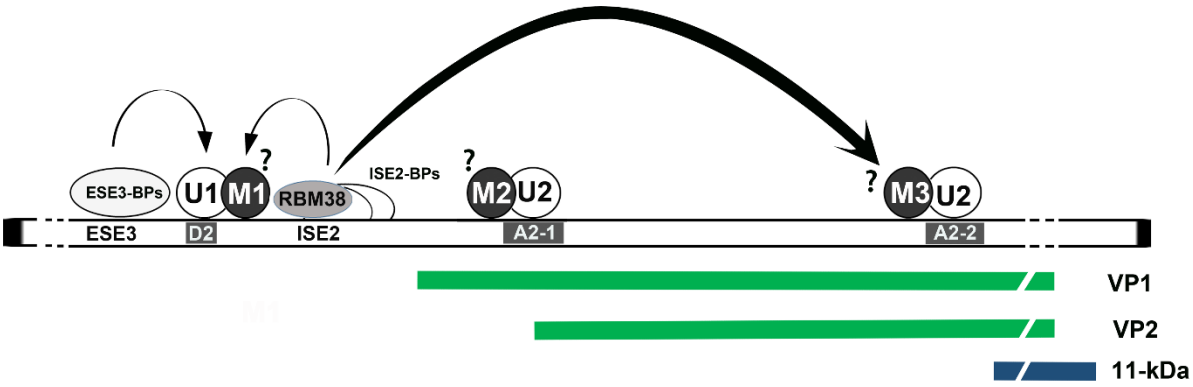
ESE3-BPs
U1
M1
?
RBM38
ISE2-BPs
?
M2
U2
?
M3
U2
ESE3
D2
ISE2
A2-1
A2-2
VP1
VP2
11-kDa

Fig. 3-9

Chapter 4:

Conclusions and Discussion

Parvovirus B19 (B19V) is one of the few parvoviruses that is pathogenic to humans (1). Approximately 40-60% of the world's population is infected with B19V (203); however, B19V infection mostly remains asymptomatic or manifests only with mild nonspecific symptoms, e.g. flu-like symptoms or arthralgia, with low levels of viremia. The viral load shoots up when the infected individual is under immune-suppression or when erythrocytes are at a high rate of turnover, such as in sickle cell disease patients. The presence of a high virus titer leads to extensive cell death of erythroid progenitor cells which causes anemia (115). In non-erythroid tissues, the B19V infection leads to inflammatory diseases like cardiomyopathy, arthopathy, etc. (19). Upon B19V infection, the single-stranded DNA genome is converted to the double-stranded replicative form, which forms a functional origin of DNA replication (Ori) of 67-bp at both ends of the genome (77). The Ori contains two NS1 binding elements (NSBE1&2), a terminal resolution site (trs) where the DNA is nicked (58), and a STAT5 binding element (STAT5BE) (78). NS1 binds Ori as a multimer (5-7), opens up the double-stranded replicative form at the Ori, and then nicks the ssDNA form Ori at the trs (62). NS1 plays a very critical role in viral DNA replication (61). It is believed that B19V replicates its genome following the rolling hairpin model of DNA replication, as described for other parvoviruses (79). Due to the limited coding capacity of the genome, the virus replication depends on cellular host factors. We have previously reported that B19V infection stalls cells in late S-phase, where the S-phase replication factors are fully utilized for viral DNA replication (68). B19V infection also induces DNA damage response by activating ATR and DNA-PKcs, which are essential for virus replication (67). The virus has a restricted tropism to erythroid progenitor cells from the bone marrow and the fetal liver (17), which depend on erythropoietin for their survival and development (87). EPO binds the EPO receptor (EPO-R), which activates three major pathways, i.e., MEK/ERK, PI3K and JAK2/STAT5 (89). Our previous

results showed that EPO signaling is essential for B19V replication (17). On further examination of the EPO-signaling cascade, our results demonstrated that the MEK/ERK pathway negatively regulates B19V replication, whereas the PI3K pathway did not play any significant role in virus infection (18). However, the JAK2-STAT5 pathway is essential for B19V replication (18). We also showed that B19V replicates efficiently under hypoxia, that the STAT5 signaling is upregulated and that the MEK/ERK signaling is downregulated during hypoxia, which in turn favor efficient B19V replication (18).

EPO-activated JAK2 phosphorylates STAT5, which undergoes dimerization and enters the nucleus (170). Phosphorylated STAT5 is critical for B19V DNA replication. Our results demonstrated that inhibition of STAT5 phosphorylation abolishes viral DNA replication **(Fig. 2-1)**. STAT5A is predominantly expressed in erythroid lineage cells rather than in STAT5B **(Fig. 2-12)**. Knockdown of STAT5A inhibits virus replication in B19V infected EPCs (18), and overexpression of a constitutively phosphorylated STAT5 mutant (STAT5A1*6) further enhances virus replication (18). Phosphorylated STAT5 is actively recruited to the viral DNA replication centers **(Fig. 2-3)**. During the late S phase arrest, the virus replicates its genome using various S-phase replication factors, such as DNA polymerases, proliferating cell nuclear antigen (PCNA), replication factor A-32 (RPA32), and minichromosome maintenance (MCM) complex, etc. (68,80). In cellular DNA replication, the ORC-CDC-CDT1 complex binds to the replication origin and CDT1 recruits MCM complex to the origin, which then uses helicase activity to unwind the DNA or helps in the recruitment of other replication factors via CDC45 (169). However, parvovirus DNA replication initiation does not require the ORC-CDC6-CDT1 complex, but rather depends on the MCM complex (68). NS1 binds B19V Ori (58), but does not interact with the MCM complex **(Fig. 2-7)**. Our *in-silico* analysis revealed that the B19V Ori

contains a consensus STAT5-binding element, which binds phosphorylated STAT5 both *in vitro* as well as *in vivo* **(Fig. 2-2, -3, -4)**. Our results revealed two important interactions: STAT5 with viral Ori, and STAT5 with the MCM complex. Of note, the interaction between STAT5 and the MCM complex is independent of the virus infection, implying that the interaction might be essential for other cellular functions, which warrants further investigation. Upon inhibition of STAT5 phosphorylation, the abundance of the MCM complex on viral Ori decreases significantly **(Fig. 2-8)**. STAT5, MCM2 and the replicating viral genome colocalize in the nuclei of B19V-infected EPCs **(Fig. 2-8)**, suggesting that B19V utilizes the STAT5-Ori interaction to recruit the MCM complex to the viral replication origin. In conclusion, our studies propose a novel model of initiation of DNA replication in parvoviruses.

To expand the coding capacity of the genome, the single precursor mRNA (pre-mRNA) transcribed from the B19V P6 promoter is post-transcriptionally processed into twelve different mRNA transcripts. The mRNAs encode two structural (VP1 & VP2) and three non-structural proteins (NS1, 11-kDa, and 7.5-kDa) (43-45). However, it is unclear how B19V precisely regulates pre-mRNA processing to maintain varying levels of mRNAs encoding different proteins. We have previously demonstrated that the expression of all mRNAs encoding capsid proteins and the 11-kDa protein depends on viral DNA replication (49). In the absence of virus DNA replication, all mRNAs polyadenylate at the (pA) p sites, and therefore only express NS1 and the 7.5-kDa proteins (49). However, replication of the viral genome facilitates read-through of the (pA)p sites and overcomes the blockage to produce full-length mRNA transcripts. Importantly, splicing at the D2 donor site is crucial for the expression of the three important viral proteins (VP1, VP2, and 11-kDa) (52). The D2 site is a weak splice donor site and the *cis-acting* elements flanking the D2 site play a key role in processing different mRNA transcripts (52). The

D2 site is flanked by exon splicing enhancer 3 (ESE3) and intronic splicing enhancer 2 (ISE2), that regulate the expression of three important viral proteins (VP1, VP2, and 11-kDa) (52). In *in-silico* analysis, we identified a motif of 5'-UGUGUG-3', a potential binding site for RBM38, in the ISE2 region of the viral pre-mRNA flanking the D2 site **(Fig. 3-2)**. Our results demonstrate that RBM38 specifically binds to ISE2 under *in-vitro* conditions **(Fig. 3-2)**. Interestingly, erythroid progenitor cells express RBM38 during the middle stages of erythropoiesis **(Fig. 3-3)**, when cells are also highly susceptible to B19V infection. Upon knockdown of RBM38 in M20-transfected UT7/Epo-S1 cells, the splicing efficiency at the D2 site decreased significantly **(Fig. 3-4)**, which, however, only affects the 11-kDa encoding mRNA **(Fig. 3-5)**. Also, RBM38 knockdown affected only 11-kDa expression in both M20-transfected UT7/Epo-S1 cells and B19V-infected $CD36^{+}$ EPCs **(Fig. 3-5)**.

Further on, our result revealed that the 11-kDa protein facilitates B19V DNA replication (~10 fold) and thereby also affects virion release **(Fig. 3-7)**. The facts that RBM38 knockdown affected virus replication **(Fig. 3-6)** and that the complementation with 11-kDa rescued the phenotype **(Fig. 3-8)** indicate that RBM38 regulates B19V replication by promoting the expression of the 11-kDa protein. The underlying mechanism of 11-kDa mediated augmentation of virus replication is unclear; however, we speculate that 11-kDa interaction with Grb2 (90) may disrupt the MEK/ERK pathway to promote virus replication. We have previously demonstrated that the MEK/ERK pathway negatively regulates B19V replication (18). Since both ISE2 and ESE3 elements are critical for splicing at the D2 site, we hypothesize that ISE2 and ESE3 interact with other host factors, and that the interplay of *cis-acting* elements and *trans-acting* factors regulates splicing at D2, thereby determining the expression of VP1, VP2, and 11-kDa proteins **(Fig. 3-9)**. In conclusion, RBM38 is an essential factor for B19V pre-mRNA

processing that ensures the expression of the 11-kDa protein, which in turn facilitates viral DNA replication and regulates the virion release.

There is neither specific treatment nor a vaccine for B19V infection and B19V-related pathologies. Our current studies identified two key host factors which can be targeted to prevent B19V infection. Importantly, phosphorylation of STAT5 is a pre-requisite for B19V replication. We showed that pimozide, a STAT5-phosphorylation inhibitor, abolishes virus replication in *ex-vivo* expanded $CD36^+$ EPCs **(Fig. 2-1)**. Our results show that pimozide inhibits virus replication with an IC_{50} of 2.7 µM **(Fig. 2-9)**. Pimozide doesn't significantly alter the cell cycle progression and colony formation of EPCs up to 15 µM **(Fig. 2-1 & Fig. 2-9)**. Thus, pimozide, an FDA-approved anti-psychotic drug, holds promise as a new treatment for B19V related pathologies in the future.

References

1. Qiu, J., Soderlund-Venermo, M., and Young, N. S. (2017) Human Parvoviruses. *Clinical microbiology reviews* **30**, 43-113
2. Cossart, Y. E., Field, A. M., Cant, B., and Widdows, D. (1975) Parvovirus-like particles in human sera. *Lancet (London, England)* **1**, 72-73
3. Young, N., Harrison, M., Moore, J., Mortimer, P., and Humphries, R. K. (1984) Direct demonstration of the human parvovirus in erythroid progenitor cells infected in vitro. *The Journal of clinical investigation* **74**, 2024-2032
4. Srivastava, A., and Lu, L. (1988) Replication of B19 parvovirus in highly enriched hematopoietic progenitor cells from normal human bone marrow. *Journal of virology* **62**, 3059-3063
5. Ozawa, K., Kurtzman, G., and Young, N. (1986) Replication of the B19 parvovirus in human bone marrow cell cultures. *Science (New York, N.Y.)* **233**, 883-886
6. Sosa, C. E., Mahony, J. B., Luinstra, K. E., Sternbach, M., and Chernesky, M. A. (1992) Replication and cytopathology of human parvovirus B19 in human umbilical cord blood erythroid progenitor cells. *J Med Virol* **36**, 125-130
7. Srivastava, C. H., Zhou, S., Munshi, N. C., and Srivastava, A. (1992) Parvovirus B19 replication in human umbilical cord blood cells. *Virology* **189**, 456-461
8. Serke, S., Schwarz, T. F., Baurmann, H., Kirsch, A., Hottentrager, B., Von Brunn, A., Roggendorf, M., Huhn, D., and Deinhardt, F. (1991) Productive infection of in vitro generated haemopoietic progenitor cells from normal human adult peripheral blood with parvovirus B19: studies by morphology, immunocytochemistry, flow-cytometry and DNA-hybridization. *Br J Haematol* **79**, 6-13
9. Schwarz, T. F., Serke, S., Hottentrager, B., von Brunn, A., Baurmann, H., Kirsch, A., Stolz, W., Huhn, D., Deinhardt, F., and Roggendorf, M. (1992) Replication of parvovirus B19 in hematopoietic progenitor cells generated in vitro from normal human peripheral blood. *Journal of virology* **66**, 1273-1276
10. Yaegashi, N., Shiraishi, H., Takeshita, T., Nakamura, M., Yajima, A., and Sugamura, K. (1989) Propagation of human parvovirus B19 in primary culture of erythroid lineage cells derived from fetal liver. *Journal of virology* **63**, 2422-2426
11. Morey, A. L., and Fleming, K. A. (1992) Immunophenotyping of fetal haemopoietic cells permissive for human parvovirus B19 replication in vitro. *Br J Haematol* **82**, 302-309
12. Munshi, N. C., Zhou, S., Woody, M. J., Morgan, D. A., and Srivastava, A. (1993) Successful replication of parvovirus B19 in the human megakaryocytic leukemia cell line MB-02. *Journal of virology* **67**, 562-566
13. Shimomura, S., Komatsu, N., Frickhofen, N., Anderson, S., Kajigaya, S., and Young, N. S. (1992) First continuous propagation of B19 parvovirus in a cell line. *Blood* **79**, 18-24
14. Morita, E., Tada, K., Chisaka, H., Asao, H., Sato, H., Yaegashi, N., and Sugamura, K. (2001) Human parvovirus B19 induces cell cycle arrest at G(2) phase with accumulation of mitotic cyclins. *Journal of virology* **75**, 7555-7563
15. Takahashi, T., Ozawa, K., Takahashi, K., Okuno, Y., Takahashi, T., Muto, Y., Takaku, F., and Asano, S. (1993) DNA replication of parvovirus B 19 in a human erythroid leukemia cell line (JK-1) in vitro. *Arch Virol* **131**, 201-208
16. Miyagawa, E., Yoshida, T., Takahashi, H., Yamaguchi, K., Nagano, T., Kiriyama, Y., Okochi, K., and Sato, H. (1999) Infection of the erythroid cell line, KU812Ep6 with

human parvovirus B19 and its application to titration of B19 infectivity. *J Virol Methods* **83**, 45-54
17. Chen, A. Y., Guan, W., Lou, S., Liu, Z., Kleiboeker, S., and Qiu, J. (2010) Role of erythropoietin receptor signaling in parvovirus B19 replication in human erythroid progenitor cells. *Journal of virology* **84**, 12385-12396
18. Chen, A. Y., Kleiboeker, S., and Qiu, J. (2011) Productive parvovirus B19 infection of primary human erythroid progenitor cells at hypoxia is regulated by STAT5A and MEK signaling but not HIFalpha. *PLoS pathogens* **7**, e1002088
19. Adamson-Small, L. A., Ignatovich, I. V., Laemmerhirt, M. G., and Hobbs, J. A. (2014) Persistent parvovirus B19 infection in non-erythroid tissues: possible role in the inflammatory and disease process. *Virus research* **190**, 8-16
20. Munakata, Y., Kato, I., Saito, T., Kodera, T., Ishii, K. K., and Sasaki, T. (2006) Human parvovirus B19 infection of monocytic cell line U937 and antibody-dependent enhancement. *Virology* **345**, 251-257
21. Schmidt-Lucke, C., Zobel, T., Schrepfer, S., Kuhl, U., Wang, D., Klingel, K., Becher, P. M., Fechner, H., Pozzuto, T., Van Linthout, S., Lassner, D., Spillmann, F., Escher, F., Holinski, S., Volk, H. D., Schultheiss, H. P., and Tschope, C. (2015) Impaired Endothelial Regeneration Through Human Parvovirus B19-Infected Circulating Angiogenic Cells in Patients With Cardiomyopathy. *The Journal of infectious diseases* **212**, 1070-1081
22. Schmidt-Lucke, C., Spillmann, F., Bock, T., Kuhl, U., Van Linthout, S., Schultheiss, H. P., and Tschope, C. (2010) Interferon beta modulates endothelial damage in patients with cardiac persistence of human parvovirus b19 infection. *The Journal of infectious diseases* **201**, 936-945
23. von Kietzell, K., Pozzuto, T., Heilbronn, R., Grossl, T., Fechner, H., and Weger, S. (2014) Antibody-mediated enhancement of parvovirus B19 uptake into endothelial cells mediated by a receptor for complement factor C1q. *Journal of virology* **88**, 8102-8115
24. Brown, K. E., Anderson, S. M., and Young, N. S. (1993) Erythrocyte P antigen: cellular receptor for B19 parvovirus. *Science (New York, N.Y.)* **262**, 114-117
25. Weigel-Kelley, K. A., Yoder, M. C., and Srivastava, A. (2001) Recombinant human parvovirus B19 vectors: erythrocyte P antigen is necessary but not sufficient for successful transduction of human hematopoietic cells. *Journal of virology* **75**, 4110-4116
26. Munakata, Y., Saito-Ito, T., Kumura-Ishii, K., Huang, J., Kodera, T., Ishii, T., Hirabayashi, Y., Koyanagi, Y., and Sasaki, T. (2005) Ku80 autoantigen as a cellular coreceptor for human parvovirus B19 infection. *Blood* **106**, 3449-3456
27. Weigel-Kelley, K. A., Yoder, M. C., and Srivastava, A. (2003) Alpha5beta1 integrin as a cellular coreceptor for human parvovirus B19: requirement of functional activation of beta1 integrin for viral entry. *Blood* **102**, 3927-3933
28. Ros, C., Gerber, M., and Kempf, C. (2006) Conformational changes in the VP1-unique region of native human parvovirus B19 lead to exposure of internal sequences that play a role in virus neutralization and infectivity. *Journal of virology* **80**, 12017-12024
29. Bonsch, C., Kempf, C., and Ros, C. (2008) Interaction of parvovirus B19 with human erythrocytes alters virus structure and cell membrane integrity. *Journal of virology* **82**, 11784-11791

30. Bonsch, C., Zuercher, C., Lieby, P., Kempf, C., and Ros, C. (2010) The globoside receptor triggers structural changes in the B19 virus capsid that facilitate virus internalization. *Journal of virology* **84**, 11737-11746
31. Leisi, R., Ruprecht, N., Kempf, C., and Ros, C. (2013) Parvovirus B19 uptake is a highly selective process controlled by VP1u, a novel determinant of viral tropism. *Journal of virology* **87**, 13161-13167
32. Leisi, R., Von Nordheim, M., Ros, C., and Kempf, C. (2016) The VP1u Receptor Restricts Parvovirus B19 Uptake to Permissive Erythroid Cells. *Viruses* **8**
33. Leisi, R., Di Tommaso, C., Kempf, C., and Ros, C. (2016) The Receptor-Binding Domain in the VP1u Region of Parvovirus B19. *Viruses* **8**, 61
34. Harbison, C. E., Chiorini, J. A., and Parrish, C. R. (2008) The parvovirus capsid odyssey: from the cell surface to the nucleus. *Trends Microbiol* **16**, 208-214
35. Quattrocchi, S., Ruprecht, N., Bonsch, C., Bieli, S., Zurcher, C., Boller, K., Kempf, C., and Ros, C. (2012) Characterization of the early steps of human parvovirus B19 infection. *Journal of virology* **86**, 9274-9284
36. Cotmore, S. F., and Tattersall, P. (2014) Parvoviruses: Small Does Not Mean Simple. *Annual review of virology* **1**, 517-537
37. Blundell, M. C., Beard, C., and Astell, C. R. (1987) In vitro identification of a B19 parvovirus promoter. *Virology* **157**, 534-538
38. Doerig, C., Beard, P., and Hirt, B. (1987) A transcriptional promoter of the human parvovirus B19 active in vitro and in vivo. *Virology* **157**, 539-542
39. Momoeda, M., Kawase, M., Jane, S. M., Miyamura, K., Young, N. S., and Kajigaya, S. (1994) The transcriptional regulator YY1 binds to the 5'-terminal region of B19 parvovirus and regulates P6 promoter activity. *Journal of virology* **68**, 7159-7168
40. Blundell, M. C., and Astell, C. R. (1989) A GC-box motif upstream of the B19 parvovirus unique promoter is important for in vitro transcription. *Journal of virology* **63**, 4814-4823
41. Raab, U., Bauer, B., Gigler, A., Beckenlehner, K., Wolf, H., and Modrow, S. (2001) Cellular transcription factors that interact with p6 promoter elements of parvovirus B19. *J Gen Virol* **82**, 1473-1480
42. Liu, J. M., Fujii, H., Green, S. W., Komatsu, N., Young, N. S., and Shimada, T. (1991) Indiscriminate activity from the B19 parvovirus p6 promoter in nonpermissive cells. *Virology* **182**, 361-364
43. Ozawa, K., Ayub, J., Hao, Y. S., Kurtzman, G., Shimada, T., and Young, N. (1987) Novel transcription map for the B19 (human) pathogenic parvovirus. *Journal of virology* **61**, 2395-2406
44. Yoto, Y., Qiu, J., and Pintel, D. J. (2006) Identification and characterization of two internal cleavage and polyadenylation sites of parvovirus B19 RNA. *Journal of virology* **80**, 1604-1609
45. Beard, C., St Amand, J., and Astell, C. R. (1989) Transient expression of B19 parvovirus gene products in COS-7 cells transfected with B19-SV40 hybrid vectors. *Virology* **172**, 659-664
46. Luo, W., and Astell, C. R. (1993) A novel protein encoded by small RNAs of parvovirus B19. *Virology* **195**, 448-455
47. St Amand, J., and Astell, C. R. (1993) Identification and characterization of a family of 11-kDa proteins encoded by the human parvovirus B19. *Virology* **192**, 121-131

48. Liu, J. M., Green, S. W., Shimada, T., and Young, N. S. (1992) A block in full-length transcript maturation in cells nonpermissive for B19 parvovirus. *Journal of virology* **66**, 4686-4692
49. Guan, W., Cheng, F., Yoto, Y., Kleiboeker, S., Wong, S., Zhi, N., Pintel, D. J., and Qiu, J. (2008) Block to the production of full-length B19 virus transcripts by internal polyadenylation is overcome by replication of the viral genome. *Journal of virology* **82**, 9951-9963
50. Bua, G., Manaresi, E., Bonvicini, F., and Gallinella, G. (2016) Parvovirus B19 Replication and Expression in Differentiating Erythroid Progenitor Cells. *PloS one* **11**, e0148547
51. Bonvicini, F., Filippone, C., Delbarba, S., Manaresi, E., Zerbini, M., Musiani, M., and Gallinella, G. (2006) Parvovirus B19 genome as a single, two-state replicative and transcriptional unit. *Virology* **347**, 447-454
52. Guan, W., Cheng, F., Huang, Q., Kleiboeker, S., and Qiu, J. (2011) Inclusion of the central exon of parvovirus B19 precursor mRNA is determined by multiple splicing enhancers in both the exon and the downstream intron. *Journal of virology* **85**, 2463-2468
53. Guan, W., Huang, Q., Cheng, F., and Qiu, J. (2011) Internal polyadenylation of the parvovirus B19 precursor mRNA is regulated by alternative splicing. *The Journal of biological chemistry* **286**, 24793-24805
54. Ganaie, S. S., Chen, A. Y., Huang, G., Xu, P., Kleiboeker, S., Du, A., and Qiu, J. (2018) RNA Binding Protein RBM38 Regulates Expression of the 11-kDa Protein of Parvovirus B19 which Facilitates Viral DNA Replication. *Journal of virology*
55. Cotmore, S. F., McKie, V. C., Anderson, L. J., Astell, C. R., and Tattersall, P. (1986) Identification of the major structural and nonstructural proteins encoded by human parvovirus B19 and mapping of their genes by procaryotic expression of isolated genomic fragments. *Journal of virology* **60**, 548-557
56. Ozawa, K., and Young, N. (1987) Characterization of capsid and noncapsid proteins of B19 parvovirus propagated in human erythroid bone marrow cell cultures. *Journal of virology* **61**, 2627-2630
57. Wan, Z., Zhi, N., Wong, S., Keyvanfar, K., Liu, D., Raghavachari, N., Munson, P. J., Su, S., Malide, D., Kajigaya, S., and Young, N. S. (2010) Human parvovirus B19 causes cell cycle arrest of human erythroid progenitors via deregulation of the E2F family of transcription factors. *The Journal of clinical investigation* **120**, 3530-3544
58. Tewary, S. K., Zhao, H., Deng, X., Qiu, J., and Tang, L. (2014) The human parvovirus B19 non-structural protein 1 N-terminal domain specifically binds to the origin of replication in the viral DNA. *Virology* **449**, 297-303
59. Momoeda, M., Wong, S., Kawase, M., Young, N. S., and Kajigaya, S. (1994) A putative nucleoside triphosphate-binding domain in the nonstructural protein of B19 parvovirus is required for cytotoxicity. *Journal of virology* **68**, 8443-8446
60. Lou, S., Luo, Y., Cheng, F., Huang, Q., Shen, W., Kleiboeker, S., Tisdale, J. F., Liu, Z., and Qiu, J. (2012) Human parvovirus B19 DNA replication induces a DNA damage response that is dispensable for cell cycle arrest at phase G2/M. *Journal of virology* **86**, 10748-10758
61. Zhi, N., Mills, I. P., Lu, J., Wong, S., Filippone, C., and Brown, K. E. (2006) Molecular and functional analyses of a human parvovirus B19 infectious clone demonstrates

essential roles for NS1, VP1, and the 11-kilodalton protein in virus replication and infectivity. *Journal of virology* **80**, 5941-5950
62. Sanchez, J. L., Romero, Z., Quinones, A., Torgeson, K. R., and Horton, N. C. (2016) DNA Binding and Cleavage by the Human Parvovirus B19 NS1 Nuclease Domain. *Biochemistry* **55**, 6577-6593
63. Raab, U., Beckenlehner, K., Lowin, T., Niller, H. H., Doyle, S., and Modrow, S. (2002) NS1 protein of parvovirus B19 interacts directly with DNA sequences of the p6 promoter and with the cellular transcription factors Sp1/Sp3. *Virology* **293**, 86-93
64. Gareus, R., Gigler, A., Hemauer, A., Leruez-Ville, M., Morinet, F., Wolf, H., and Modrow, S. (1998) Characterization of cis-acting and NS1 protein-responsive elements in the p6 promoter of parvovirus B19. *Journal of virology* **72**, 609-616
65. Moffatt, S., Yaegashi, N., Tada, K., Tanaka, N., and Sugamura, K. (1998) Human parvovirus B19 nonstructural (NS1) protein induces apoptosis in erythroid lineage cells. *Journal of virology* **72**, 3018-3028
66. Poole, B. D., Zhou, J., Grote, A., Schiffenbauer, A., and Naides, S. J. (2006) Apoptosis of liver-derived cells induced by parvovirus B19 nonstructural protein. *Journal of virology* **80**, 4114-4121
67. Luo, Y., Lou, S., Deng, X., Liu, Z., Li, Y., Kleiboeker, S., and Qiu, J. (2011) Parvovirus B19 infection of human primary erythroid progenitor cells triggers ATR-Chk1 signaling, which promotes B19 virus replication. *Journal of virology* **85**, 8046-8055
68. Luo, Y., Kleiboeker, S., Deng, X., and Qiu, J. (2013) Human parvovirus B19 infection causes cell cycle arrest of human erythroid progenitors at late S phase that favors viral DNA replication. *Journal of virology* **87**, 12766-12775
69. Morita, E., Nakashima, A., Asao, H., Sato, H., and Sugamura, K. (2003) Human parvovirus B19 nonstructural protein (NS1) induces cell cycle arrest at G(1) phase. *Journal of virology* **77**, 2915-2921
70. Xu, P., Zhou, Z., Xiong, M., Zou, W., Deng, X., Ganaie, S. S., and Kleiboeker, S. (2017) Parvovirus B19 NS1 protein induces cell cycle arrest at G2-phase by activating the ATR-CDC25C-CDK1 pathway. *PLoS pathogens* **13**, e1006266
71. Chen, A. Y., Zhang, E. Y., Guan, W., Cheng, F., Kleiboeker, S., Yankee, T. M., and Qiu, J. (2010) The small 11 kDa nonstructural protein of human parvovirus B19 plays a key role in inducing apoptosis during B19 virus infection of primary erythroid progenitor cells. *Blood* **115**, 1070-1080
72. Ozawa, K., Ayub, J., and Young, N. (1988) Translational regulation of B19 parvovirus capsid protein production by multiple upstream AUG triplets. *The Journal of biological chemistry* **263**, 10922-10926
73. Pillet, S., Annan, Z., Fichelson, S., and Morinet, F. (2003) Identification of a nonconventional motif necessary for the nuclear import of the human parvovirus B19 major capsid protein (VP2). *Virology* **306**, 25-32
74. Dorsch, S., Kaufmann, B., Schaible, U., Prohaska, E., Wolf, H., and Modrow, S. (2001) The VP1-unique region of parvovirus B19: amino acid variability and antigenic stability. *J Gen Virol* **82**, 191-199
75. Dorsch, S., Liebisch, G., Kaufmann, B., von Landenberg, P., Hoffmann, J. H., Drobnik, W., and Modrow, S. (2002) The VP1 unique region of parvovirus B19 and its constituent phospholipase A2-like activity. *Journal of virology* **76**, 2014-2018

76. Zadori, Z., Szelei, J., Lacoste, M. C., Li, Y., Gariepy, S., Raymond, P., Allaire, M., Nabi, I. R., and Tijssen, P. (2001) A viral phospholipase A2 is required for parvovirus infectivity. *Dev Cell* **1**, 291-302
77. Guan, W., Wong, S., Zhi, N., and Qiu, J. (2009) The genome of human parvovirus b19 can replicate in nonpermissive cells with the help of adenovirus genes and produces infectious virus. *Journal of virology* **83**, 9541-9553
78. Ganaie, S. S., Zou, W., Xu, P., Deng, X., Kleiboeker, S., and Qiu, J. (2017) Phosphorylated STAT5 directly facilitates parvovirus B19 DNA replication in human erythroid progenitors through interaction with the MCM complex. **13**, e1006370
79. Tattersall P, B. M., Bloom ME, Brown KE, Linden RM, Muzyczka N, Parrish CR, Tijssen P. . (2005) *Family Parvoviridae*, Elsevier/Academic Press, San Diego
80. Zou, W., Wang, Z., Xiong, M., Chen, A. Y., Xu, P., Ganaie, S. S., Badawi, Y., Kleiboeker, S., Nishimune, H., Ye, S. Q., and Qiu, J. (2017) Human Parvovirus B19 Utilizes Cellular DNA Replication Machinery for Viral DNA Replication. *Journal of virology*
81. Testa, U. (2004) Apoptotic mechanisms in the control of erythropoiesis. *Leukemia* **18**, 1176-1199
82. Ogawa, M. (1993) Differentiation and proliferation of hematopoietic stem cells. *Blood* **81**, 2844-2853
83. Papayannopoulou, T., Brice, M., and Blau, C. A. (1993) Kit ligand in synergy with interleukin-3 amplifies the erythropoietin-independent, globin-synthesizing progeny of normal human burst-forming units-erythroid in suspension cultures: physiologic implications. *Blood* **81**, 299-310
84. Dai, C. H., Krantz, S. B., and Zsebo, K. M. (1991) Human burst-forming units-erythroid need direct interaction with stem cell factor for further development. *Blood* **78**, 2493-2497
85. Sui, X., Tsuji, K., Tajima, S., Tanaka, R., Muraoka, K., Ebihara, Y., Ikebuchi, K., Yasukawa, K., Taga, T., Kishimoto, T., and Nakahata, T. (1996) Erythropoietin-independent erythrocyte production: signals through gp130 and c-kit dramatically promote erythropoiesis from human CD34+ cells. *J Exp Med* **183**, 837-845
86. Koury, M. J., and Bondurant, M. C. (1992) The molecular mechanism of erythropoietin action. *Eur J Biochem* **210**, 649-663
87. Grebien, F., Kerenyi, M. A., Kovacic, B., Kolbe, T., Becker, V., Dolznig, H., Pfeffer, K., Klingmuller, U., Muller, M., Beug, H., Mullner, E. W., and Moriggl, R. (2008) Stat5 activation enables erythropoiesis in the absence of EpoR and Jak2. *Blood* **111**, 4511-4522
88. Takahashi, T., Ozawa, K., Takahashi, K., Asano, S., and Takaku, F. (1990) Susceptibility of human erythropoietic cells to B19 parvovirus in vitro increases with differentiation. *Blood* **75**, 603-610
89. Lodish HF, G. S., Socolovsky M, Tong W, Zhang J. (2009) Intracellular signaling by the erythropoietin receptor. in *Erythropoietins, Erythropoietic Factors and Erythropoiesis.* (Elliott SG, F. M., Molineux G ed.), Birkhäuser Verlag, Switzerland:. pp pp. 155–174.
90. Fan, M. M., Tamburic, L., Shippam-Brett, C., Zagrodney, D. B., and Astell, C. R. (2001) The small 11-kDa protein from B19 parvovirus binds growth factor receptor-binding protein 2 in vitro in a Src homology 3 domain/ligand-dependent manner. *Virology* **291**, 285-291

91. Wong, S., and Brown, K. E. (2006) Development of an improved method of detection of infectious parvovirus B19. *Journal of clinical virology : the official publication of the Pan American Society for Clinical Virology* **35**, 407-413
92. Takano, T., and Yamada, K. (2007) Quantitation of human parvovirus B19 DNA by real-time polymerase chain reaction. *Pediatrics international : official journal of the Japan Pediatric Society* **49**, 459-462
93. Rogers, H. M., Yu, X., Wen, J., Smith, R., Fibach, E., and Noguchi, C. T. (2008) Hypoxia alters progression of the erythroid program. *Experimental hematology* **36**, 17-27
94. Koller, M. R., Bender, J. G., Miller, W. M., and Papoutsakis, E. T. (1992) Reduced oxygen tension increases hematopoiesis in long-term culture of human stem and progenitor cells from cord blood and bone marrow. *Experimental hematology* **20**, 264-270
95. Caillet-Fauquet, P., Draps, M. L., Di Giambattista, M., de Launoit, Y., and Laub, R. (2004) Hypoxia enables B19 erythrovirus to yield abundant infectious progeny in a pluripotent erythroid cell line. *J Virol Methods* **121**, 145-153
96. Luo, Y., and Qiu, J. (2015) Human parvovirus B19: a mechanistic overview of infection and DNA replication. *Future Virol* **10**, 155-167
97. Deleu, L., Pujol, A., Faisst, S., and Rommelaere, J. (1999) Activation of promoter P4 of the autonomous parvovirus minute virus of mice at early S phase is required for productive infection. *Journal of virology* **73**, 3877-3885
98. Oleksiewicz, M. B., and Alexandersen, S. (1997) S-phase-dependent cell cycle disturbances caused by Aleutian mink disease parvovirus. *Journal of virology* **71**, 1386-1396
99. Parris, D. S., and Bates, R. C. (1976) Effect of bovine parvovirus replication on DNA, RNA, and protein synthesis in S phase cells. *Virology* **73**, 72-78
100. Ciccia, A., and Elledge, S. J. (2010) The DNA damage response: making it safe to play with knives. *Molecular cell* **40**, 179-204
101. Trigg, B. J., and Ferguson, B. J. (2015) Functions of DNA damage machinery in the innate immune response to DNA virus infection. *Current opinion in virology* **15**, 56-62
102. Nunoue, T., Okochi, K., Mortimer, P. P., and Cohen, B. J. (1985) Human parvovirus (B19) and erythema infectiosum. *The Journal of pediatrics* **107**, 38-40
103. Anderson, M. J., Higgins, P. G., Davis, L. R., Willman, J. S., Jones, S. E., Kidd, I. M., Pattison, J. R., and Tyrrell, D. A. (1985) Experimental parvoviral infection in humans. *The Journal of infectious diseases* **152**, 257-265
104. Shneerson, J. M., Mortimer, P. P., and Vandervelde, E. M. (1980) Febrile illness due to a parvovirus. *British medical journal* **280**, 1580
105. Broliden, K., Tolfvenstam, T., and Norbeck, O. (2006) Clinical aspects of parvovirus B19 infection. *Journal of internal medicine* **260**, 285-304
106. Anderson, L. J., Tsou, C., Parker, R. A., Chorba, T. L., Wulff, H., Tattersall, P., and Mortimer, P. P. (1986) Detection of antibodies and antigens of human parvovirus B19 by enzyme-linked immunosorbent assay. *J Clin Microbiol* **24**, 522-526
107. Heegaard, E. D., and Brown, K. E. (2002) Human parvovirus B19. *Clinical microbiology reviews* **15**, 485-505
108. Naides, S. J. (1999) Infection with Parvovirus B19. *Current infectious disease reports* **1**, 273-278

109. Woolf, A. D., Campion, G. V., Chishick, A., Wise, S., Cohen, B. J., Klouda, P. T., Caul, O., and Dieppe, P. A. (1989) Clinical manifestations of human parvovirus B19 in adults. *Archives of internal medicine* **149**, 1153-1156
110. Riipinen, A., Vaisanen, E., Nuutila, M., Sallmen, M., Karikoski, R., Lindbohm, M. L., Hedman, K., Taskinen, H., and Soderlund-Venermo, M. (2008) Parvovirus b19 infection in fetal deaths. *Clinical infectious diseases : an official publication of the Infectious Diseases Society of America* **47**, 1519-1525
111. Kaplan, C., Morinet, F., and Cartron, J. (1992) Virus-induced autoimmune thrombocytopenia and neutropenia. *Seminars in hematology* **29**, 34-44
112. Peng, C. Y., Graves, P. R., Ogg, S., Thoma, R. S., Byrnes, M. J., 3rd, Wu, Z., Stephenson, M. T., and Piwnica-Worms, H. (1998) C-TAK1 protein kinase phosphorylates human Cdc25C on serine 216 and promotes 14-3-3 protein binding. *Cell growth & differentiation : the molecular biology journal of the American Association for Cancer Research* **9**, 197-208
113. Dunphy, W. G., Brizuela, L., Beach, D., and Newport, J. (1988) The Xenopus cdc2 protein is a component of MPF, a cytoplasmic regulator of mitosis. *Cell* **54**, 423-431
114. Mortimer, P. P., Humphries, R. K., Moore, J. G., Purcell, R. H., and Young, N. S. (1983) A human parvovirus-like virus inhibits haematopoietic colony formation in vitro. *Nature* **302**, 426-429
115. Young, N. S., Mortimer, P. P., Moore, J. G., and Humphries, R. K. (1984) Characterization of a virus that causes transient aplastic crisis. *The Journal of clinical investigation* **73**, 224-230
116. Sol, N., Le Junter, J., Vassias, I., Freyssinier, J. M., Thomas, A., Prigent, A. F., Rudkin, B. B., Fichelson, S., and Morinet, F. (1999) Possible interactions between the NS-1 protein and tumor necrosis factor alpha pathways in erythroid cell apoptosis induced by human parvovirus B19. *Journal of virology* **73**, 8762-8770
117. Bonvicini, F., Manaresi, E., Di Furio, F., De Falco, L., and Gallinella, G. (2012) Parvovirus b19 DNA CpG dinucleotide methylation and epigenetic regulation of viral expression. *PloS one* **7**, e33316
118. Kerr, J. R. (2000) Pathogenesis of human parvovirus B19 in rheumatic disease. *Annals of the rheumatic diseases* **59**, 672-683
119. Duechting, A., Tschope, C., Kaiser, H., Lamkemeyer, T., Tanaka, N., Aberle, S., Lang, F., Torresi, J., Kandolf, R., and Bock, C. T. (2008) Human parvovirus B19 NS1 protein modulates inflammatory signaling by activation of STAT3/PIAS3 in human endothelial cells. *Journal of virology* **82**, 7942-7952
120. Polcz, M. E., Adamson, L. A., Lu, X., Chang, M. N., Fowler, L. J., and Hobbs, J. A. (2013) Increased IL-6 detection in adult and pediatric lymphoid tissue harboring parvovirus B19. *Journal of clinical virology : the official publication of the Pan American Society for Clinical Virology* **57**, 233-238
121. Lu, J., Zhi, N., Wong, S., and Brown, K. E. (2006) Activation of synoviocytes by the secreted phospholipase A2 motif in the VP1-unique region of parvovirus B19 minor capsid protein. *The Journal of infectious diseases* **193**, 582-590
122. Wang, J. H., Zhang, W. P., Liu, H. X., Wang, D., Li, Y. F., Wang, W. Q., Wang, L., He, F. R., Wang, Z., Yan, Q. G., Chen, L. W., and Huang, G. S. (2008) Detection of human parvovirus B19 in papillary thyroid carcinoma. *British journal of cancer* **98**, 611-618

123. Li, Y., Wang, J., Zhu, G., Zhang, X., Zhai, H., Zhang, W., Wang, W., and Huang, G. (2007) Detection of parvovirus B19 nucleic acids and expression of viral VP1/VP2 antigen in human colon carcinoma. *The American journal of gastroenterology* **102**, 1489-1498
124. Poole, B. D., Karetnyi, Y. V., and Naides, S. J. (2004) Parvovirus B19-induced apoptosis of hepatocytes. *Journal of virology* **78**, 7775-7783
125. Pasquinelli, G., Bonvicini, F., Foroni, L., Salfi, N., and Gallinella, G. (2009) Placental endothelial cells can be productively infected by Parvovirus B19. *Journal of clinical virology : the official publication of the Pan American Society for Clinical Virology* **44**, 33-38
126. Kurtzman, G. J., Cohen, B. J., Field, A. M., Oseas, R., Blaese, R. M., and Young, N. S. (1989) Immune response to B19 parvovirus and an antibody defect in persistent viral infection. *The Journal of clinical investigation* **84**, 1114-1123
127. Gray, J. J., Cohen, B. J., and Desselberger, U. (1993) Detection of human parvovirus B19-specific IgM and IgG antibodies using a recombinant viral VP1 antigen expressed in insect cells and estimation of time of infection by testing for antibody avidity. *J Virol Methods* **44**, 11-23
128. Brown, C. S., Jensen, T., Meloen, R. H., Puijk, W., Sugamura, K., Sato, H., and Spaan, W. J. (1992) Localization of an immunodominant domain on baculovirus-produced parvovirus B19 capsids: correlation to a major surface region on the native virus particle. *Journal of virology* **66**, 6989-6996
129. von Poblotzki, A., Hemauer, A., Gigler, A., Puchhammer-Stockl, E., Heinz, F. X., Pont, J., Laczika, K., Wolf, H., and Modrow, S. (1995) Antibodies to the nonstructural protein of parvovirus B19 in persistently infected patients: implications for pathogenesis. *The Journal of infectious diseases* **172**, 1356-1359
130. Anderson, S., Momoeda, M., Kawase, M., Kajigaya, S., and Young, N. S. (1995) Peptides derived from the unique region of B19 parvovirus minor capsid protein elicit neutralizing antibodies in rabbits. *Virology* **206**, 626-632
131. Norbeck, O., Isa, A., Pohlmann, C., Broliden, K., Kasprowicz, V., Bowness, P., Klenerman, P., and Tolfvenstam, T. (2005) Sustained CD8+ T-cell responses induced after acute parvovirus B19 infection in humans. *Journal of virology* **79**, 12117-12121
132. von Poblotzki, A., Gerdes, C., Reischl, U., Wolf, H., and Modrow, S. (1996) Lymphoproliferative responses after infection with human parvovirus B19. *Journal of virology* **70**, 7327-7330
133. Isa, A., Lundqvist, A., Lindblom, A., Tolfvenstam, T., and Broliden, K. (2007) Cytokine responses in acute and persistent human parvovirus B19 infection. *Clin Exp Immunol* **147**, 419-425
134. Franssila, R., Auramo, J., Modrow, S., Mobs, M., Oker-Blom, C., Kapyla, P., Soderlund-Venermo, M., and Hedman, K. (2005) T helper cell-mediated interferon-gamma expression after human parvovirus B19 infection: persisting VP2-specific and transient VP1u-specific activity. *Clin Exp Immunol* **142**, 53-61
135. Hsu, G. J., Tzang, B. S., Tsai, C. C., Chiu, C. C., Huang, C. Y., and Hsu, T. C. (2011) Effects of human parvovirus B19 on expression of defensins and Toll-like receptors. *Chin J Physiol* **54**, 367-376
136. Guo, Y. M., Ishii, K., Hirokawa, M., Tagawa, H., Ohyagi, H., Michishita, Y., Ubukawa, K., Yamashita, J., Ohteki, T., Onai, N., Kawakami, K., Xiao, W., and Sawada, K. (2010)

CpG-ODN 2006 and human parvovirus B19 genome consensus sequences selectively inhibit growth and development of erythroid progenitor cells. *Blood* **115**, 4569-4579
137. Kishore, J., and Kapoor, A. (2000) Erythrovirus B19 infection in humans. *The Indian journal of medical research* **112**, 149-164
138. Gigler, A., Dorsch, S., Hemauer, A., Williams, C., Kim, S., Young, N. S., Zolla-Pazner, S., Wolf, H., Gorny, M. K., and Modrow, S. (1999) Generation of neutralizing human monoclonal antibodies against parvovirus B19 proteins. *Journal of virology* **73**, 1974-1979
139. O'Sullivan, M. G., Anderson, D. C., Fikes, J. D., Bain, F. T., Carlson, C. S., Green, S. W., Young, N. S., and Brown, K. E. (1994) Identification of a novel simian parvovirus in cynomolgus monkeys with severe anemia. A paradigm of human B19 parvovirus infection. *The Journal of clinical investigation* **93**, 1571-1576
140. Cotmore, S. F., Agbandje-McKenna, M., Chiorini, J. A., Mukha, D. V., Pintel, D. J., Qiu, J., Soderlund-Venermo, M., Tattersall, P., Tijssen, P., Gatherer, D., and Davison, A. J. (2014) The family Parvoviridae. *Arch Virol* **159**, 1239-1247
141. Deiss, V., Tratschin, J. D., Weitz, M., and Siegl, G. (1990) Cloning of the human parvovirus B19 genome and structural analysis of its palindromic termini. *Virology* **175**, 247-254
142. Young, N. S., and Brown, K. E. (2004) Parvovirus B19. *New England Journal of Medicine* **350**, 586-597
143. Brown, K. E., and Young, N. S. (1997) Parvovirus B19 in human disease. *Annual review of medicine* **48**, 59-67
144. Gallinella, G. (2013) Parvovirus B19 Achievements and Challenges. *ISRN Virology* **2013**, 33
145. Young, N. S. (1995) B19 parvovirus. *Bailliere's clinical haematology* **8**, 25-56
146. Chen, A. Y., and Qiu, J. (2010) Parvovirus infection-induced cell death and cell cycle arrest. *Future Virol* **5**, 731-743
147. Wong, S., Zhi, N., Filippone, C., Keyvanfar, K., Kajigaya, S., Brown, K. E., and Young, N. S. (2008) Ex vivo-generated CD36+ erythroid progenitors are highly permissive to human parvovirus B19 replication. *Journal of virology* **82**, 2470-2476
148. Muller, J., Sperl, B., Reindl, W., Kiessling, A., and Berg, T. (2008) Discovery of chromone-based inhibitors of the transcription factor STAT5. *Chembiochem : a European journal of chemical biology* **9**, 723-727
149. Nelson, E. A., Walker, S. R., Weisberg, E., Bar-Natan, M., Barrett, R., Gashin, L. B., Terrell, S., Klitgaard, J. L., Santo, L., Addorio, M. R., Ebert, B. L., Griffin, J. D., and Frank, D. A. (2011) The STAT5 inhibitor pimozide decreases survival of chronic myelogenous leukemia cells resistant to kinase inhibitors. *Blood* **117**, 3421-3429
150. Deng, X., Xu, P., Zou, W., Shen, W., Peng, J., Liu, K., Engelhardt, J. F., Yan, Z., and Qiu, J. (2017) DNA Damage Signaling Is Required for Replication of Human Bocavirus 1 DNA in Dividing HEK293 Cells. *Journal of virology* **91**
151. Zhi, N., Zadori, Z., Brown, K. E., and Tijssen, P. (2004) Construction and sequencing of an infectious clone of the human parvovirus B19. *Virology* **318**, 142-152
152. Soldaini, E., John, S., Moro, S., Bollenbacher, J., Schindler, U., and Leonard, W. J. (2000) DNA binding site selection of dimeric and tetrameric Stat5 proteins reveals a large repertoire of divergent tetrameric Stat5a binding sites. *Molecular and cellular biology* **20**, 389-401

153. Jutras, B. L., Verma, A., and Stevenson, B. (2012) Identification of novel DNA-binding proteins using DNA-affinity chromatography/pull down. *Current protocols in microbiology* **Chapter 1**, Unit1F.1
154. Shen, W., Deng, X., Zou, W., Engelhardt, J. F., Yan, Z., and Qiu, J. (2016) Analysis of cis and trans Requirements for DNA Replication at the Right-End Hairpin of the Human Bocavirus 1 Genome. *Journal of virology* **90**, 7761-7777
155. Lu, D., Han, C., and Wu, T. (2014) 15-PGDH inhibits hepatocellular carcinoma growth through 15-keto-PGE2/PPARgamma-mediated activation of p21WAF1/Cip1. *Oncogene* **33**, 1101-1112
156. Gade, P., and Kalvakolanu, D. V. (2012) Chromatin immunoprecipitation assay as a tool for analyzing transcription factor activity. *Methods in molecular biology (Clifton, N.J.)* **809**, 85-104
157. Ganaie, S. S., Haque, A., Cheng, E., Bonny, T. S., Salim, N. N., and Mir, M. A. (2014) Ribosomal protein S19-binding domain provides insights into hantavirus nucleocapsid protein-mediated translation initiation mechanism. *The Biochemical journal* **464**, 109-121
158. Salim, N. N., Ganaie, S. S., Roy, A., Jeeva, S., and Mir, M. A. (2016) Targeting a Novel RNA-Protein Interaction for Therapeutic Intervention of Hantavirus Disease. *The Journal of biological chemistry* **291**, 24702-24714
159. Jamieson AM, F. M., Decker T. (2012) *How stats interact with the molecular machinery of transcriptional activation in Jak-stat signaling: From basics to diseases.* , Springer-Verlag Wien.
160. Ehret, G. B., Reichenbach, P., Schindler, U., Horvath, C. M., Fritz, S., Nabholz, M., and Bucher, P. (2001) DNA binding specificity of different STAT proteins. Comparison of in vitro specificity with natural target sites. *The Journal of biological chemistry* **276**, 6675-6688
161. Lin, J. X., Li, P., Liu, D., Jin, H. T., He, J., Ata Ur Rasheed, M., Rochman, Y., Wang, L., Cui, K., Liu, C., Kelsall, B. L., Ahmed, R., and Leonard, W. J. (2012) Critical Role of STAT5 transcription factor tetramerization for cytokine responses and normal immune function. *Immunity* **36**, 586-599
162. Soderberg, O., Gullberg, M., Jarvius, M., Ridderstrale, K., Leuchowius, K. J., Jarvius, J., Wester, K., Hydbring, P., Bahram, F., Larsson, L. G., and Landegren, U. (2006) Direct observation of individual endogenous protein complexes in situ by proximity ligation. *Nature methods* **3**, 995-1000
163. Bashir, T., Rommelaere, J., and Cziepluch, C. (2001) In vivo accumulation of cyclin A and cellular replication factors in autonomous parvovirus minute virus of mice-associated replication bodies. *Journal of virology* **75**, 4394-4398
164. Young, P. J., Jensen, K. T., Burger, L. R., Pintel, D. J., and Lorson, C. L. (2002) Minute virus of mice NS1 interacts with the SMN protein, and they colocalize in novel nuclear bodies induced by parvovirus infection. *Journal of virology* **76**, 3892-3904
165. Sun, J., and Kong, D. (2010) DNA replication origins, ORC/DNA interaction, and assembly of pre-replication complex in eukaryotes. *Acta biochimica et biophysica Sinica* **42**, 433-439
166. Bell, S. P., and Dutta, A. (2002) DNA replication in eukaryotic cells. *Annual review of biochemistry* **71**, 333-374
167. Stenlund, A. (2003) Initiation of DNA replication: lessons from viral initiator proteins. *Nature reviews. Molecular cell biology* **4**, 777-785

168. Nash, K., Chen, W., and Muzyczka, N. (2008) Complete in vitro reconstitution of adeno-associated virus DNA replication requires the minichromosome maintenance complex proteins. *Journal of virology* **82**, 1458-1464
169. Takisawa, H., Mimura, S., and Kubota, Y. (2000) Eukaryotic DNA replication: from pre-replication complex to initiation complex. *Current opinion in cell biology* **12**, 690-696
170. Buitenhuis, M., Coffer, P. J., and Koenderman, L. (2004) Signal transducer and activator of transcription 5 (STAT5). *The international journal of biochemistry & cell biology* **36**, 2120-2124
171. Fahrenkamp, D., Li, J., Ernst, S., Schmitz-Van de Leur, H., Chatain, N., Kuster, A., Koschmieder, S., Luscher, B., Rossetti, G., and Muller-Newen, G. (2016) Intramolecular hydrophobic interactions are critical mediators of STAT5 dimerization. *Scientific reports* **6**, 35454
172. Oda, A., Sawada, K., Druker, B. J., Ozaki, K., Takano, H., Koizumi, K., Fukada, Y., Handa, M., Koike, T., and Ikeda, Y. (1998) Erythropoietin induces tyrosine phosphorylation of Jak2, STAT5A, and STAT5B in primary cultured human erythroid precursors. *Blood* **92**, 443-451
173. Hong, S., Cheng, S., Iovane, A., and Laimins, L. A. (2015) STAT-5 Regulates Transcription of the Topoisomerase IIbeta-Binding Protein 1 (TopBP1) Gene To Activate the ATR Pathway and Promote Human Papillomavirus Replication. *mBio* **6**, e02006-02015
174. Watanabe, S., Zeng, R., Aoki, Y., Itoh, T., and Arai, K. (2001) Initiation of polyoma virus origin-dependent DNA replication through STAT5 activation by human granulocyte-macrophage colony-stimulating factor. *Blood* **97**, 1266-1273
175. Simmons, D. T. (2000) SV40 large T antigen functions in DNA replication and transformation. *Advances in virus research* **55**, 75-134
176. Cotmore SF, T. P. (2005) *A rolling-haipin strategy: basic mechanisms of DNA replication in the parvoviruses*, London: Hoddler Arond
177. Nash, K., Chen, W., Salganik, M., and Muzyczka, N. (2009) Identification of cellular proteins that interact with the adeno-associated virus rep protein. *Journal of virology* **83**, 454-469
178. Christensen, J., Cotmore, S. F., and Tattersall, P. (1997) Parvovirus initiation factor PIF: a novel human DNA-binding factor which coordinately recognizes two ACGT motifs. *Journal of virology* **71**, 5733-5741
179. Christensen, J., Cotmore, S. F., and Tattersall, P. (1999) Two new members of the emerging KDWK family of combinatorial transcription modulators bind as a heterodimer to flexibly spaced PuCGPy half-sites. *Molecular and cellular biology* **19**, 7741-7750
180. Christensen, J., Cotmore, S. F., and Tattersall, P. (2001) Minute virus of mice initiator protein NS1 and a host KDWK family transcription factor must form a precise ternary complex with origin DNA for nicking to occur. *Journal of virology* **75**, 7009-7017
181. Kast, R. E. (2010) Glioblastoma chemotherapy adjunct via potent serotonin receptor-7 inhibition using currently marketed high-affinity antipsychotic medicines. *British journal of pharmacology* **161**, 481-487
182. Bar-Natan, M., Nelson, E. A., Walker, S. R., Kuang, Y., Distel, R. J., and Frank, D. A. (2012) Dual inhibition of Jak2 and STAT5 enhances killing of myeloproliferative neoplasia cells. *Leukemia* **26**, 1407-1410

183. Morfin, F., Dupuis-Girod, S., Frobert, E., Mundweiler, S., Carrington, D., Sedlacek, P., Bierings, M., Cetkovsky, P., Kroes, A. C., van Tol, M. J., and Thouvenot, D. (2009) Differential susceptibility of adenovirus clinical isolates to cidofovir and ribavirin is not related to species alone. *Antiviral therapy* **14**, 55-61
184. St Amand, J., Beard, C., Humphries, K., and Astell, C. R. (1991) Analysis of splice junctions and in vitro and in vivo translation potential of the small, abundant B19 parvovirus RNAs. *Virology* **183**, 133-142
185. Liu, Z., Qiu, J., Cheng, F., Chu, Y., Yoto, Y., O'Sullivan, M. G., Brown, K. E., and Pintel, D. J. (2004) Comparison of the transcription profile of simian parvovirus with that of the human erythrovirus B19 reveals a number of unique features. *Journal of virology* **78**, 12929-12939
186. Jia, R., Liu, X., Tao, M., Kruhlak, M., Guo, M., Meyers, C., Baker, C. C., and Zheng, Z. M. (2009) Control of the papillomavirus early-to-late switch by differentially expressed SRp20. *Journal of virology* **83**, 167-180
187. Wu, K. K. (2006) Analysis of protein-DNA binding by streptavidin-agarose pulldown. *Methods in molecular biology (Clifton, N.J.)* **338**, 281-290
188. Rio, D. C. (2014) Electrophoretic mobility shift assays for RNA-protein complexes. *Cold Spring Harbor protocols* **2014**, 435-440
189. Wang, Z., Deng, X., Zou, W., Engelhardt, J. F., Yan, Z., and Qiu, J. (2017) Human Bocavirus 1 Is a Novel Helper for Adeno-Associated Virus Replication. *Journal of virology*
190. Sowd, G. A., Li, N. Y., and Fanning, E. (2013) ATM and ATR activities maintain replication fork integrity during SV40 chromatin replication. *PLoS pathogens* **9**, e1003283
191. Pillay, S., Zou, W., Cheng, F., Puschnik, A. S., Meyer, N. L., Ganaie, S. S., Deng, X., Wosen, J. E., Davulcu, O., Yan, Z., Engelhardt, J. F., Brown, K. E., Chapman, M. S., Qiu, J., and Carette, J. E. (2017) AAV serotypes have distinctive interactions with domains of the cellular receptor AAVR. *Journal of virology* **vol. 91** e00391-00317
192. Kuroyanagi, H., Ohno, G., Mitani, S., and Hagiwara, M. (2007) The Fox-1 family and SUP-12 coordinately regulate tissue-specific alternative splicing in vivo. *Molecular and cellular biology* **27**, 8612-8621
193. Ohno, G., Ono, K., Togo, M., Watanabe, Y., Ono, S., Hagiwara, M., and Kuroyanagi, H. (2012) Muscle-specific splicing factors ASD-2 and SUP-12 cooperatively switch alternative pre-mRNA processing patterns of the ADF/cofilin gene in Caenorhabditis elegans. *PLoS genetics* **8**, e1002991
194. Anyanful, A., Ono, K., Johnsen, R. C., Ly, H., Jensen, V., Baillie, D. L., and Ono, S. (2004) The RNA-binding protein SUP-12 controls muscle-specific splicing of the ADF/cofilin pre-mRNA in C. elegans. *The Journal of cell biology* **167**, 639-647
195. Heinicke, L. A., Nabet, B., Shen, S., Jiang, P., van Zalen, S., Cieply, B., Russell, J. E., Xing, Y., and Carstens, R. P. (2013) The RNA binding protein RBM38 (RNPC1) regulates splicing during late erythroid differentiation. *PloS one* **8**, e78031
196. Lee, Y., and Rio, D. C. (2015) Mechanisms and Regulation of Alternative Pre-mRNA Splicing. *Annual review of biochemistry* **84**, 291-323
197. Lowenstein, E. J., Daly, R. J., Batzer, A. G., Li, W., Margolis, B., Lammers, R., Ullrich, A., Skolnik, E. Y., Bar-Sagi, D., and Schlessinger, J. (1992) The SH2 and SH3 domain-

containing protein GRB2 links receptor tyrosine kinases to ras signaling. *Cell* **70**, 431-442
198. Bandziulis, R. J., Swanson, M. S., and Dreyfuss, G. (1989) RNA-binding proteins as developmental regulators. *Genes & development* **3**, 431-437
199. Gerstberger, S., Hafner, M., and Tuschl, T. (2014) A census of human RNA-binding proteins. *Nature reviews. Genetics* **15**, 829-845
200. Zhou, X. J., Wu, J., Shi, L., Li, X. X., Zhu, L., Sun, X., Qian, J. Y., Wang, Y., Wei, J. F., and Ding, Q. (2017) PTEN expression is upregulated by a RNA-binding protein RBM38 via enhancing its mRNA stability in breast cancer. *Journal of experimental & clinical cancer research : CR* **36**, 149
201. Zhang, M., Xu, E., Zhang, J., and Chen, X. (2015) PPM1D phosphatase, a target of p53 and RBM38 RNA-binding protein, inhibits p53 mRNA translation via dephosphorylation of RBM38. *Oncogene* **34**, 5900-5911
202. Alvarez-Dominguez, J. R., Zhang, X., and Hu, W. (2017) Widespread and dynamic translational control of red blood cell development. **129**, 619-629
203. Marano, G., Vaglio, S., Pupella, S., Facco, G., Calizzani, G., Candura, F., Liumbruno, G. M., and Grazzini, G. (2015) Human Parvovirus B19 and blood product safety: a tale of twenty years of improvements. *Blood transfusion = Trasfusione del sangue* **13**, 184-196